

# **The Dynamics of Molecular Glasses Studied by Light Scattering**

Der Universität Bayreuth  
Zur Erlangung des Grades eines  
Doktors der Naturwissenschaften (Dr. rer. nat.)  
vorgelegte Abhandlung

von

**Sergei Adichtchev**  
Geboren am 2. Februar 1974 in Nowosibirsk

1. Gutachter: Prof. Dr. E. Rössler
2. Gutachter: Prof. Dr. W. Köhler

Tag der Einreichung: 29. Juni 2006  
Tag des Kolloquiums: 7. December 2006



# Contents

<b>1</b>	<b>Introduction</b>	<b>1</b>
<b>2</b>	<b>Phenomenology of the dynamics in supercooled liquids and glasses</b>	<b>4</b>
2.1	The correlation function. . . . .	4
2.2	The Mode-Coupling theory. . . . .	7
2.2.1	Mode-Coupling theory equations. . . . .	7
2.2.2	The asymptotic scaling laws of MCT . . . . .	10
2.3	Models of fast dynamics in glasses ( $T < T_g$ ). . . . .	13
<b>3</b>	<b>Light scattering experiment</b>	<b>17</b>
3.1	Introduction . . . . .	17
3.2	Experimental setup . . . . .	19
3.2.1	Tandem Fabry-Perot interferometer . . . . .	20
3.2.2	Light scattering setup . . . . .	23
<b>4</b>	<b>Light scattering in 2 - picoline and m-tricresyl phosphate</b>	<b>25</b>
4.1	Experimental check of the MCT predictions. . . . .	25
4.2	Light - scattering spectra . . . . .	27
4.3	Spectra analysis . . . . .	28
4.4	Phenomenological analysis . . . . .	33
4.5	Discussion and conclusions . . . . .	38
<b>5</b>	<b>Reexamination of the evolution of the dynamic susceptibility of glycerol</b>	<b>40</b>
5.1	Introduction . . . . .	40
5.2	Phenomenological description of the susceptibility . . . . .	43

5.3	Results . . . . .	45
5.3.1	Spectra analysis . . . . .	45
5.3.2	Mode coupling theory analysis. . . . .	51
5.4	Discussion and conclusion. . . . .	54
<b>6</b>	<b>Fast relaxation processes in glasses tested by quasi-elastic light scattering</b>	<b>58</b>
6.1	Introduction . . . . .	58
6.2	Light-scattering spectra . . . . .	61
6.3	Spectra analysis . . . . .	63
<b>7</b>	<b>Study of the structural glass and glassy crystal of ethanol and cyano cyclohexane</b>	<b>68</b>
7.1	Introduction . . . . .	68
7.2	Experimental conditions . . . . .	69
7.3	Results and analysis . . . . .	72
7.3.1	Depolarized light scattering . . . . .	72
7.3.2	Brillouin scattering . . . . .	78
7.4	Discussion . . . . .	81
7.5	Conclusion . . . . .	84
<b>8</b>	<b>Summary</b>	<b>86</b>
<b>9</b>	<b>Zusammenfassung</b>	<b>88</b>
<b>A</b>	<b>Appendix</b>	<b>90</b>
	<b>Bibliography</b>	<b>94</b>
	<b>List of Publications</b>	<b>103</b>
	<b>Acknowledgments</b>	<b>104</b>

# 1 Introduction

There is a large amount of materials, called amorphous or disordered systems, which have no long range order. Liquids, glasses, and polymers are well known and useful examples of disordered systems. Also crystals with orientational disorder may be included in this list. Because of their importance, amorphous systems are in the focus of different kind of investigations.

The most common way to make a glass is by cooling a liquid below its melting temperature fast enough to avoid crystallization. During the cooling one can see a dramatic increase of the viscosity  $\eta$ , changing from  $\eta \sim 10^{-3}$  Pa·s, which is typical for a simple liquid, to  $\eta \sim 10^{12}$  Pa·s for a solid body. This transition from a liquid to an amorphous solid (glass) is called the glass transition. Along with increasing of viscosity the molecular motions in supercooled liquid slow down and the structural relaxation time  $\tau_\alpha$  continuously grows from, say,  $10^{-13}$ s up to  $10^2$ s at the glass transition temperature  $T_g$ . Around this temperature the liquid falls out of equilibrium since the structural relaxation time becomes larger than experimental timescale. By the glass formation the liquid does not undergo a distinct structural change. However some properties, like density or heat capacity, change their temperature dependence by passing  $T_g$ . For instance, heat capacity exhibits a pronounced step at  $T_g$ . This property is commonly used to determine  $T_g$  experimentally by differential scanning calorimetry.

One of the distinguishing properties of glasses is the existence of relaxational processes on the frequency scale from zero to, say, 1 THz. These relaxational features were actively studied in recent years by monitoring the evolution of the susceptibility spectra. Near  $T_g$ , the relaxation spectra spread over more than 14 decades in frequency.

One can phenomenologically distinguish four different regimes of relaxation, which are schematically shown in Fig. 1: (a) low-density fluid,

where relaxation and microscopic dynamics have essentially merged, (b) a liquid of moderate viscosity with its characteristic two-step relaxation, (c) a highly viscous liquid close to  $T_g$  where additional, slow secondary relaxations emerge, and (d) the glassy state below  $T_g$ . In the glass, structural relaxation is absent and the susceptibility spectra are determined by the vibrational and secondary relaxational dynamics.

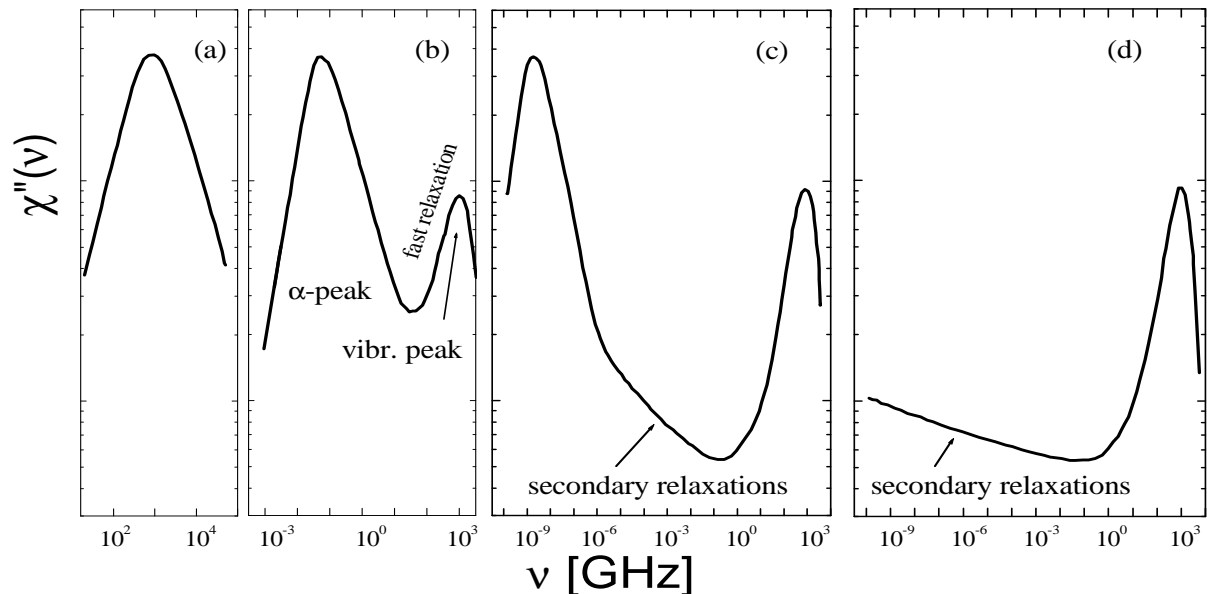


**Figure 1.1:** A schematic plot of the temperature evolution of the susceptibility spectra of simple molecular liquids upon passing from low-density fluid (a) to the glass (d).

As said before, the dynamics of the glass transition occur on the frequency scale from zero to say 1 THz. Great technical progress in instrumentations made it possible in recent years to measure the dielectric response of super-cooled liquids in the complete dynamic range associated with the glass transition phenomenon [13]. This was realized for a few glass formers by covering a frequency range of  $10^{-6}\text{Hz} < \nu < 10^{13}\text{Hz}$ . Spectra with high signal-to-noise ratio were compiled by depolarized light-scattering (DLS). Starting with the pioneering work of Cummins and co-workers [15], DLS spectroscopy in the GHz-THz range, made possible by the use of tandem Fabry-Perot interferometer [23], was applied to study supercooled liquids.

In contrast to that, the molecular dynamics in the glass, *i.e.*, below

---

$T_g$ , is less investigated. Since the main relaxation ( $\alpha$ -process) is frozen all persisting relaxational contributions are characterized by small amplitudes, and broad band spectra allowing for a systematic description down to cryogenic temperatures are rare. On the other hand, the anomalies of glasses at low temperatures attracted a lot of attention; however, most of the works focused on temperatures below say 4 K, and mainly inorganic network glasses were studied [25, 26, 27]. In order to describe the low-temperature anomalies of glasses, in particular the anomalous specific heat, the tunneling model was introduced which postulates the existence of certain defects that are described by asymmetric double well potentials (ADWP), and at low temperatures the barrier is crossed via tunneling [25].

There are many models invented in order to describe the glass transition phenomenon (cf. a review [3]). The most applied models are the Adam-Gibbs theory [4] and the free volume model [5]. These models do describe relaxation time but don't make clear experimental predictions for the dynamic susceptibility of the glass-formers. Understanding the dynamic susceptibility of glass formers as it evolves from high temperatures down to the glass transition temperature  $T_g$  is the main goal of the present investigations.

The model, aimed to describe the dynamics in glass-forming liquids is the Mode Coupling Theory (MCT) [7, 8, 9]. It is the most discussed theory of the glass transition at the moment. The MCT is a microscopic theory, which predicts a dynamical transition at some critical temperature  $T_c$ , which is turned out to be higher than the glass transition temperature  $T_g$ . MCT makes a number of quantitative predictions for the dynamic response in the glass transition region. The possibility to check these predictions experimentally makes the MCT very attractive for researchers of the glass transition phenomenon.

The present work is devoted to the experimental study of the dynamical response of the molecular glass formers by applying light-scattering technique, *i.e.* a tandem Fabry-Perot interferometer.

The results of this thesis are presented in Chapters 4-7. Every chapter is devoted to some special aspect of the dynamics in glasses. Thus, each chapter is self contained and follows at least in parts the corresponding publication (cf. List of publications).

# 2 Phenomenology of the dynamics in supercooled liquids and glasses

## 2.1 The correlation function.

For describing the dynamics of liquids on a microscopic level the fluctuations of the local density  $\delta\rho(\mathbf{r}, t) = \sum_{j=1}^N \delta(\mathbf{r} - \mathbf{r}_j(t))$  may be considered. In the reciprocal space  $\delta\rho(\mathbf{r}, t) = \sum_{j=1}^N \exp(i\mathbf{q}\mathbf{r}_j(t))$ . The normalized density-density correlation function

$$\phi_q(t) = \frac{S_q(t)}{S_q(0)} = \frac{\langle \delta\rho_q^*(t)\delta\rho_q(0) \rangle}{\langle \delta\rho_q^*(0)\delta\rho_q(0) \rangle}, \quad (2.1)$$

where the index  $q$  means the  $q$ th component of the Fourier transform,  $S_q(t)$  and  $S_q(0)$  are dynamic and static structure factors, respectively.  $N$  is the number of atoms.

The dynamics can be studied also in the frequency domain by investigating the dynamic susceptibility  $\chi_q''(\omega)$ :

$$\chi_q''(\omega) = \omega\phi_q''(\omega) \quad (2.2)$$
$$\phi_q''(\omega) = \int_0^\infty \phi_q(t)\cos(\omega t)dt$$

Experimentally these properties can be determined by neutron scattering that provides information on the translational dynamics on microscopic scales. There are however other variables pertaining to the structure of molecular liquids, notably the molecular orientations. It is the dynamics of the orientational degrees of freedom that is accessible experimentally, for example by light scattering or dielectric spectroscopy.



In the Maxwell theory of viscosity the correlation function of the structural relaxation ( $\alpha$ -relaxation) is described by the exponential function:

$$\phi_q(t) \propto \exp(-t/\tau_\alpha) \quad (2.3)$$

In the frequency domain this is a Lorentzian (Debye curve)

$$\phi_q''(\omega) \propto \Im[(1 - i\omega\tau_\alpha)]^{-1} \quad (2.4)$$

However, in real glass-forming liquids the  $\alpha$ -process correlation function, *i.e.*, the long-time decay of  $\phi(t)$  is generally found to be better described by a stretched-exponential, so-called Kohlrausch-Williams-Watts (KWW) function:

$$\phi_\alpha(t) \propto \exp[-(t/\tau_\alpha)^{\beta_{KWW}}], 0 < \beta_{KWW} < 1 \quad (2.5)$$

The average relaxation time of the  $\alpha$ -process is:

$$\langle \tau \rangle = \int_0^\infty \phi(t) dt = \frac{\tau}{\beta_{KWW}} \Gamma\left(\frac{1}{\beta_{KWW}}\right), \quad (2.6)$$

where  $\Gamma$  denotes the gamma function.

In the frequency domain one may also apply the so-called Cole-Davidson (CD) function [34]:

$$\phi_{CD}''(\omega) \propto \Im[(1 - i\omega\tau_{CD})]^{-\beta_{CD}}, 0 < \beta_{CD} < 1 \quad (2.7)$$

The average relaxation time of the  $\alpha$ -process in the Cole-Davidson approximation is:

$$\tau_\alpha = \int_0^\infty \phi(t) dt = \beta_{CD} \tau_{CD} \quad (2.8)$$

As new experimental techniques evolved and measurements were extended to shorter times (respectively higher frequencies), it was found that there is also some fast relaxation process present. These observations suggest that the relaxation function, normalized to  $\phi(0)=1$ , might be represented approximately by

$$\phi_q(t) = (1 - f)g(t) + f \exp[-(t/\tau_\alpha)^\beta] \quad (2.9)$$

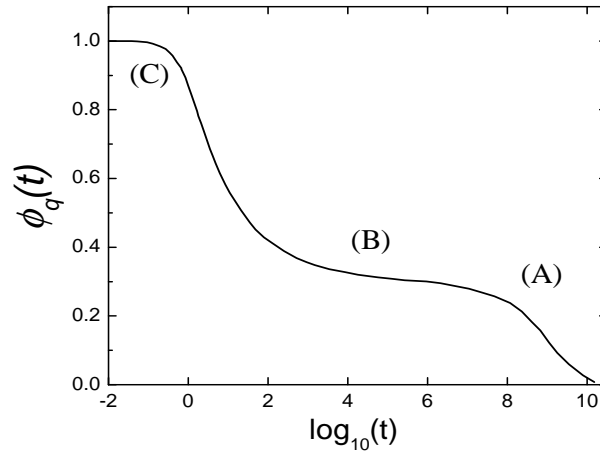


**Figure 2.1:** A schematic plot of  $\phi_q(t)$  versus  $\log(t)$  for a supercooled liquid; (A) the long-time  $\alpha$ -relaxation region; (C) the short-time (microscopic) region; (B) the intermediate region exhibiting two-step relaxation. This figure is adapted from [6].

where  $f$  is the relaxation strength of the  $\alpha$ -relaxation. A schematic version of  $\phi_q(t)$  is shown in Fig.2.1 where, on a logarithmic time scale the slow  $\alpha$ -relaxation as well as the fast relaxation can be seen.

In Fig. 2.2 the dielectric loss data of glycerol compiled by Lunkenheimer *et al.* [13] are shown. This data covers essentially the complete response

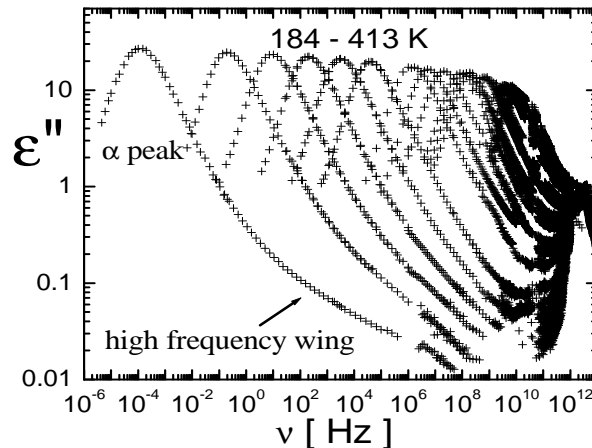


**Figure 2.2:** Dielectric loss data of glycerol [13]

of a glass former in the frequency domain. The  $\alpha$ -process leads to a strong loss peak (cf. Fig. 2.2) shifting to high frequencies with increasing temperature. This peak can be well described by the CD function. At

low temperatures, in addition to the  $\alpha$ -peak, another contribution, the so-called excess high frequency wing appears. Including that it is not sufficient to interpolate the glass dynamics spectra applying only the CD function. Up to now there is no commonly accepted microscopic model of the origin of the excess wing in glass-forming materials. At frequencies in GHz-THz range a minimum in  $\varepsilon''$  is present. At a few THz another peak shows up that can be identified with the microscopic band including the so called *boson peak*, which is also seen in the light-scattering spectra.

## 2.2 The Mode-Coupling theory.

In 1984, Bengtzelius, Götze and Sjölander [7] and Leutheusser [8] introduced a new theoretical approach (which is now called *Mode Coupling Theory* (MCT)), which leads to a dynamical singularity with characteristics distinctive for the liquid-glass transition.

### 2.2.1 Mode-Coupling theory equations.

The MCT is formulated in terms of the normalized density-density correlation function  $\phi_q(t)$  (cf. Eq. 2.1) and starts with an equation of motion for the  $\phi_q(t)$  (cf. Eq. 2.1) which can be derived from the Zwanzig-Mori formalism [9]:

$$\ddot{\phi}_q(t) + \Omega_q^2 \phi_q(t) + \int_0^t M_q(t-t') \dot{\phi}_q(t') dt' = 0 \quad (2.10)$$

with initial conditions  $\phi_q(0)=1$  and  $\dot{\phi}_q(0)=0$ .  $\Omega_q = qv/\sqrt{S_q}$  is the microscopic mode frequency,  $v$  is the thermal velocity of the liquid particles. The memory kernel  $M_q(t)$  splits into fast (regular) and slow fluctuating parts:  $\gamma_q \delta(t)$  and  $\Omega_q^2 m_q(t)$ , respectively. Equation 2.10 becomes

$$\ddot{\phi}_q(t) + \gamma_q \dot{\phi}_q(t) + \Omega_q^2 \phi_q(t) + \Omega_q^2 \int_0^t m_q(t-t') \dot{\phi}_q(t') dt' = 0 \quad (2.11)$$

The most important part of the idealized version of the MCT is the kernel  $m_q$ , which can be expressed in terms of the correlation function itself [9]:

$$m_q(t) = \frac{1}{2} \sum_{k,p} V(q, kp) \phi_k(t) \phi_p(t) \quad (2.12)$$

The vertices (or coupling constants)  $V(q, kp)$  represent the coefficients for the coupling of pair of density fluctuations to fluctuating forces. They are completely determined by the static structure factors  $S_q$ , and assumed to depend on external control parameters, *e.g.*, temperature  $T$  or density  $\rho$ .

An important quantity is the non-ergodicity parameter  $f_q(T)$  which describes the long-time behavior of  $\phi_q(T)$ , *i.e.*,  $\phi_q(t \rightarrow \infty) = f_q(T)$ . In its idealized version, MCT predicts a discontinuous change at a critical temperature  $T_c$ :

$$\begin{aligned} f_q(T) &= 0 & T > T_c \\ f_q(T) &> 0 & T < T_c \end{aligned} \quad (2.13)$$

Whereas the correlation function  $\phi_q(t)$  decays to zero in the liquid state, this is no longer the case below  $T_c$ , where the system becomes non-ergodic. In other words, the non-ergodicity parameter  $f_q(T)$  changes discontinuously, although structural changes remain continuous and smooth. This constitutes the paradigm of the glass transition as a dynamic phase transition, without diverging static susceptibilities.

The corresponding correlation functions are schematically shown for characteristic temperatures in Fig. 2.3. The critical temperature  $T_c$  marks the crossover from an ergodic state (liquid) to a non-ergodic state (glass). In the liquid state, a two-step process describes the decay of the correlation function (cf. Fig. 2.3), where  $f_q$  is the fraction relaxed by the slow process ( $\alpha$ -process) and  $1 - f_q$  the part decaying due to the fast dynamics. As at long times the correlation function actually always decays to zero at  $T > T_g$  an "effective Debye-Waller factor" is defined which presents the amplitude of the  $\alpha$ -process and this is what is meant by non-ergodicity parameter  $f_q$  in the following.

The two-step density correlation functions emerging from the idealized theory exhibit characteristic power-law decays towards and from the

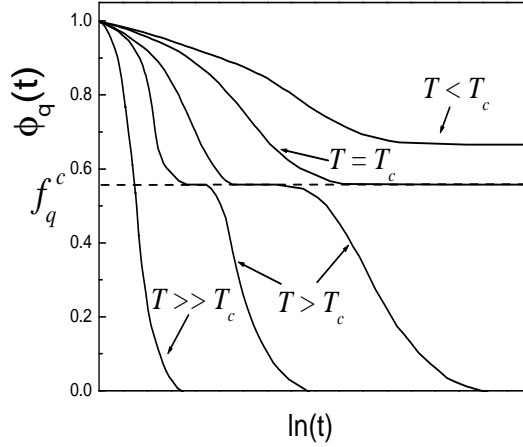


**Figure 2.3:** Correlation functions at different temperatures with respect to the critical temperature  $T_c$ . From a one-step function, a two-step function emerges while cooling; the plateau characterized denoted by  $f_q^c$  is the relaxation strength of the  $\alpha$ -process.

plateau. Their experimental identification and analysis allow to determine the crossover temperature  $T_c$ . The two power-law exponents are not independent but depend on a single parameter, the so-called critical exponent  $\lambda$ , which is specific for a given interaction potential, *i.e.*, hard spheres. As an example, Fig. 2.4 shows susceptibility spectra of the hard sphere system at a particular  $q$ . The packing fraction  $\varphi$  is used as a parameter. Above the critical packing fraction  $\varphi_c$  ( $\varepsilon > 0$ ), which corresponds to  $T < T_c$ , the  $\alpha$ -process is absent (frozen) and only the fast dynamics is present. At  $\varphi < \varphi_c$  the  $\alpha$ -peak and the corresponding susceptibility minimum shift to lower frequencies with increasing  $\varphi$ , so that the closer  $\varphi$  is to the critical value  $\varphi_c$ , the better the critical decay of the fast dynamics can be identified (curve *c* in Fig. 2.4).

The main predictions of MCT are: relaxation occurs in two steps and a dynamic transition happens at some temperature  $T_c$ , the slow relaxation is frozen below  $T_c$  and only the fast relaxation remains. Qualitatively MCT predicts that at short time scale atoms move in a cage created by their neighbors. This is the fast relaxation. The motion is restricted by the cage and fluctuations do not relax to zero. At longer times the particle can escape from the cage due to motions of the neighboring atoms. This is the slow relaxation. In this case fluctuations relax to zero. At some critical temperature  $T_c$  the atom becomes arrested in the cage. This corresponds

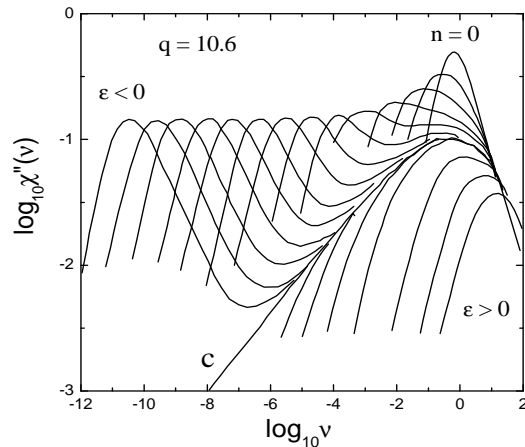


**Figure 2.4:** Solutions of idealized MCT for the hard sphere system.  $\varepsilon = (\varphi - \varphi_c)/\varphi_c$  measures the departure of the packing fraction  $\varphi$  from the critical value  $\varphi_c$ . The solid line marked  $c$  represents the critical spectrum  $\varphi_c$  (taken from [6]).

to a transition from a liquid-like to a solid-like dynamics.

## 2.2.2 The asymptotic scaling laws of MCT

Close to the crossover temperature  $T_c$  the solution of the idealized MCT equations can be expanded around the non-ergodicity parameter  $f_q^c$  at  $T_c$  and some generic laws can be derived. These results establish, so-called asymptotic laws of MCT, which can be regarded as generic features of the MCT dynamics at  $T > T_c$ .

The asymptotic scaling laws of MCT describe the crossover from the fast relaxation to the onset of the slow relaxation, that is a power-law decay of  $\phi(t)$  towards the plateau with an exponent  $a_{mct}$ , and another power-law decay away from the plateau with an exponent  $b_{mct}$ :

$$\begin{aligned} \phi_q(t) &= f_q^c + |\sigma|^{1/2} h(t/t_\sigma)^{-a_{mct}} & t_0 < t \leq \tau_\sigma \\ \phi_q(t) &= f_q^c - |\sigma|^{1/2} hB(t/t_\sigma)^{b_{mct}} & t_\sigma < t < \tau_\alpha \quad B > 0 \end{aligned} \quad (2.14)$$

where  $f_q^c$  is the temperature independent non-ergodicity parameter,  $h$  a temperature independent amplitude and  $t_\sigma = t_0/|\sigma|^{1/(2a_{mct})}$  a rescaling time determined by the some microscopic time  $t_0$ . The temperature enters via  $\sigma = (T_c - T)/T_c$ . The exponents  $a_{mct}$  and  $b_{mct}$  are not independent.

They are connected by the, critical exponent  $\lambda$  via the transcendental equation involving the gamma function

$$\lambda = \frac{\Gamma^2(1 - a_{mct})}{\Gamma(1 - 2a_{mct})} = \frac{\Gamma^2(1 + b_{mct})}{\Gamma(1 + 2b_{mct})} \quad (2.15)$$

The spectra shown on Fig. 2.4 can be interpolated by simple analytical expressions, which can be applied to test MCT by experiments. As an example, the susceptibility spectra versus frequency at different temperatures are shown qualitatively in Fig. 2.5. Note that it is on a log-log scale. In the low-frequency part of the spectrum a peak, which moves to the lower frequencies with decreasing temperature. This peak corresponds to the slow  $\alpha$ -process. At high frequencies the fast relaxation is seen. For temperatures  $T > T_c$  MCT predicts that the fast process is temperature independent.

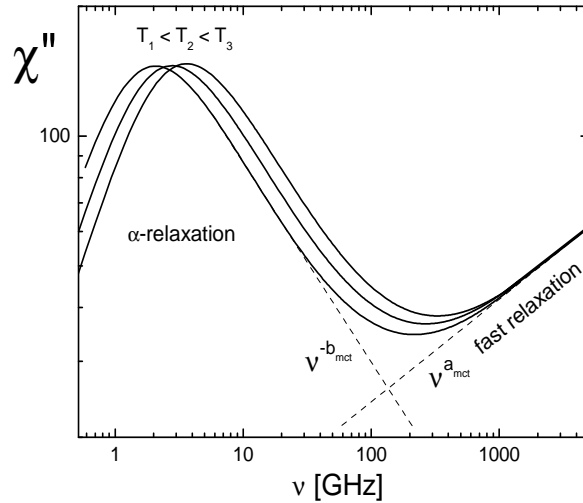


**Figure 2.5:** MCT scenario for high temperatures  $T > T_c$ .

Because of the interplay of the  $\alpha$ -process and the fast relaxation there is a minimum in the susceptibility spectrum (cf. Fig. 2.5) which can be interpolated in first approximation at  $T > T_c$  by two power-laws [9]

$$\chi''(\nu) = \chi''_{\min} \left[ \frac{b_{mct} (\nu/\nu_{\min})^{a_{mct}} + a_{mct} (\nu/\nu_{\min})^{-b_{mct}}}{a_{mct} + b_{mct}} \right], \quad (2.16)$$

where  $\nu_{\min}$  and  $\chi''_{\min}$  are the frequency and the amplitude of the minimum, respectively. The exponents  $a_{mct}$  and  $b_{mct}$  describe the low-frequency behavior of the fast dynamics and the high-frequency part of the  $\alpha$ -process, respectively; they are connected by the parameter  $\lambda$  (cf. Eq. 2.15). The temperature dependence of  $\nu_{\min}$  and  $\chi''_{\min}$  at temperatures  $T > T_c$  are described by

$$\begin{aligned}\chi''_{\min} &\propto (T - T_c)^{1/2} \\ \nu_{\min} &\propto (T - T_c)^{1/2a_{mct}}\end{aligned}\tag{2.17}$$

The time scale of the  $\alpha$ -process (relaxation time)  $\tau_\alpha$  obeys another power-law,

$$\tau_\alpha \propto \frac{\eta}{T} \propto (T - T_c)^{-\gamma_{mct}},\tag{2.18}$$

where  $\eta$  is a viscosity. The exponent  $\gamma_{mct}$  is related to the exponents  $a_{mct}$  and  $b_{mct}$  via

$$\gamma_{mct} = \frac{1}{2a_{mct}} + \frac{1}{2b_{mct}}.\tag{2.19}$$

Applying Eqs. 2.17, 2.18, 2.19, a further relation can be derived

$$\chi''_{\min} \propto (\nu_{\min}\tau_\alpha)^{-b_{mct}}.\tag{2.20}$$

From Eq. 2.16 it follows that rescaling the susceptibility spectra  $\chi''_{\min}$  measured for different temperatures by  $\chi''_{\min}$  and  $\nu_{\min}$  leads to a master curve. The exponents  $a_{mct}$  and  $b_{mct}$  can be extracted from this master curve using Eq. 2.16. The crossover temperature  $T_c$  can be determined graphically, by using linearized plots of the experimental  $\chi''_{\min}$ ,  $\nu_{\min}$  and  $\tau_\alpha$  temperature dependencies.  $T_c$  marks the end of the high temperature regime of MCT.

Below  $T_c$  the fast relaxation spectrum changes its shape. A crossover from a power-law with an exponent  $a = a_{mct}$  to a white noise spectrum ( $a = 1$ ) at low frequencies is expected. As a consequence of the appearance of this "knee" at  $T_c$  and its shifting up in frequency with decreasing the temperature, the strength of the fast relaxation, *i.e.*, its integrated spectral density, decreases upon cooling. This is further reflected in the characteristic temperature dependence, or an anomaly, of the non-ergodicity



parameter  $f$ , since  $f$  is the strength of  $\alpha$ -relaxation, and therefore  $1 - f$  equals the strength of the fast relaxation. Specifically,

$$\begin{aligned} f(T) &= f_c & T > T_c \\ f(T) &= f_c + h(T_c - T)^{1/2} & T < T_c, \end{aligned} \quad (2.21)$$

This is, so-called square-root cusp singularity in  $f(T)$ . Correspondingly,  $1 - f$  specifies the relaxation strength of the fast relaxation and is given by the integral over the susceptibility of the fast relaxation  $\chi''_{fast}$ :

$$1 - f \propto \int_0^\infty \chi''_{fast} d \ln \nu. \quad (2.22)$$

The asymptotic laws are expected to hold when the liquid approaches the critical temperature  $T_c$  from above. Below  $T_c$  the theory is far from complete.

## 2.3 Models of fast dynamics in glasses ( $T < T_g$ ).

Below the glass transition temperature  $T_g$  the  $\alpha$ -process is frozen and only so-called secondary relaxation processes survive.

Fast dynamics in glasses consists of relaxational and vibrational contributions. The former shows up in the LS spectra as a quasi-elastic contribution. Recently, the quasi-elastic LS (QELS) in two inorganic glasses (silica and CKN) was described by the asymmetric double-well potential (ADWP) model [81, 82, 83]. We apply this model for interpreting the QELS spectra of molecular glasses too. The model assumes that the main mechanism of relaxation is a jump process of groups of atoms from one configuration to another in an ADWP with potential barrier heights  $V$  and asymmetry  $\Delta$ . Theodorakopolous and Jäckle considered the relaxation in symmetric double well potentials [76]. The model was generalized by Gilroy and Phillips (GP) [78] and Jäckle [79]. In this model the dynamic susceptibility is expressed via the parameters of the ADWPs by the following equation:

$$\chi''(\nu) = \frac{A}{T} \int_0^{\infty} \int_0^{\infty} \frac{2\pi\nu\tau(\Delta, T)}{1 + (2\pi\nu\tau(\Delta, T))^2} \operatorname{sech}^2\left(\frac{\Delta}{2T}\right) f(\Delta) g(V) d\Delta dV, \quad (2.23)$$

where  $A$  is a constant determined by the specific experiment,  $g(V)$  is the distribution of barrier heights  $V$ ,  $f(\Delta)$  is the distribution of the asymmetry parameter  $\Delta$ . The relaxation time  $\tau(\Delta, T)$  is determined by a thermally activated process,  $\tau(\Delta, T) = \tau_0 \exp(V/T) \operatorname{sech}(\Delta/2T)$  where  $\tau_0 \sim 10^{-12} - 10^{-13}$  sec is a typical molecular attempt time. Eq. 2.23 describes both LS and acoustic attenuation data,  $Q^{-1}(\nu)$  (internal friction) [78], *i.e.*,  $\chi''(\nu) \propto Q^{-1}(\nu)$  is expected to hold.

If the thermal energy is high enough with respect to the asymmetry parameter  $\Delta$ , *i.e.*,  $\Delta < 2T$ , and the distribution function of  $f(\Delta)$  is flat,  $f(\Delta) = f_0$ , Eq. 2.23 reduces to [78]:

$$\chi''(\nu) = 2Af_0 \int_0^{\infty} \frac{2\pi\nu\tau}{1 + (2\pi\nu\tau)^2} g(V) d(V), \quad (2.24)$$

where now  $\tau = \tau_0 \exp(V/T)$ . Expression Eq. 2.24 is similar to the corresponding result of the symmetric double-well potential model. Note, however, the absence of the factor  $T$  in the denominator of Eq. 2.24 in comparison with Eq. 2.23; this is a consequence of the effective cut-off of the integration over  $\Delta$  by the factor  $T$  and is an important difference between the ADWP model and symmetric double-well potential model. We mention that an equation of the form of Eq. 2.24 can formally be used for any temperature activated processes, such as the much slower Johari-Goldstein  $\beta$ -process [47, 48, 49]. The absence of a temperature-dependent pre-factor is, however, specific to the GP model. Gilroy and Phillips assumed an exponential distribution  $g(V) = V_0^{-1} \exp(-V/V_0)$ . With this  $g(V)$  one finds from Eq. 2.24:

$$\chi''(\nu) = 2Af_0\alpha(2\pi\nu\tau_0)^\alpha \int_{2\pi\nu\tau_0}^{\infty} \frac{x^{-\alpha} dx}{1 + x^2}, \quad (2.25)$$

where  $x=2\pi\nu\tau$  and  $\alpha = T/V_0$ . Equation 2.25 describes the susceptibility  $\chi''(\nu)$  as an asymmetric peak. The peak is similar to a Cole-Davidson one, but with low-frequency and high-frequency wings interchanged, *i.e.*, the high-frequency wing of  $\chi''(\nu)$  exhibits a Debye behavior,  $\chi''(\nu) = B/\nu$ , with  $B = f_0 A \alpha / 2(\alpha + 1)$ , while the low-frequency wing ( $\nu \ll 1/2\pi\tau_0$ ) at  $T \ll V_0$  is described by a power-law with the exponent equal to  $\alpha$ :

$$\chi''(\nu) = \pi f_0 A \alpha (2\pi\nu\tau_0)^\alpha. \quad (2.26)$$

As in the GP model there is no low-energy cut-off in  $g(V)$ , no relaxation peak shifting with temperature is expected. Instead, the relaxation peak overlaps with the vibration band. It was shown that the same result can be obtained in the soft-potential (SP) model under the additional assumption that the distribution of force constants has a Gaussian cut-off [77].

As said, the power-law spectrum 2.26 was observed in some inorganic glasses and also polystyrene [81, 82] and indeed an exponential distribution  $g(V)$  was confirmed in fair approximation. Within the ADWP model, the integral of the spectral density  $\chi''(\nu)/\nu$  over frequency does not depend on temperature, which results from the assumption  $f(\Delta) = f_0$  (see above). Specifically, for any  $g(V)$  one has

$$S_{ADWP} = \int_{fast} \chi''(\nu) \frac{d\nu}{\nu} = \pi f_0 A. \quad (2.27)$$

Thus, a power-law wing with an exponent proportional to temperature, Eq. 2.26, and a temperature-independent integrated spectral density are predictions of the GP model of fast relaxation. The anharmonicity of vibrations is also considered to be a source of QELS [111]. The so-called anharmonic model predicts a power-law wing of the relaxation spectrum with a temperature independent exponent. Contrary to the ADWP model, the anharmonic contribution  $S_{anh}$  increases with temperature,  $S_{anh} \propto T$ . Thus, the two models give different predictions that can be compared to experimental data.

At higher frequencies, say 100 - 500 GHz, the relaxation spectrum eventually merges with the vibrational band (boson peak). In order to separate vibrational and relaxational contributions, one needs to know the

frequency dependence of the vibrational spectrum. In glasses the spectral density in the THz region is dominated by the boson peak that reflects the excess density of vibrational states over the Debye density of states. At elevated temperatures, its low-frequency wing is partially covered by the fast relaxation spectrum. The SP model [77] predicts that the low-frequency wing of the boson peak density of states is described by a power-law,  $g(\nu) \propto \nu^h$ , where  $h = 4$ . The Debye density of states corresponds to  $g(\nu) \propto \nu^3$ . Experimentally, the low-temperature LS spectra [81, 82] where the relaxation contribution is negligible, give a power-law behavior with an intermediate value of the exponent  $h$ . This exponent can be connected to that of the vibrational susceptibility  $\chi''_{vib}(\nu)$ . According to Shuker and Gammon [80], the LS intensity in glasses at frequencies where the vibration coherence length is shorter than the optical wavelength, in particular, in the region of the boson peak, can be expressed as

$$\chi''_{vib}(\nu) = C(\nu)g(\nu)/\nu, \quad (2.28)$$

where  $C(\nu)$  is the light-to-vibration coupling constant. It is known that at the low-frequency side of the boson peak, *i.e.*, between the region where the fast relaxation dominates and the maximum of the boson peak,  $C(\nu) \propto \nu$  [84]. Thus, in this frequency range  $\chi''_{vib}(\nu) \propto g(\nu)$ . Finally, we note that at lowest frequencies (a few GHz) a nearly constant loss spectrum was observed in some glasses by LS [89]. This NCL spectrum was described by a power-law with a small negative exponent  $\sim -0.1$  and shows some similarity to what was found in the dielectric spectra of glasses covering several decades though at lower frequencies [13, 47, 49, 63, 65]. Its temperature dependence is described by an exponential factor similar to that of Debye-Waller. The nature of this contribution is yet unknown.

# 3 Light scattering experiment

## 3.1 Introduction

The light-scattering (LS) technique is a powerful experimental method, which is intensively used for studying the dynamics in supercooled liquids.

In Fig. 3.1 a scheme of the LS experiment is shown. The photon with frequency  $\nu_0$  and wave vector  $\vec{k}_0$  passes through the investigated matter. Due to interactions with atoms of the investigated substance the incident light is scattered, *i.e.*, the photon changes its frequency and wave vector to  $\nu_s$  and  $\vec{k}_s$ , respectively (cf. Fig. 3.1).

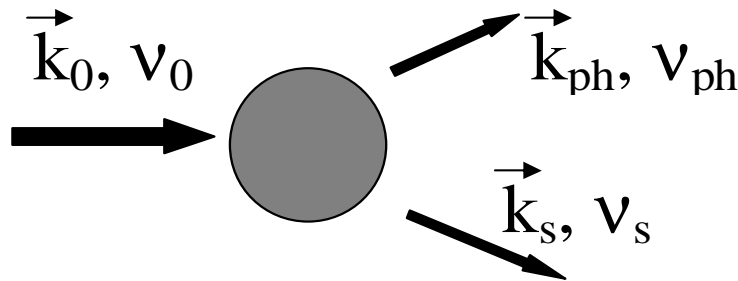


**Figure 3.1:** Schematic picture of the light scattering.

The scattering process is accompanied by creating (or annihilation) an excitation (phonon) of energy  $h\nu_{ph}$  and momentum  $h\vec{k}_{ph}$  in the scattered medium. From the conservation of energy and momentum [11]:

$$\begin{aligned}\vec{k}_s &= \vec{k}_0 - \vec{k}_{ph} \\ \nu_s &= \nu_0 - \nu_{ph}\end{aligned}\tag{3.1}$$

In the case of light scattering on localized vibrations or relaxational excitations in disordered media the momentum conservation rule (first equation

### 3 Light scattering experiment

---

in Eq. 3.1) is not applicable. The LS feels the fluctuations  $\delta\varepsilon$  of the dielectric tensors  $\varepsilon$ , which is connected with the dielectric susceptibility  $\chi$  by  $\varepsilon = 1 + \chi$ ,  $\delta\varepsilon(\mathbf{q}, t) \equiv \delta\chi(\mathbf{q}, t)$ . Dynamic susceptibility has real and imaginary parts:  $\chi(\mathbf{q}, \nu) = \chi'(\mathbf{q}, \nu) + i\chi''(\mathbf{q}, \nu)$

The spectral density of the light scattering is [11]

$$S_{LS}(\mathbf{q}, \nu) = \frac{I_0 k_f^4}{16\pi^2 R^2 \varepsilon_0^2} \frac{1}{2\pi} \int_{-\infty}^{\infty} e^{-i\nu t} \langle \delta\chi_{if}^*(\mathbf{q}, t) \delta\chi_{if}(\mathbf{q}, 0) \rangle dt \quad (3.2)$$

The imaginary part of the dynamic susceptibility is connected to the spectral density by an equation [11]:

$$\chi''(\mathbf{q}, \nu) = \frac{1}{2\hbar} [1 - e^{-\frac{\hbar\nu}{k_B T}}] \cdot S_{LS}(\mathbf{q}, \nu) = \frac{1}{2\hbar} \frac{S_{LS}(\mathbf{q}, \nu)}{[n(\nu) + 1]} \quad (3.3)$$

where  $n$  is the Bose factor

$$n(\nu) = \frac{1}{e^{\frac{\hbar\nu}{k_B T}} - 1} \quad (3.4)$$

It is convenient to present LS data in the form of LS susceptibility  $\chi''(\nu)$ .

Generally, scattering of electromagnetic radiation at optical frequencies (light scattering) occurs through the secondary emission of electromagnetic radiation from a fluctuating electronic polarization induced by the excitation field. It reflects therefore fluctuations of the electronic polarizability tensor that occur due to fluctuations of the molecular positions and orientations. Compared to the dielectric spectroscopy, it involves a second rank tensor property (electronic polarizability) rather than the electric polarization vector. The two main sources of the fluctuating polarizability are rotations of anisotropic molecules that modulate the off-diagonal elements of the tensor, and fluctuations of the particle density that contribute to its diagonal (isotropic) part. In addition, one has to consider the so-called "interaction induced" mechanisms of second order, generally weak scattering, whereby the polarizability of a molecule is influenced by nearby molecules due to *e.g.* molecular collisions or dipole-dipole interactions. The anisotropic scattering, by its mechanism, is thus comparable with the dielectric absorption in non-ionic molecular liquids, which pre-

dominantly occurs due to rotating molecular dipoles. The isotropic scattering, on the contrary, has no direct counterpart in the dielectric spectroscopy, except for relatively weak interaction induced effects. Isotropic and anisotropic parts of the scattered field can be separated experimentally owing to their different polarization properties. Isotropic scattering always occurs with the same polarization as the (linearly polarized) excitation field, while the anisotropically scattered field has components in all polarizations. Choosing therefore the orthogonal, so-called depolarized scattering component, one excludes isotropic scattering off the density fluctuations. Selecting furthermore the back-scattered radiation, one also excludes scattering from shear waves, which is then forbidden by symmetry. Otherwise, transverse waves give rise to a relatively weak anisotropic scattering through orientation-to-shear coupling. The resulting scattering geometry is commonly referred to as "depolarized back scattering".

The momentum  $\mathbf{q}$  of the excitations that are probed in LS experiments is of the order  $2\pi/\lambda$ . Since optical wavelength  $\lambda$  is much longer than the intermolecular distances and since there are no conceivable intermolecular interactions that could lead to orientational correlations between different molecules on such long length scales, depolarized light scattering is essentially  $\mathbf{q}$ -independent, which is commonly referred to as the  $\mathbf{q} = 0$  limit. In this respect, too, it is comparable with the dielectric spectroscopy, which also operates in the  $\mathbf{q} = 0$  limit. Of course, light scattered in any other geometry than the depolarized backscattering will include coherent, momentum-allowed contributions from long-wavelength shear and/or longitudinal waves, which naturally are  $\mathbf{q}$ -dependent.

## 3.2 Experimental setup

For investigation of the relaxation processes in the glass-forming liquids, polymers and glasses by dynamic LS it is necessary to be able to measure the scattered light at frequencies lower than 1 THz ( $30\text{ cm}^{-1}$ ). Normally with Raman spectrometers it is possible to measure the spectra down till tens of GHz [19]. In order to get more information about relaxation processes, especially about  $\alpha$ -relaxation, it is desirable to extend the frequency range to lower frequencies. Usually in this frequency range a

Fabry-Perot-Interferometer (FPI) is used. With the FPI one is able to get spectra down to 0.1 GHz with spectral resolution about 10-100 MHz [22]. The main problem with using FPI is that it has limited *free spectral range* (*FSR*). Only within the *FSR* one can interpret the measured data unambiguously. This is not a problem to measure the position and the width of a narrow Brillouin line, but overlapping of the transmission orders makes the measurements in a frequency range, which is broader than *FSR*, impossible. Another problem is a relatively low contrast  $\sim 10^2$  of the FPI. With such low contrast it is very difficult to measure Brillouin spectra when the elastic scattering from the sample is high, because in this case it is impossible to distinguish the spectrum from the elastic contribution. It is possible to solve these problems by creating a multi-pass tandem of interferometers Fabry-Perot [22]. At the moment the best known spectrometer based on the multi-pass tandem of two interferometers Fabry-Perot was innovated by J.R. Sandercock and produced by *JRS Scientific Instruments* [23, 24]. Using a Sandercock tandem Fabry-Perot interferometer (TFPI) one can measure the spectrum in the frequency range 0.3 GHz-1500 GHz. Because of the very good technical characteristics, high stability, convenience in alignment and measurement TFPI became very popular in Brillouin spectroscopy. The group of H.Z. Cummins was the first who used the TFPI for measurements of the quasi-elastic light scattering spectra of the supercooled glass-forming liquids [14, 15]. Spectra extending over more than four decades in frequency became accessible when the TFPI combined with a double monochromator. Their works have stimulated other researching groups to use TFPI for the experimental investigation of the glass-forming substances.

#### 3.2.1 Tandem Fabry-Perot interferometer

The TFPI is a very useful tool in the high resolution spectroscopy where a resolution on the order of MHz to GHz is required, *e.g.*, in a Brillouin spectroscopy. A standard plane FPI consists of two plane mirrors mounted accurately parallel to one another. For a given spacing  $L$  between mirrors the interferometer will transmit only certain wavelength  $\lambda$  as determined



by the transmission function of a single Fabry-Perot etalon [22]

$$I_t = \frac{I_0}{1 + \frac{4F^2}{\pi^2} \sin^2\left(\frac{2\pi nL}{\lambda}\right)} \quad (3.5)$$

where  $F$  is the *finesse* of the etalon, which characterizes the quality of the mirror reflectivity and flatness and  $n$  is the refractive index of the medium between the plates. From Eq. 3.5 it follows that only the wavelengths which satisfy

$$nL = \frac{1}{2}p\lambda \quad (3.6)$$

for integral values of  $p$ , will be transmitted. The finesse  $F$  is related to the spacing between the successive transmitted wavelengths  $\Delta\lambda$  (free spectral range,  $FSR$ ) and the width of a transmission peak by  $F = \Delta\lambda / \delta\lambda$  (cf. Fig.3.2).

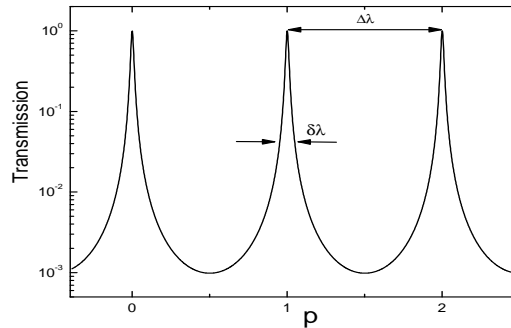


**Figure 3.2:** Transmission of the interferometer Fabry-Perot.

The FPI can be used as a spectrometer by varying the spacing  $L$  so as to scan the light intensity at different wavelengths. However, it is immediately apparent that the measured intensity at a given spacing is the sum of the intensities at all wavelengths satisfying condition of Eq. 3.6. An unambiguous interpretation of the spectrum is thus impossible unless it is known *a priori* that the spectrum of the light lies entirely within a wavelength spread  $\Delta\lambda = \lambda^2 / 2L$  [22]. For a given  $L$  the  $FSR$  can be expressed in a frequency range [22] as:

$$\delta\nu = \frac{c}{2nL} \quad (3.7)$$

### 3 Light scattering experiment

where  $c$  is the speed of light.

In order to increase the measurable frequency range a combination of two FPIs with slightly different spacings can be used. In the Sandercock tandem Fabry-Perot interferometer there are two FPIs with spacings  $L_1$  and  $L_2 = 0.95L_1$ . They are mounted in the same platform in such a way that their spacings can be changed simultaneously during scanning keeping the ratio  $L_1/L_2 = \text{const.}$  (cf. Fig. 3.3).

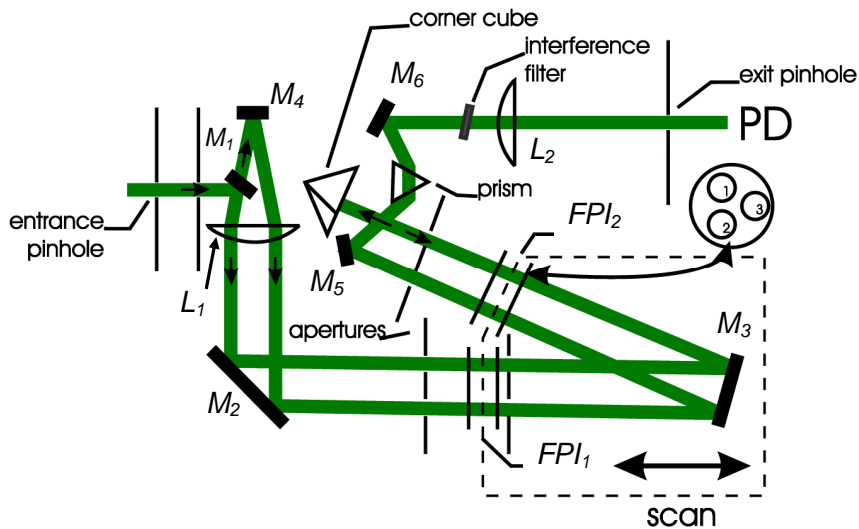


Figure 3.3: Tandem Fabry-Perot interferometer.

The scattered light enters the spectrometer at an adjustable entrance pinhole. The mirror  $M_1$  reflects the light towards the lens  $L_1$  where it is collimated and directed via the mirror  $M_2$  and through aperture 1 to  $FP_1$ . Then the light is directed via mirror  $M_3$  to  $FP_2$ .

After transmission of  $FP_2$  the light strikes the corner cube where it is reflected downwards and returned parallel to itself towards to  $FP_2$ . It continuous through the aperture 2 to  $FP_1$ . After transmission through  $FP_1$  it passes through lens  $L_1$ , underneath mirror  $M_1$ , and is again collimated and directed through  $FP_1$ .

After the final pass through the interferometers, through the aperture 3, the light strikes the mirror  $M_5$ , where it directed to the prism  $PR_1$ . This prism, in combination with the lens  $L_2$  and the output pinhole  $P_2$ , forms a bandpass filter with a width determined by the size of the pinhole.

The mirror  $M_6$  sends the light to the output pinhole.

The scattered light passes three times through this system and the transmission function of the TFPI is

$$I_t = I_0 \left[ 1 + \frac{4F^2}{\pi^2} \sin^2\left(\frac{\pi\nu}{\delta\nu}\right) \right]^{-3} \left[ 1 + \frac{4F^2}{\pi^2} \sin^2\left(0.95\frac{\pi\nu}{\delta\nu}\right) \right]^{-3} \quad (3.8)$$

Note that  $\nu$  is a Brillouin shift from the elastic light. The transmission function 3.8 is shown on a Fig.3.4

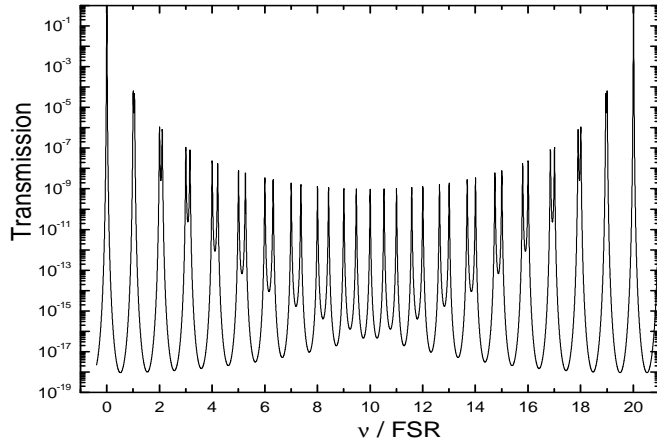


Figure 3.4: Transmission of the TFPI.

It is seen that all transmission orders up to the 20th are suppressed and instead of them so called "ghosts" peaks in the LS spectra are present (cf. [24]). The magnitude of these "ghosts" is by a factor of  $10^3$ - $10^7$  smaller than magnitude of transmitted elastic light. In order to suppress the high orders of the light transmitted through the interferometer an interference filter was used. The necessity of using the interference filter was widely discussed in [20, 21].

### 3.2.2 Light scattering setup

The experimental setup consists of the  $Ar^+$ - laser (*Coherent Radiation*), optical helium cryostat (*Cryovac*), Sandercock TFPI (*JRS Scientific Instruments*) and optical elements, which are necessary for performing the light-scattering experiment. The whole system is mounted on an optical table. In the Fig. 3.5 the complete experimental setup is shown.

### 3 Light scattering experiment

---

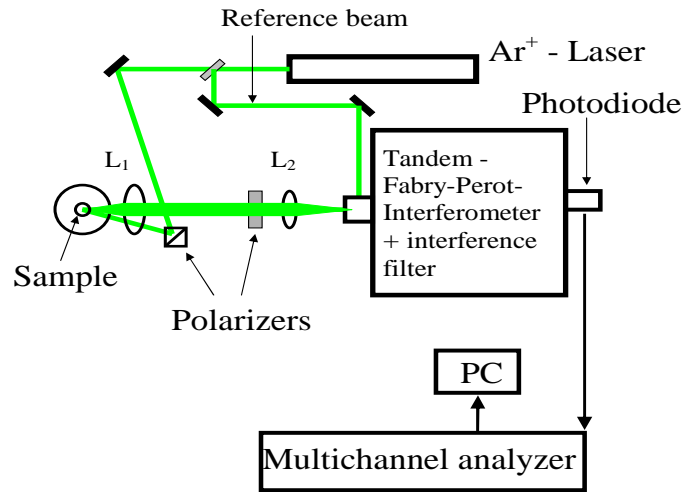


**Figure 3.5:** The experimental setup.

Lens  $L_1$  focuses the incident laser beam onto the sample placed inside of the optical helium cryostat. As well as focusing the incident light to approximately  $30\mu\text{m}$  in diameter the lens  $L_1$  collects the light scattered from the sample and collimates it into a beam up to 10 mm in diameter. Lens  $L_2$  focuses this parallel beam onto the entrance pinhole of the TFPI. In order to subtract or transmit vertically polarized component of the scattered light (depolarized and polarized experiment, respectively), there is a Si polarizer placed between  $L_1$  and  $L_2$ . By rotating this polarizer it is possible to carry out depolarized or polarized light-scattering experiment. Detecting of measured light is performed by a Si photodiode.

## 4 Light scattering in 2 - picoline and m-tricresyl phosphate

This chapter is dedicated to the experimental study of two molecular glass-former liquids, namely 2-picoline and m-tricresyl phosphate. One of the goals of this study is trying to verify the qualitative MCT predictions, which are discussed in Chapter 2.2.2.

### 4.1 Experimental check of the MCT predictions.

The MCT motivated many experimental works which appeared in the last years (cf. *e.g.* [15, 19, 29, 41, 42]). First experimental attempts to check the MCT predictions were done in the group of H.Z. Cummins [14, 15]. They measured many substances applying the LS technique. For instance, they reported in [15] their results of study the liquid-glass transition of  $Ca_{0.4}K_{0.6}(NO_3)_{1.4}$ . They measured LS spectra using a tandem Fabry-Perrot interferometer and a double monochromator. Analyzing the data they found a good agreement with the scaling law predictions of the MCT.

In ref [19] Rössler and coworkers studied by LS spectroscopy a number of glass-forming liquids:  $B_2O_3$ , glycerol, m-tricresyl phosphate (m-TCP), and  $K_3Ca_2(NO_3)_7$  (CKN) again in order to check applicability of the scaling laws predicted by MCT. A qualitative agreement for CKN, m-TCP and glycerol was found. However, the predicted relation between the exponents  $a_{mct}$  and  $b_{mct}$  was not always reproduced. The largest deviations were found for glycerol. In the case of  $B_2O_3$  no minimum in the susceptibility spectra was observed up to 1000 K. Thus, no test of MCT was possible.

The hydrogen bonded glass-forming liquid glycerol was also experimentally investigated by incoherent neutron and depolarized LS [29] as well as using dielectric spectroscopy [41] in the same frequency range. The neutron and depolarized LS data show qualitatively similar spectra. The authors applied an analysis of the data in the frame of MCT. A large difference between  $T_c$  extracted from the susceptibility spectra and  $T_c$  obtained from the viscosity data [30] was found. In the first case  $T_c = 225$  K, in the second  $T_c = 305$  K. In [41] the dielectric data of glycerol in very broad frequency range ( $10^{-6} - 10^{12}$  Hz) were measured. The authors have analyzed the dielectric loss spectra  $\varepsilon''(\nu)$ . They found out, that the observed spectral minimum can not be described according to the MCT predictions and an additional temperature dependent constant loss contribution has to be assumed for it. The critical temperature  $T_c$  was extracted from the measured data using the scaling laws for the spectral minima predicted by MCT.  $T_c$  was found about 262 K. One can see, that MCT works satisfactory on a qualitative level, but there are quantitative discrepancies.

The authors conclude, that although the frequency and temperature dependencies of the measured data are in a rather good agreement with the MCT predictions, the existent deviations from the MCT predictions do not allow to say surely that MCT predictions are valid in the case of glycerol.

So, one can see that in glycerol MCT works satisfactory on a qualitative level, although some quantitative discrepancies were found. These works demonstrate that MCT describes quite correctly the dynamics of investigated liquids for temperatures above  $T_c$ . However, for temperatures below  $T_c$  the MCT does not work well, for example, a predicted by MCT spectral feature called "knee" was not observed experimentally (cf. [17, 20, 21]). This fact should be a good motivation for researchers to find a new approach for describing the dynamics below  $T_c$ . Such attempt was done in [17] where a phenomenological approach for describing the light scattering data of toluene was suggested. This approach allows to single out the fast dynamics spectral contribution and to determine the non-ergodicity parameter  $f$ . Moreover, an anomaly of the Debye-Waller factor near the temperature close to  $T_c$  was observed. Such anomaly is predicted by MCT [17]. This fact also demonstrates that a dynamic sin-

gularity predicted by MCT can be analyzed also beyond a frame of MCT. Unfortunately, toluene has a strong tendency to crystallize, that is why there are no experimental data between 128 K and 148 K. This gap in the data does not allow to make a clear conclusion about the glassy dynamics below  $T_c$ .

## 4.2 Light - scattering spectra

Light - scattering (LS) spectra of 2-picoline and m-tricresyl phosphate (m-TCP) are measured using a Sandercock Tandem Fabry - Perot - Interferometer (TFPI) and an  $\text{Ar}^+$  laser at a wavelength 514.5 nm with a power of 1W. The depolarized light - scattering experiments (cf. chapter 3) were performed at  $\sim 170^\circ$  (backscattering geometry). Three different Free Spectral Ranges (FSRs): 15 GHz, 150 GHz and 750 GHz) were measured. In order to suppress contributions from higher transmission orders of the TFPI (cf. Chapter 3), for FSR = 15 GHz and 150 GHz the additional interference filters with width ( FWHM ) 185 GHz and 1150 GHz, respectively, were used. For a FSR = 750 GHz the suppression was achieved by a prism (cf. [24]). The agreement between the spectra measured with different FSRs was checked in overlapping frequency ranges in order to control the quality of the spectra and the absence of high order contributions. Typical mismatches did not exceed 1-3%. The temperature inside the illuminated sample was determined by comparing the Stokes and anti-Stokes sides of the spectrum. Typical overheating in the illuminated volume was about 3K at low temperatures ( $T < 50K$ ). Dark signal of the detector was  $\sim 2.5$  counts/sec (cf. Chapter 3).

Fig. 4.1(a) and 4.1(b) display the susceptibility spectra of 2-picoline and m-TCP, respectively. The spectra were normalized by the amplitude of the  $\alpha$ -relaxation peak for high temperatures ( $180K \leq T \leq 320K$  for 2-picoline and  $300K \leq T \leq 320K$  for m-TCP) and by the amplitude of the vibrational peak (at frequency  $\sim 1000$  GHz) for low temperatures ( $13K \leq T \leq 170K$  for 2-picoline and  $56K \leq T \leq 290K$  for m-TCP). The strong low-frequency peak in the susceptibility spectra corresponds to the main relaxation process ( $\alpha$ -process) and at highest frequencies the vibrational modes are found. While the  $\alpha$ -peak shifts to lower frequen-

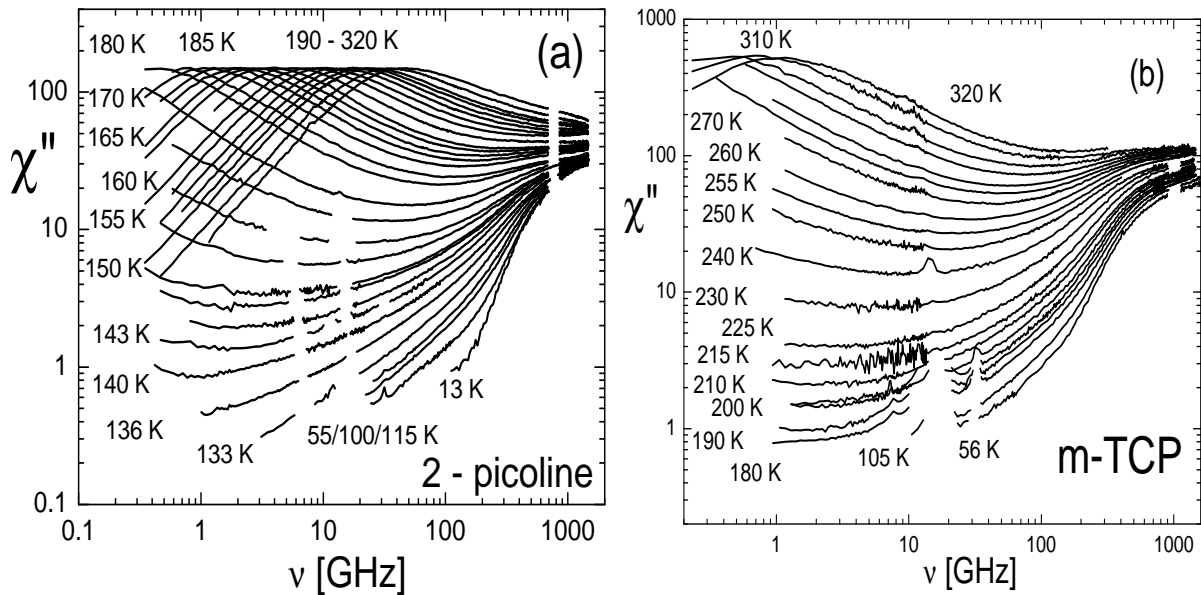


**Figure 4.1:** (a) LS spectra of 2- picoline for various temperatures (13K, 55K, 100K, 115K, 133K, 136K, 143K, 145K, 148K, 150K, 155K, 160K, 165K, 170K, 180K, 185K, 190K, 195K, 200K, 205K, 210K, 220K, 230K, 240K, 250K, 260K, 280K, 300K, 320K); (b) LS spectra of m-TCP for various temperatures (56K, 105K, 180K, 190K, 200K, 205K, 210K, 215K, 225K, 230K, 240K, 250K, 255K, 260K, 270K, 280K, 290K, 300K, 310K, 320K)

cies upon cooling a fast relaxation process is recognized in the frequency range between the  $\alpha$ -peak and the high-frequency vibrational contributions. The crossover from the  $\alpha$ -process and this fast dynamics is marked by the occurrence of a minimum in  $\chi''(\nu)$ . This minimum is the focus of the MCT predictions.

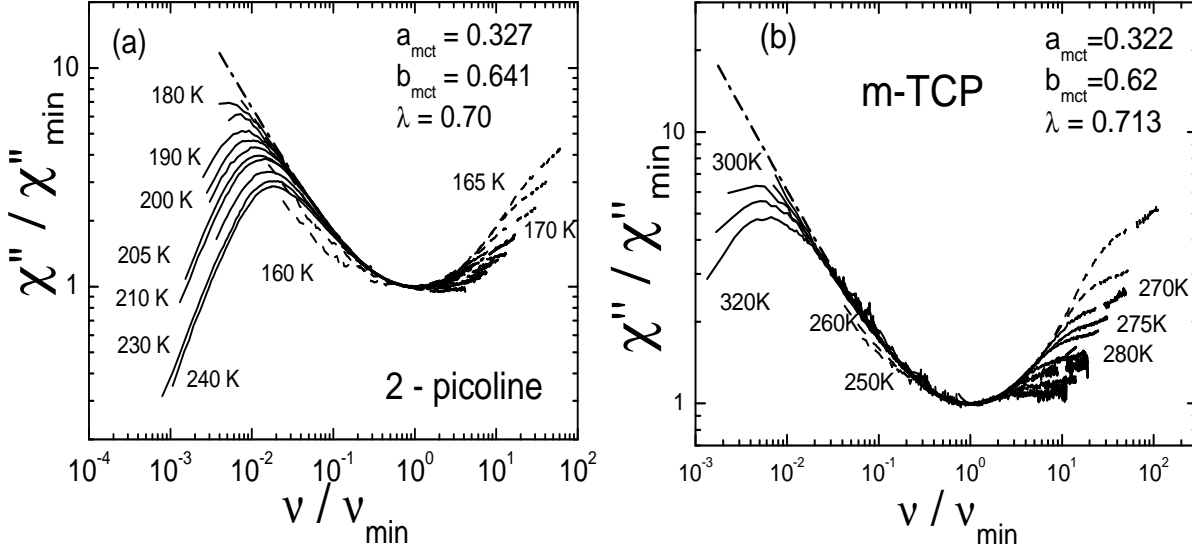
We want to emphasize that it was possible to measure LS spectra below  $T_g$  (for 2-picoline  $T_g \approx 133K$  and for m-TCP  $T_g \approx 210K$ ) where the signal is weak. It demonstrates the very good characteristics of the experimental setup. Moreover, since quasi-elastic contributions are observed even at cryogenic temperatures, LS is able to study fast dynamics below  $T_g$ .

### 4.3 Spectra analysis

According to the asymptotic laws of idealized MCT the high temperature data in Figs. 4.1(a) and 4.1(b) should collapse to a single master curve if the frequency and susceptibility axes are rescaled by the position and



amplitude of the susceptibility minimum  $\nu_{\min}$  and  $\chi''_{\min}$ , respectively (cf. Eq. 2.5).



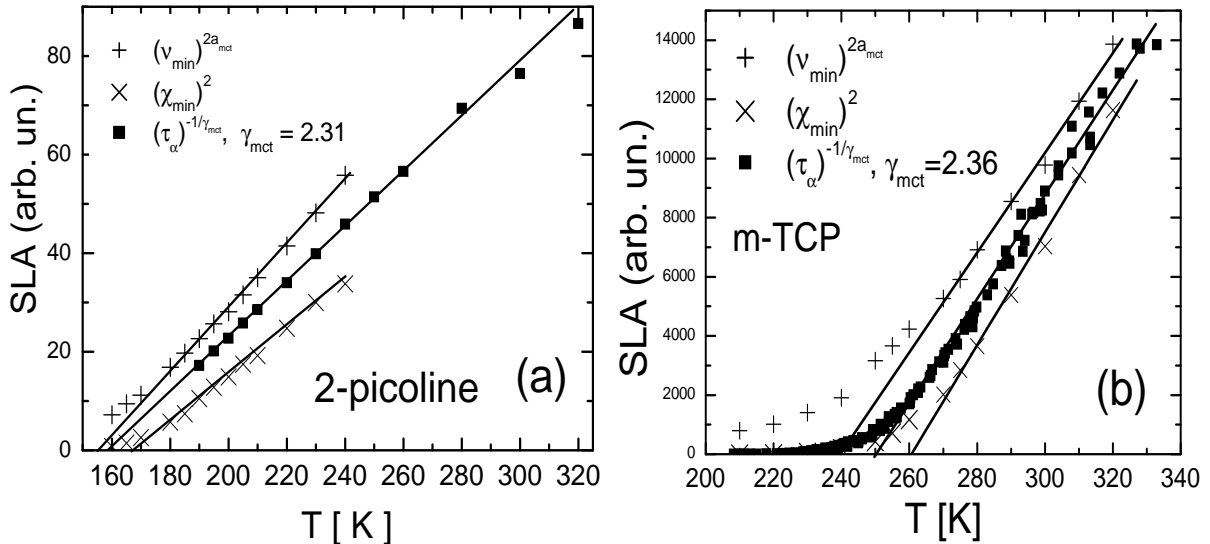
**Figure 4.2:** Rescaled plot of  $\chi''$ :  $\chi'' / \chi''_{\min}$  versus  $\nu / \nu_{\min}$  for different temperatures in the case of (a) 2- picoline; dashed lines: 160K, 165K, 170K; solid lines: 180K, 185K, 190K, 195K, 200K, 205K, 210K, 220K, 230K, 240K; dash dot line: theoretical curve with  $a_{\text{mct}} = 0.327$  and  $b_{\text{mct}} = 0.641$  (cf. Eq. 2.16); (b) m-TCP dashed lines: 250K and 260K; solid lines: 270K, 280K, 290K, 300K, 310K, 320K; dash dot line: theoretical curve with  $a_{\text{mct}} = 0.322$  and  $b_{\text{mct}} = 0.62$  (cf. Eq. 2.16).

Fig. 4.2(a) and 4.2(b) present these rescaled data for 2-picoline and for m-TCP. One can see in this plot that around the minimum the envelope of the high temperature data (dashed-dotted lines) falls on a single curve, which coincides with the theoretical curve (cf. Eq. 2.16) using  $a_{\text{mct}} = 0.327$ ,  $b_{\text{mct}} = 0.641$  for 2-picoline,  $a_{\text{mct}} = 0.322$  and  $b_{\text{mct}} = 0.62$  for m-TCP.

These values correspond to an exponent parameter  $\lambda = 0.70$  for 2-picoline and  $\lambda = 0.713$  for m-TCP (cf. Eq. 2.15). At high rescaled frequencies deviations from the MCT interpolation are observed, which are probably due to the vibrational contribution to  $\chi''(\nu)$ . One can also see deviations from the MCT minimum interpolation at low temperatures ( $T < 180\text{K}$  for 2-picoline and  $T < 270\text{K}$ ) at low rescaled frequencies. It is clearly seen that the susceptibility minima become flatter below a certain temperature with decreasing temperature.

MCT implies certain predictions concerning the temperature dependence of the parameters  $\chi''_{\min}$  and  $\nu_{\min}$  (cf. Eq. 2.17) applied in Fig. 4.2.

These relations are also checked in Fig. 4.3(a) and 4.3(b) by plotting the parameters with the exponents, taken from the interpolation of the susceptibility minima, as a function of temperature (scaling laws). Within



**Figure 4.3:** Test of MCT scaling laws: temperature dependence of  $\chi''_{\min}$  and  $\nu_{\min}$  in (a) 2-picoline and (b) m-TCP, plotted in a way to reveal linear behavior; SLA: scaling law amplitude. In the case of m-TCP values for  $\tau_{\alpha}$  are taken from [33]

the accuracy of the experiment the predicted linear relationships are reproduced. The critical temperature  $T_c$  taken as average from both lines can be estimated as  $T_c = 162 \pm 5K$  for 2-picoline and  $T_c = 250 \pm 10K$  for m-TCP. Thus, in the case of 2-picoline idealized MCT provides a consistent interpolation even up to quite high temperatures. In the case of m-TCP the agreement is less good. The deviations from the scaling laws are found already at temperatures somewhat above  $T_c$  for 2-picoline and for m-TCP, as well. The possible origin of these deviations will be discussed later in this section.

The critical temperature  $T_c$  can also be determined by studying the temperature dependence of the time constant  $\tau_{\alpha}$  of the  $\alpha$ -relaxation by applying MCT predictions (cf. Eq. 2.18). Fig. 4.4 displays the temperature dependence of the time constant  $\tau_{\alpha}$ , which has been extracted by analyzing the  $\alpha$ -process measured with different experimental techniques: (a) light scattering (LS) (cf. Section 4.2), neutron scattering (NS) [35]

and dielectric spectroscopy (DS) [31] for 2- picoline and (b) light scattering (LS), NMR [33] and dielectric spectroscopy (DS) [36] for m- TCP. In

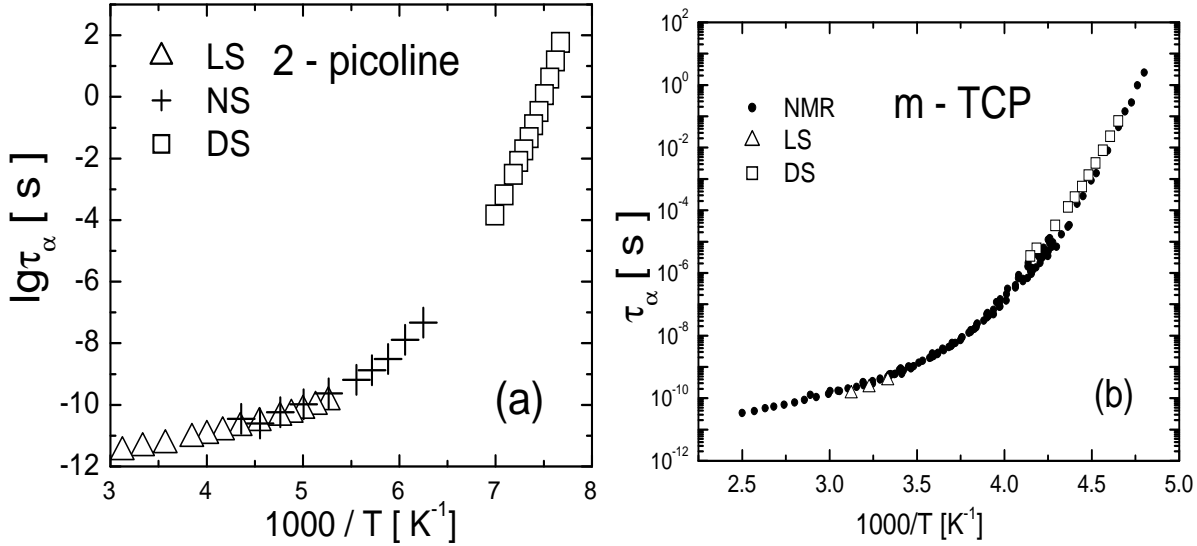


**Figure 4.4:** Temperature dependence of the time constant  $\tau_\alpha$  for (a) 2-picoline and (b) m-TCP as obtained by LS, NS [35], DS [31, 36] and NMR [33].

Figs. 4.3(a) and 4.3(b)  $\tau_\alpha^{-1/\gamma_{mct}}$  is plotted as a function of temperature. In the case of 2-picoline the time constants  $\tau_\alpha$  were extracted from the susceptibility spectra by fitting the  $\alpha$ -peak with a Cole- Davidson (CD) function,  $\chi''_{CD}(\nu) \propto \Im(1 + i\omega\tau)^{-b}$  (cf. Fig. 4.7). There are no many LS data of m-TCP with  $\alpha$ -peak. Therefore, for our analysis we used the time constants  $\tau_\alpha$  extracted from the NMR data [33]. The exponent  $\gamma_{mct}$  was calculated from the exponents  $a_{mct}$  and  $b_{mct}$  using the relation Eq. 2.19. A linear behavior is found, and the extracted critical temperature is in good agreement with the value of  $T_c$  extracted from the temperature dependence of  $\chi''_{\min}$  and  $\nu_{\min}$ .

In order to understand the origin of the deviations from the MCT scaling laws in Fig. 4.3 we plot LS data of 2-picoline and m-TCP  $\chi''$  as a function of  $\nu\tau_\alpha$  (cf. Fig.4.5), where  $\tau_\alpha$  is taken from interpolating  $\tau_\alpha(T)$  (cf. Fig. 4.4). As can be seen in Fig. 4.5, at high temperatures the low frequency part of the  $\alpha$ -peak collapses to a single curve, as expected by MCT, and this part is well interpolated by a CD susceptibility (solid line). In other words, the width of the  $\alpha$ -peak is essentially temperature inde-

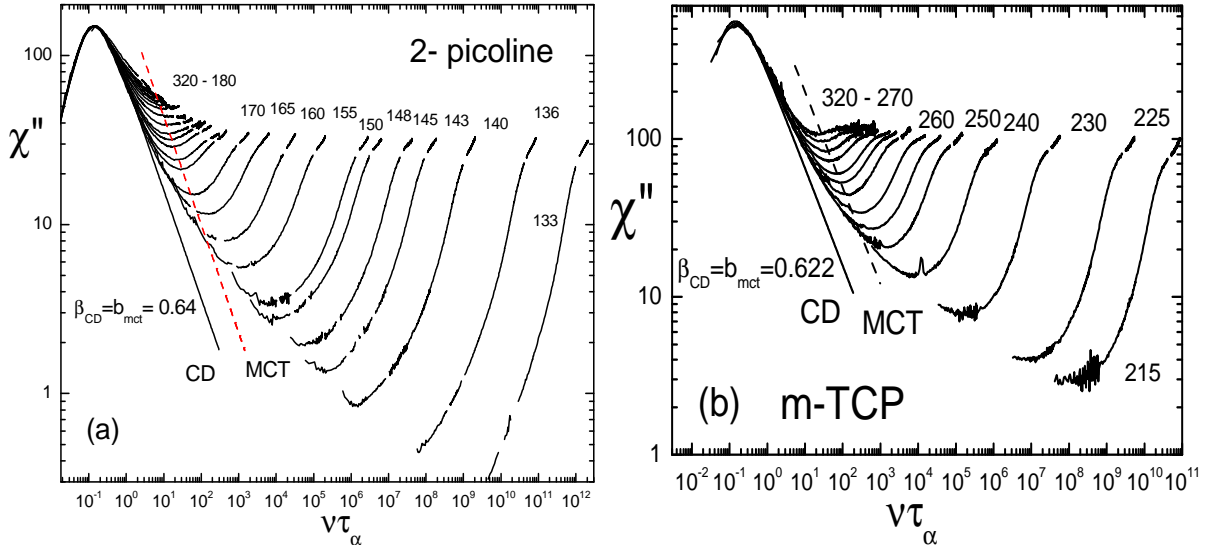


**Figure 4.5:** LS spectra of 2- picoline (a) and m-TCP (b) as function of reduced frequency  $\nu\tau_\alpha$ . Solid line: interpolation of the  $\alpha$  - peak by a Cole - Davidson susceptibility; dashed line: MCT prediction for the position of the minimum.

pendent. According to Eq. 2.20 position and height of the susceptibility minima should be described by a straight line with a slope  $-b_{mct}$  in the double logarithmic plot (dashed line). This is indeed observed for temperatures above 180K for 2-picoline and above 270K for m-TCP. Below this temperature deviations are observed which become larger at lower temperatures. It appears that the minima are shifted to higher reduced frequencies ( $\nu\tau_\alpha$ ) and to higher amplitudes  $\chi''_{\min}$  as compared to MCT predictions.

The deviations observed at low temperatures ( $T \lesssim T_c$ ) can be explained if some additional spectral contributions are assumed to be present between the frequency range of the  $\alpha$ - relaxation peak and the contribution of the fast dynamics. Possible candidates are the high frequency excess wing of the  $\alpha$ - process identified by dielectric spectroscopy and/or the Johari-Goldstein  $\beta$ - process [67] (cf. Fig. 2.2 in Chapter 2). Since 2- picoline and m-TCP do not exhibit a slow  $\beta$ - process in the DS spectra, the only candidate for a change of the susceptibility is the excess wing, which indeed is clearly seen in the DS spectra (cf. Fig. 4.6(a), Fig. 4.6(b) and Fig. 4.9).

From the DS data of glycerol and propylene carbonate [13], which were

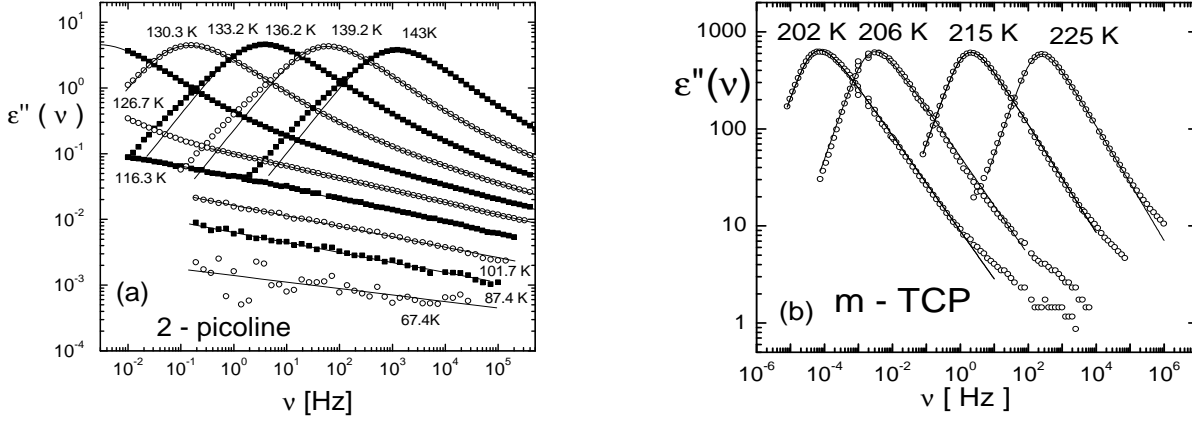


**Figure 4.6:** (a) DS spectra of 2-picoline for various temperatures; (b) DS spectra of m-TCP for various temperatures

measured to higher frequencies, it is seen that the excess wing disappears at high temperatures. We conclude that the deviations of  $\chi''$  from the MCT description are due to the appearance of the excess wing below a certain temperature. The excess wing is observed by DS in all supercooled liquids provided that it is not obscured by the presence of a  $\beta$ - process and can be described by a power-law contribution with exponent  $\gamma < \beta_{CD}$  [31].

So, idealized MCT provides a satisfying interpolation of the susceptibility minimum at high temperatures ( $T > T_c$ ), but deviations from the scaling laws are observed below some temperature, which is little higher than the critical temperature  $T_c$ .

## 4.4 Phenomenological analysis

The open question is how to describe the evolution of the susceptibility of a glass former during cooling down from the critical temperature  $T_c$  to temperatures in the glassy state  $T \leq T_g$ . There are no predictions for this temperature range, but one can try to apply some phenomenological approach in order to describe the spectra.

A phenomenological analysis of the LS spectra presented on the Fig. 4.1 which allows one to fully interpolate the relaxation contribution including slow ( $\alpha$ -process) and fast dynamics will be described in this section. This

approach does not rely on MCT although the relation among the exponents characterizing  $\alpha$ -process and fast dynamics are incorporated. For performing this interpolation some assumptions are needed.

First of all, the  $\alpha$ -process contribution is completely interpolated by a Cole-Davidson (CD) susceptibility.

Second, slow and fast dynamics can be described by an additive superposition of a CD susceptibility and a power-law contribution,  $\nu^a$  [17, 31]:

$$\chi''(\nu) = A\chi''_{CD} + B\nu^a, \quad T > T_c \quad (4.1)$$

where  $A$  and  $B$  are constants to be determined by the fit. Here, we assume that the values of the exponents  $\beta_{CD}$  and  $a$  are fixed by the MCT predictions (cf. Eq. 2.19). We take  $\beta_{CD} = b_{mct} = 0.641$ ,  $a = a_{mct} = 0.327$  for 2-picoline and  $\beta_{CD} = b_{mct} = 0.62$ ,  $a = a_{mct} = 0.322$  for m-TCP. Figs. 4.7(a) and 4.7(b) display the LS spectra of 2-picoline at temperatures  $190K \leq T \leq 320K$  and LS spectra of m-TCP at temperatures  $300K \leq T \leq 320K$  with the fit curves. It is clear seen in this plot that the fit

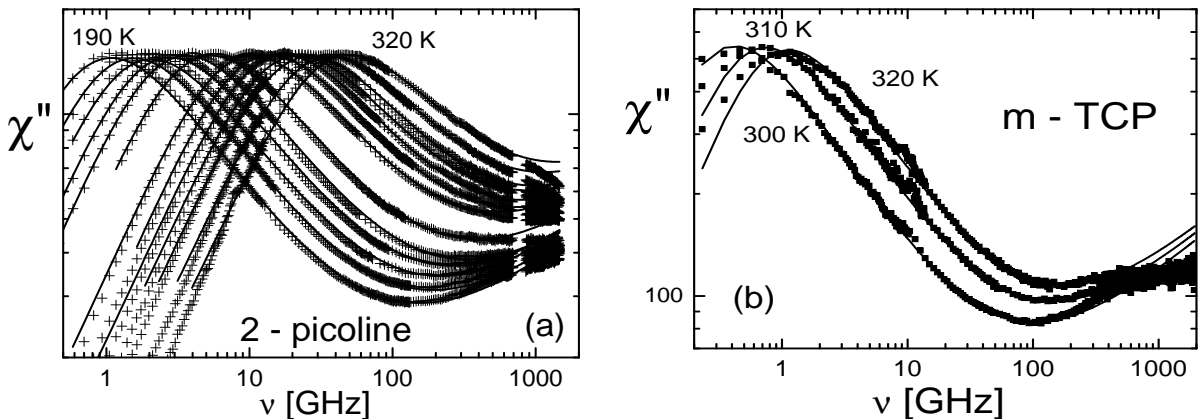


**Figure 4.7:** (a) LS spectra of picoline above 185K (190K, 195K, 200K, 205K, 210K, 220K, 250K, 270K, 280K, 300K, 320K, pluses), fit by applying the phenomenological approach (solid lines); (b) LS spectra of m-TCP for 300K, 310K, 320K (squares), fit by the phenomenological approach (solid lines).

works well for 2-picoline. For m-TCP the fit works also well apart the low frequency side of the  $\alpha$ -peak where some deviations from the data are observed.

Furthermore, we assume, that the susceptibility spectra at temperatures below 190K in the case of 2-picoline and below 300K for m-TCP

can be described by a sum of two power-law contributions,

$$\chi''(\nu) = A\nu^{-\gamma} + B\nu^a, \quad T < T_c \quad (4.2)$$

where the exponents  $\gamma$  and  $a$  are attributed to the slow and fast dynamics, respectively. It is important to quantify  $\gamma(T)$ .

Recently, a distribution of correlation times which allows to fit the spectral shape of both the  $\alpha$ -process peak and the wing and to extract the exponent  $\gamma$  from the DS spectra was proposed [53, 54]. Fig. 4.6(a) displays the DS spectra of 2-picoline, where such fits are included (cf. [53]). Moreover, analyzing the DS data of several glass formers it was found [53, 55] that  $\gamma$  shows a universal behavior when plotted as function of  $\lg(\tau_\alpha)$  (cf. Fig. 4.8).

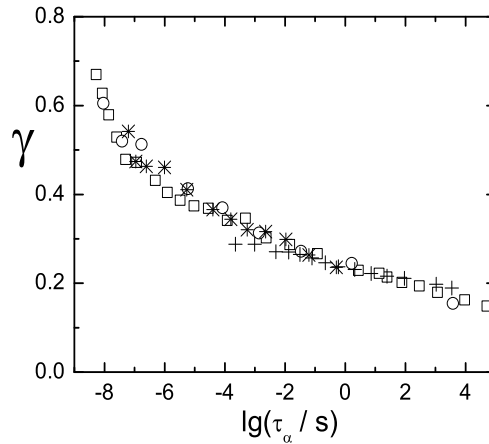


**Figure 4.8:** Exponent of the excess wing in the DS spectra of:  $\circ$ -glycerol [55],  $*$ -propylene carbonate [53],  $\square$ -glycerol [53],  $+$ -2-picoline [53]

*A priori* there are no arguments that this universality holds for the LS data, however, recent LS measurements of glycerol show that the wing manifests itself in a very similar way as in DS [32].

One can also try to compare LS and DS data of 2-picoline and m-TCP directly (cf. Fig. 4.9). In this figures again the susceptibility as a function of  $\nu\tau_\alpha$  is plotted like in Fig. 4.5. It is possible to say that the excess wing is at least similar for both methods. For proceeding further we assume that  $\gamma(T)$  is the same in both DS and LS.

Let's try to fit the data applying the phenomenological formula (Eq. 4.2) with the parameter  $\gamma$  extracted from DS spectra in Fig. 4.8

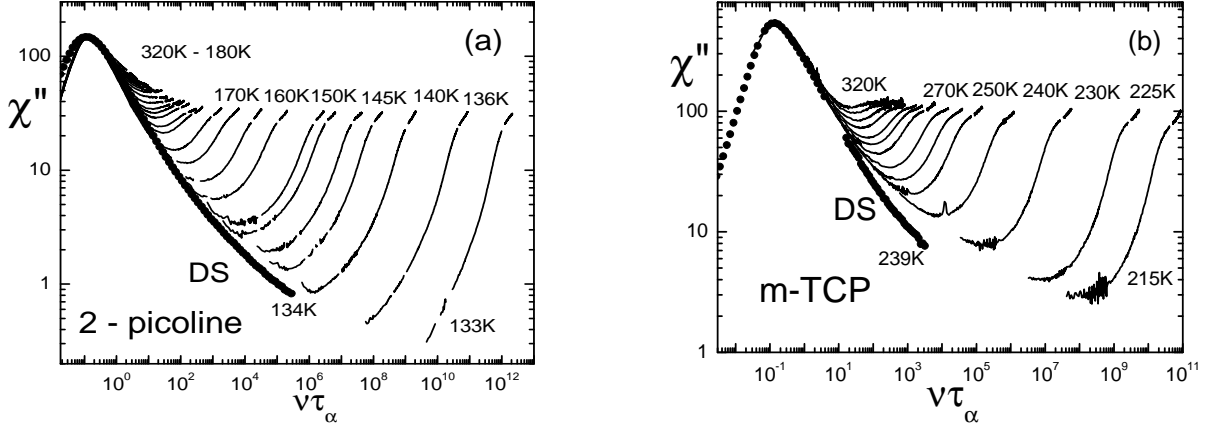


**Figure 4.9:** LS spectra of 2- picoline (a) and m-TCP (b) as a function of reduced frequency  $\nu\tau_\alpha$ . Circles: DS spectrum for 2- picoline (a) and m-TCP (b), respectively.

for each temperature. The fit parameters  $a$ ,  $A$ , and  $B$  are kept free. Figs. 4.10(a) and 4.10(b) display the LS data of 2-picoline at tempera-

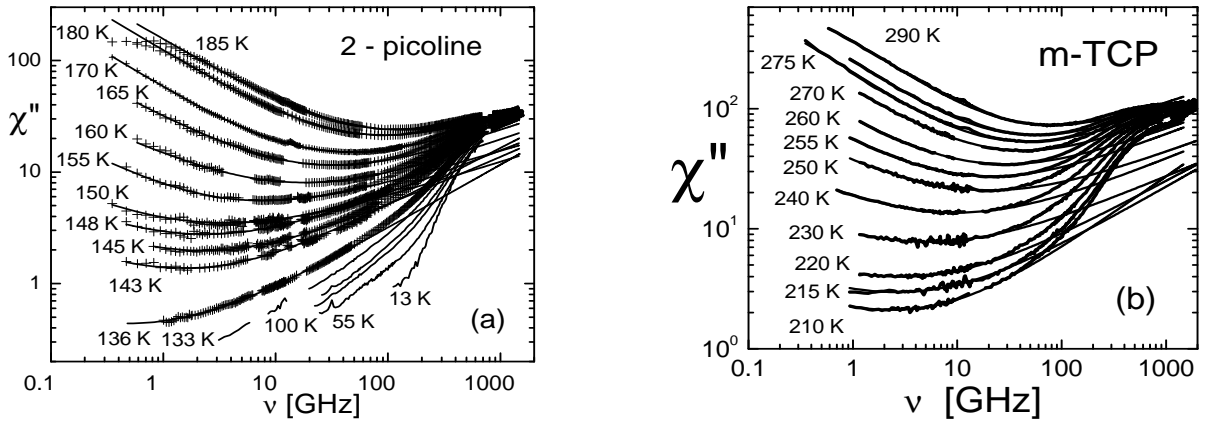


**Figure 4.10:** (a) LS spectra of 2- picoline below 185K (pluses), fit by the superposition of two power-laws (solid lines); (b) LS spectra of m-TCP below 290K (pluses), fit by the superposition of two power-laws (solid lines).

tures  $T \leq 185K$  and the LS data of m-TCP at temperatures  $T \leq 290K$ , respectively, with the fit curves. One can see from these plots that this fit works well for 2-picoline and m-TCP.

The exponents  $a$  for 2-picoline and m-TCP are shown in the Fig. 4.11. It is clear that  $a$  is temperature dependent in the temperature interval  $T_g < T < T_c$  and increase from  $a = a_{mct} = 0.327$  to  $a = 0.725$  for 2-picoline and from  $a = a_{mct} = 0.322$  to  $a = 0.8$  for m-TCP. For temperatures  $T \leq T_g$



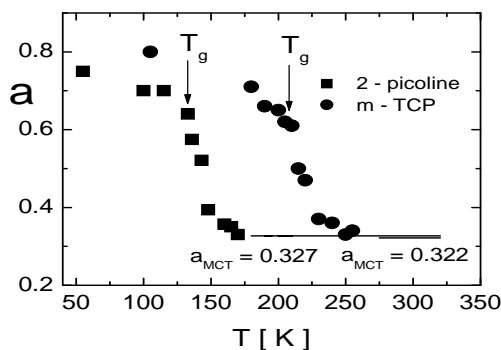


**Figure 4.11:** Temperature dependence of the exponent  $a$ .

$a$  can directly be read from the data since no interference with the wing contribution is expected. In this temperature interval  $a$  is essentially constant.

Fig. 4.12 shows the LS spectra of 2-picoline and m-TCP after subtracting the contribution of the  $\alpha$ -process including the excess wing.

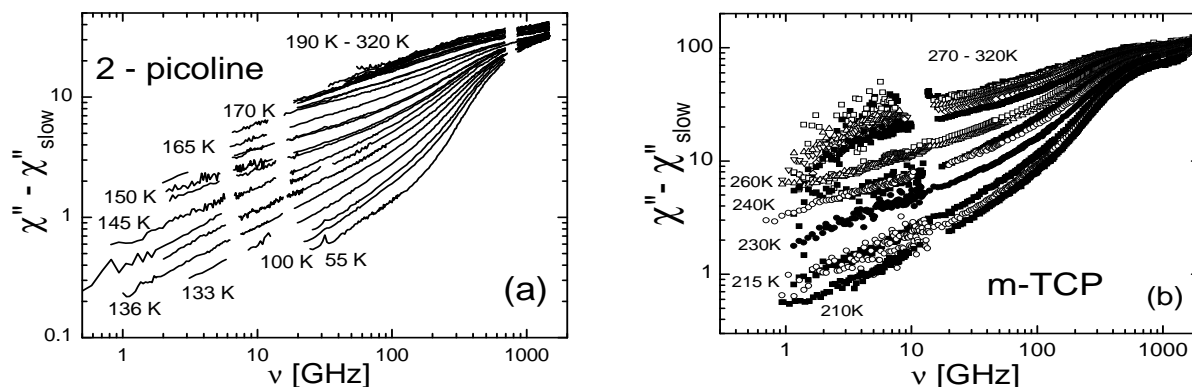


**Figure 4.12:** Fast dynamics spectra singled out by applying the phenomenological model for (a) 2- picoline and (b) m-TCP.

In agreement with the phenomenological fit in Figs. 4.7 and 4.10 the power-law of the fast dynamics with a constant amplitude and an exponent  $a = a_{mct}$  is rediscovered at  $T > T_c$ .

Having singled out the fast dynamics contribution one is able to determine the non-ergodicity parameter  $f$  (cf. Eq. 2.22 in Chapter 2). The integration is performed in the frequency interval 0-200 GHz. Fig. 4.13 displays  $1 - f$ . Obviously, the anomaly expected by MCT is discovered: above 180K for 2-picoline and above 260K for m-TCP only a weak temperature dependence of  $1 - f$  is discernible; below a strong decrease is

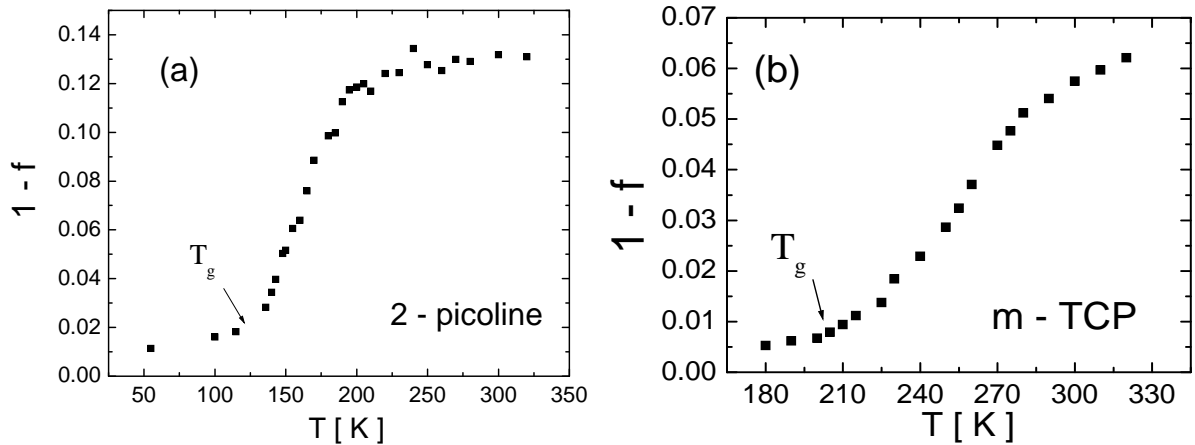


**Figure 4.13:** Temperature dependence of  $1 - f$  for (a) 2-picoline and (b) m-TCP.

observed with decreasing temperature (cf. Fig. 4.13). At  $T_g$  the strong temperature dependence halts and only a weak one persists at  $T < T_g$ .

## 4.5 Discussion and conclusions

A comprehensive depolarized LS study of the molecular glass formers 2-picoline and m-TCP was performed, and an analysis within the frame of the idealized MCT was carried out. The susceptibility minimum is well described by the asymptotic laws of MCT, allowing to identify consistently the critical temperature  $T_c$ . The critical temperature was determined to be  $T_c = 162 \pm 5K$  for 2-picoline and  $T_c = 250 \pm 10K$  for m-TCP. An analysis of the full LS spectrum was carried out within a phenomenological model down to  $T \sim T_g$ . This model assumes additivity of fast and slow relaxation processes and the relation of the respective exponents is kept fixed at  $T > T_c$  as predicted by MCT. Including the  $\alpha$ -relaxation, it is sufficient to fix a single spectral shape parameter, *i.e.*,  $\beta_{CD} = b_{mct}$ , which defines the high-frequency power-law behavior of  $\alpha$ -process. Below  $T_c$  the positions of the susceptibility minima do not follow the MCT predictions because of the appearance of the excess wing. The wing is believed to be kind of precursor of the  $\alpha$ -process and/or a secondary relaxation process different from the  $\beta$ -process. Since no simple and generally accepted predictions exist for the low temperature regime ( $T < T_c$ ), and since the

frequency window is limited, our analysis is phenomenological in principle and has to rely on certain assumptions. Nevertheless, within this approach one is able to single out the fast dynamics contribution. Power-law contributions are found with an exponent being constant above  $T_c$  but increasing upon further cooling. This one can interpret as an indication that the susceptibility crosses over to a white noise spectrum as predicted by MCT. The predicted anomaly of the non-ergodicity parameter was also observed.

# 5 Reexamination of the evolution of the dynamic susceptibility of glycerol

This chapter closely follows the publication [55].

## 5.1 Introduction

In recent years significant experimental progress has been made in monitoring the evolution of the molecular dynamics in supercooled liquids. For example, the dielectric response of polar glass formers can now be measured over 18 decades in frequency ( $10^{-5}$  Hz -  $10^{13}$  Hz) [13]. Quasi-elastic light scattering is able to monitor the fast dynamics with high precision ( $10^8$  Hz -  $10^{13}$  Hz) as we demonstrated in Chapter 4. Together with molecular dynamics simulations [16] the applications of the aforementioned techniques among others have demonstrated that MCT provides a rather consistent description of the evolution of the susceptibility at the onset of the glass transition.

Most systems investigated so far were fragile molecular glass formers, characterized by the absence of strong intermolecular interactions. Here, the question arises whether MCT may also be applied to non-fragile glass formers, *i.e.*, to so-called strong systems with more or less strong intermolecular interactions. Since in such systems the cage effect is expected to play a minor role one may be reluctant to test MCT here. However, it turns out that again two-step correlation functions are observed though quantitative agreement with MCT is less convincing [38, 39].

The case of glycerol is of particular interest since the system is of intermediate degree of fragility. Several MCT studies were published but concerning the critical temperature  $T_c$  extracted from the data significant disagreement was found. In 1994 a first MCT analysis of LS as well as

neutron scattering NS data was carried out by Wuttke *et al.* [29] and the authors reported  $T_c \approx 225K$ , however no agreement with viscosity data was obtained. The latter data suppose  $T_c \approx 300K$  as pointed out by Rössler *et al.* [19]. A reanalysis of the LS data by Franosch *et al.* [40] identified  $T_c$  in the temperature interval 223 - 233 K. In 1996 an analysis of the now accessible high frequency dielectric data of glycerol were presented by Lunkenheimer *et al.* [41] and they reported  $T_c \approx 262K$ . In a review article on testing MCT predictions by NS Petry and Wuttke [43] displayed the non-ergodicity parameter for several glass formers though they hesitated to draw any conclusion in the case of glycerol. Finally, an impulsive stimulated thermal scattering study by Clearly, these contradictory results are very unsatisfying and they point to a problem for any MCT analysis, namely, that its expected range of validity is not well defined. In other words, the approximations made within the theory are not controlled. On the one hand, the theoretical predictions are expected to hold only close to the critical temperature  $T_c$ , on the other, for temperature close to  $T_c$  the high temperature scenario of MCT is expected to be disturbed by the emergence of so-called hopping transport which within the extended theory is supposed to provide the mechanism to re-establish ergodicity below  $T_c$ . It is expected that this problem is more severe in non-fragile glass formers than in fragile systems.

Experimentally, the situation turns out to be somewhat different. In a series of papers it was demonstrated that the high temperature MCT scenario is found even up to the fluid regime close to the melting point [16, 44, 45].

This allows one to easily identify first deviations from the scaling laws indicating the break down of the idealized MCT description at  $T \leq T_c$ , and provides a large enough temperature range from which the critical temperature can be accurately extrapolated. Most of the cited analyses of glycerol were carried out in a rather small temperature range which actually may be too small. As a consequence, the results of these analyses depend on the temperature interval investigated. Below  $T_c$  the evolution of the susceptibility is up to now not adequately described by theory and one has to resort to phenomenological approaches. Analyzing the dielectric loss of several glass formers including glycerol by applying a newly introduced distribution of correlation times derived from an extension of a

generalized gamma distribution first introduced by Kudlik *et al.* [47], Blochowicz *et al.* [53, 54] report that, independent of the degree of fragility, the evolution of the dynamic susceptibility including the high frequency excess wing of the  $\alpha$ -process exhibits a high degree of universality provided that the parameters of the excess wing are plotted as a function of the correlation time  $\tau_\alpha$  rather than as a function of temperature as is usually done. Within this analysis it can be shown that the excess wing appears upon cooling at  $\lg(\tau_\alpha/s) \approx -8$  and that the temperature at which this happens correlates well with the critical temperature  $T_c$ . This phenomenological analysis provides clear evidence that a high and low temperature scenario holds for the evolution of the susceptibility, and it was concluded that the break down of high temperature scenario of MCT coincides with the appearance of the excess wing. For glycerol  $T(\lg(\tau_\alpha/s) = -8) \approx 270$  K is found thus challenging most MCT analyses on glycerol published so far. Although the nature of the excess wing is not well understood, it seems to be some kind of secondary relaxation process and can not be identified with a contribution from hopping transport [56, 57].

In this contribution we reanalyze the dielectric data compiled by Lunkenheimer *et al.* [13] (cf. Fig. 5.1) which currently provide the most complete dielectric data set reported for a glass former. By applying the extension of a generalized gamma distribution function [47, 53, 54] for describing the slow response at low temperatures on the one hand, and by analyzing the dynamics at high temperatures as proposed by MCT, on the other, we will demonstrate that (i) a complete interpolation of the dielectric data covering about 17 decades in frequencies is obtained and (ii) the crossover temperature extracted from the phenomenological analysis of the slow response agrees well with that obtained from the MCT analysis. For the purpose of the latter analysis we included high temperature data [13] which were not used in the first MCT analysis of the dielectric response [41]. In this work, Lunkenheimer *et al.* analyzed directly the  $\varepsilon(\omega)$  data whereas we use normalized data for which the static permittivity has been scaled out. Actually, since glycerol is a non-fragile glass former the effect of the temperature dependence of the static susceptibility is quite strong and significantly changes the results of any line shape analysis. (iii) Finally, we will show that no difference is found for the non-fragile system glycerol with respect to a fragile glass former like,

*e.g.*, propylene carbonate.

## 5.2 Phenomenological description of the susceptibility

Glycerol is a type *A* glass former exhibiting no discernible secondary relaxation peak in the dielectric spectra. For such systems Kudlik *et al.* [47] (for details see also [53, 54]) have proposed a distribution of correlation times which excellently interpolates the  $\alpha$ -relaxation contribution including both the peak and excess wing. The distribution is an extension of a generalized gamma distribution (GGE) [53, 54] and is given by

$$G_{GGE}(\ln\tau) = N_{GGE}(\alpha, \beta, \gamma) \exp\left[-\frac{\beta}{\alpha}\left(\frac{\tau}{\tau_0}\right)^\alpha\right] \left(\frac{\tau}{\tau_0}\right)^\beta \left[1 + \left(\frac{\tau\sigma}{\tau_0}\right)^{\gamma-\beta}\right] \quad (5.1)$$

with the normalizing factor

$$N_{GGE}(\alpha, \beta, \gamma) = \alpha \left(\frac{\beta}{\alpha}\right)^{\frac{\beta}{\alpha}} \left[\Gamma\left(\frac{\beta}{\alpha}\right) + \sigma^{\gamma-\beta} \left(\frac{\alpha}{\beta}\right)^{(\gamma-\beta)/\alpha} \Gamma\left(\frac{\gamma}{\alpha}\right)\right]^{-1} \quad (5.2)$$

given by the condition  $\int_{-\infty}^{\infty} G_{GGE}(\ln\tau) d\ln\tau = 1$ , and the mean time constant

$$\langle\tau\rangle = \tau_0 \left(\frac{\alpha}{\beta}\right)^{\frac{1}{\alpha}} \frac{\Gamma\left(\frac{\beta+1}{\alpha}\right) + \sigma^{\gamma-\beta} \left(\frac{\alpha}{\beta}\right)^{(\gamma-\beta)/\alpha} \Gamma\left(\frac{\gamma+1}{\alpha}\right)}{\Gamma\left(\frac{\beta}{\alpha}\right) + \sigma^{\gamma-\beta} \left(\frac{\alpha}{\beta}\right)^{(\gamma-\beta)/\alpha} \Gamma\left(\frac{\gamma}{\alpha}\right)} \quad (5.3)$$

In addition to the parameters  $\alpha$  and  $\beta$  specifying the manifestation of the  $\alpha$ -relaxation peak two additional parameters  $\sigma$  and  $\gamma$  appear which define the onset of the wing and its exponent, respectively. Thus, in this phenomenological approach it is assumed that the wing contribution formally may be treated as a part of the  $\alpha$ -relaxation spectrum. The width parameters  $\alpha$  and  $\beta$  can assume values  $0 < \alpha, \beta < \infty$ . From Eq. 5.1 the complex dielectric permittivity  $\varepsilon(\omega)$  is:

$$\varepsilon_\alpha(\omega) - \epsilon_\infty = \Delta\varepsilon_\alpha \int_{-\infty}^{\infty} G_{GGE}(\ln\tau) \frac{1}{1 + i\omega\tau} d\ln\tau, \quad (5.4)$$

where  $\Delta\varepsilon_\alpha$  is the relaxation strength of the  $\alpha$ -process. As demonstrated by Adichtchev *et al.* [31] and by Blochowicz *et al.* [53, 54], in the case of glycerol, 2-picoline and propylene carbonate the parameters  $\sigma$  and  $\gamma$  evolve in a very similar manner provided that they are plotted as a function of  $\tau_\alpha$  (cf. also Fig. 5.5). Moreover, it has been shown that the excess contribution appears only at  $\tau_\alpha > 10^{-8}$ s and that at high temperatures the susceptibility is well described by a CD function [34], *i.e.*, by a simple peak function. It turns out that the GGE distribution provides an excellent fit of a CD susceptibility with  $\gamma = \beta_{CD}$ , when a constraint  $\sigma(\alpha, \beta, \gamma) = \sigma_c$  is introduced in such a way, that the absolute short time asymptote of the GGE and the CD distribution become identical. Explicitly, one finds

$$\sigma_c(\alpha, \beta, \gamma) = \left( \frac{(\frac{\beta}{\alpha})^{\beta/\alpha} \left( \frac{\alpha\pi}{\sin(\pi\gamma)} - (\frac{\alpha}{\beta})^{\gamma/\alpha} \Gamma(\gamma/\alpha) \right)}{\Gamma(\beta/\alpha)} \right)^{1/(\beta-\gamma)} \quad (5.5)$$

Irrespective of the particular shape of the  $\alpha$ -peak itself,  $\sigma_c$  assures that no wing is present in  $\varepsilon''(\omega)$ . Thus, although the distribution function GGE at  $\tau/\tau_0 \ll 1$  still is described by two power-law contributions with exponents  $\beta$  and  $\gamma$ , the resulting susceptibility function is a simple peak function being very close to a CD susceptibility. Note that a fit of a CD susceptibility by the GGE distribution always leads to  $\gamma = \beta_{CD}$ . Qualitatively, for the typical values of the parameters  $\alpha$  and  $\beta$  found in type A systems the onset parameter  $\sigma$  reaches values of 1 - 2, *i.e.* the onset of the excess wing shifts very close to the peak frequency  $1/(2\pi\tau_0)$  and as consequence the susceptibility becomes a simple peak function without an excess wing. Simultaneously, the parameter  $\beta$  becomes  $> 1$ . Concluding, instead of a free fit of the data the constraint (Eq. 5.5) can be applied to guarantee that the GGE is well reproducing a simple peak susceptibility. We shall call this limit the *CD limit* of the GGE distribution. As the line shape analysis shows, beyond this limit (not applying the constraint) a pronounced excess wing is characterized by an onset parameter  $\sigma \gg 1$  and a parameter  $\beta < 1$ . In order to account also for the fast dynamics we include in the phenomenological approach a power law contribution, explicitly

$$\chi''(\nu) = A\chi''_{GGE}(\nu) + B\nu^a \quad (5.6)$$



Within this phenomenological approach the  $1 - f$  is defined [53] by

$$1 - f = \frac{B \int_{-\infty}^{\ln \nu_c} \nu^a d \ln \nu}{\pi A/2 + B \int_{-\infty}^{\ln \nu_c} \nu^a d \ln \nu}, \quad (5.7)$$

where for an experimental analysis cutoff frequency  $\nu_c$  has to be properly chosen.  $A$  and  $B$  are some weighting factors that may depend on temperature.

## 5.3 Results

### 5.3.1 Spectra analysis

Fig. 5.1 (a) presents the imaginary part  $\varepsilon''(\nu)$  and Fig. 5.1 (b) the real part  $\varepsilon'(\nu)$  of glycerol as a function of frequency as compiled by Lunkenheimer et al. [13].

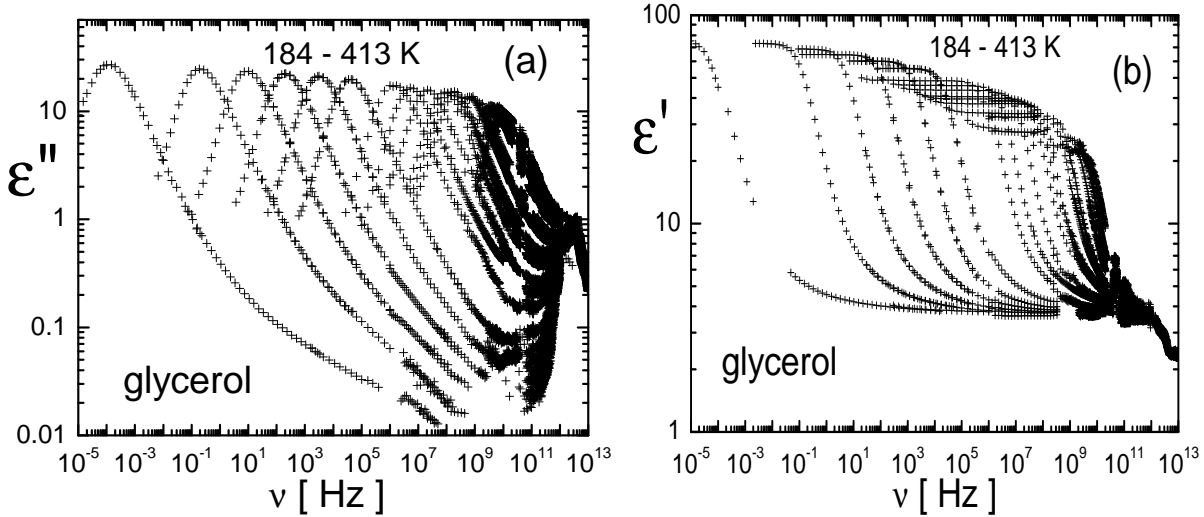


**Figure 5.1:** Dielectric permittivity of glycerol as compiled by Lunkenheimer *et al.* [13] for various temperatures. The temperature of each curve is, from left to right (in K): 184, 195, 204, 213, 223, 234, 253, 263, 273, 289, 295, 303, 323, 333, 363, 382, 403 and 413. (a) imaginary part  $\varepsilon''(\nu)$ ; (b) real part  $\varepsilon'(\nu)$ , no data for 403 K.

About 18 decades in frequency are covered. As is clearly seen from the data, the amplitude of the  $\alpha$ -relaxation peak decreases with increasing

temperature. This is a consequence of the temperature dependence of the static dielectric constant  $\varepsilon_s = \Delta\varepsilon + \varepsilon_\infty$ . The relaxation strength  $\Delta\varepsilon$  includes all contributions from intermolecular dynamics, namely that of the  $\alpha$ -process and fast dynamics as well as that of the boson peak and the microscopic peak;  $\varepsilon_\infty$  comprises all processes at optical frequencies. The quantity  $\varepsilon_s$  may be extracted from the plateau of  $\varepsilon'(\nu)$  at lowest frequencies (cf. Fig. 5.1 (b)). Fig. 5.2 displays the results. For comparison, the corresponding results reported by Lunkenheimer *et al.* [13] are included showing a good agreement.

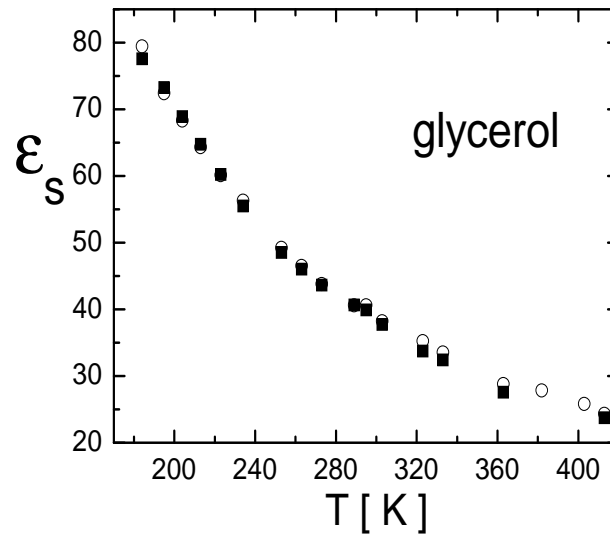


**Figure 5.2:** Temperature dependence of the static permittivity  $\varepsilon_s$  (solid squares); for comparison the data reported by Lunkenheimer *et al.* [13] are shown (open circles)

Inspecting the real part (cf. Fig. 5.1 (b)) it is found that  $\Delta\varepsilon \gg \varepsilon_\infty$  holds for all temperatures. Therefore, for obtaining a normalized susceptibility we take

$$\chi''(\nu) = \varepsilon''(\nu)/\varepsilon_s \quad (5.8)$$

and only this quantity can be compared with theory. Note that the static quantity  $\varepsilon_s$  contains no direct information on the dynamics. Thus, from analyzing its temperature dependence no conclusion can be drawn in a strict sense concerning a dynamic crossover as may be implied by the work, *e.g.*, of Lunkenheimer [58] and of Schönhal's [59]. Fig. 5.3 presents the normalized data. Within the experimental noise the  $\alpha$ -relaxation peak

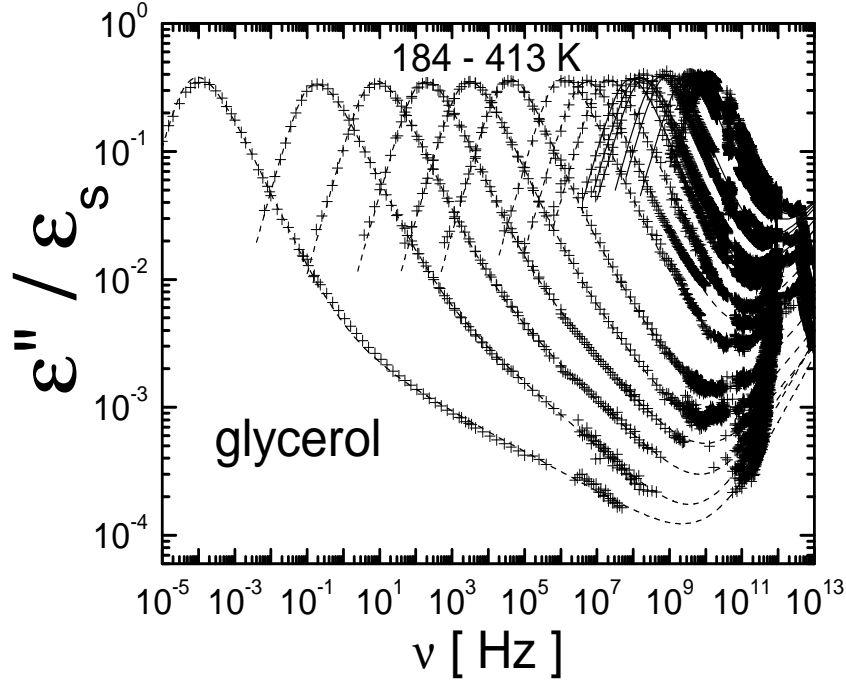


**Figure 5.3:** Imaginary part of dielectric permittivity of glycerol (cf. Fig. 5.1 (a)) scaled by the static permittivity  $\varepsilon_s$  for various temperatures, included complete interpolation of the relaxation contribution by applying Eq. 5.6. (dashed line) and by applying in addition the constraint, Eq. 5.5 (solid line), data for 403K and 413K are not fitted.

is essentially constant in amplitude for all temperatures. The fit curves (cf. Eq. 5.6) are also shown in Fig. 5.3. It is seen that the slow response ( $< 1$  GHz) at low temperature ( $T < 289$  K) including  $\alpha$ -relaxation peak and excess wing is well described by the phenomenological approach, namely by the GGE distribution, Eq. 5.1. The parameters of the fits are displayed as a function of temperature in Fig. 5.4. The onset parameter  $\sigma$  and the exponent  $\gamma$  (cf. Fig. 5.4 (a) and Fig. 5.4 (b)), both characterizing the excess wing, as well as the parameter  $\beta$  (cf. Fig. 5.4 (c)), determining together with  $\alpha$  (which for glycerol can be set to  $\alpha = 10$  for all temperatures) the width of the  $\alpha$ -relaxation peak, are found to be very similar to those reported by Blochowicz *et al.* [53, 54] who performed an analysis of a glycerol data set extending only up to 1 GHz. The exponent  $\gamma$  becomes lower the lower the temperature and  $\sigma$  strongly increases with decreasing temperature. The parameter  $\beta$  shows a trend to increase with temperature, in particular, it becomes larger than 1 at the highest temperatures.

## 5 Reexamination of the evolution of the dynamic susceptibility of glycerol

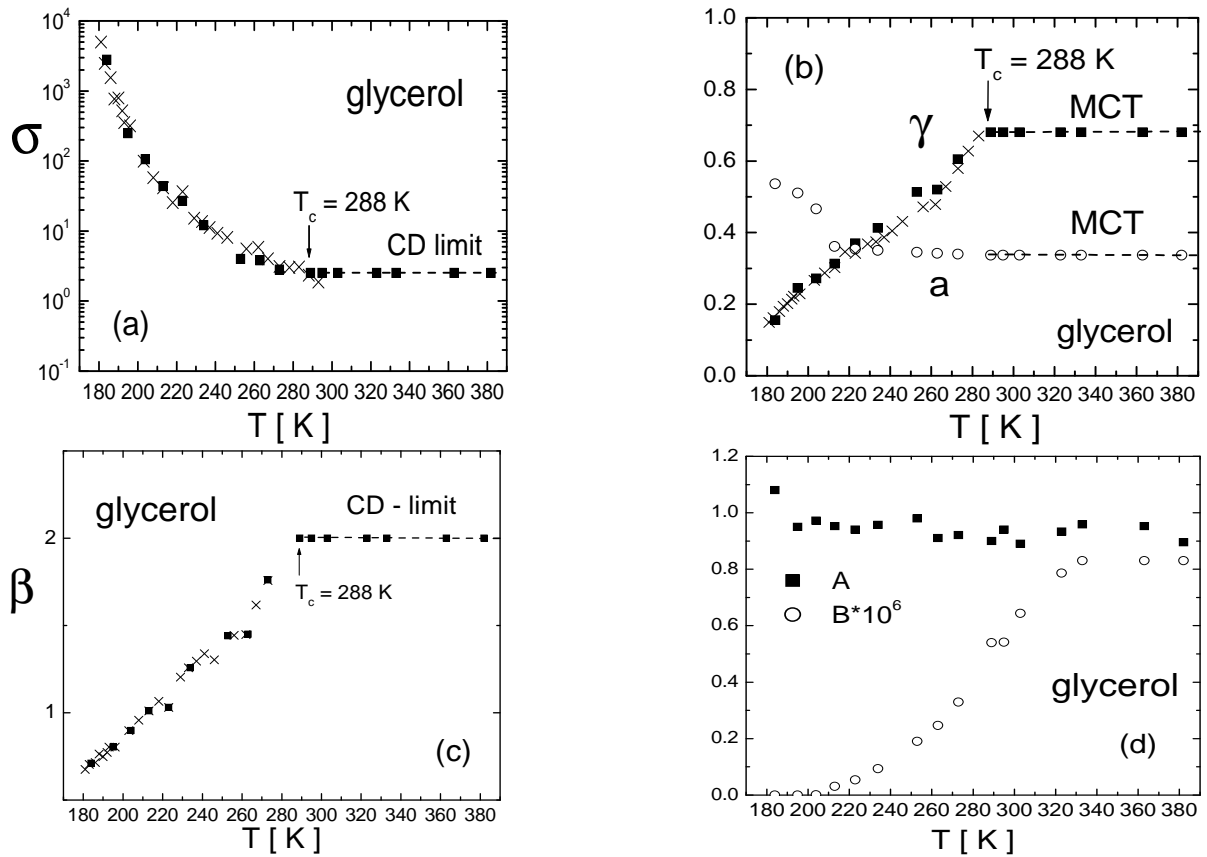


**Figure 5.4:** Fit parameters of the GGE distribution as well as the parameters of the fast dynamics contribution obtained from interpolating the dielectric spectra of glycerol in Fig. 5.3 and Fig. 5.1(a) as function of temperature **(a)** onset parameter  $\sigma$  of the excess wing; **(b)** exponent  $\gamma$  of the excess wing and exponent  $a$  of the fast dynamics contribution; **(c)** width parameter  $\beta$ ; **(d)** amplitude of the  $\alpha$ -process  $A$  and fast dynamics contribution  $B$ .

Blochowicz *et al.* [53, 54] also reported the GGE parameters of the glass formers propylene carbonate and 2-picoline which may be compared to those of glycerol if the parameters are plotted as a function of  $\lg\tau_\alpha$ . This is done in Fig. 5.5.

Although the degree of fragility is quite different within this group of materials, a quite universal behavior is found for  $\sigma$  and  $\gamma$ , and also for  $\beta$  at low temperatures. In first approximation  $\lg\sigma$  linearly increases with  $\lg\tau_\alpha$ , *i.e.*, with the state of supercooling, whereas  $\gamma$  non-linearly decreases reaching values of about 0.15 at highest  $\lg\tau_\alpha$ , that is at the lowest temperatures.

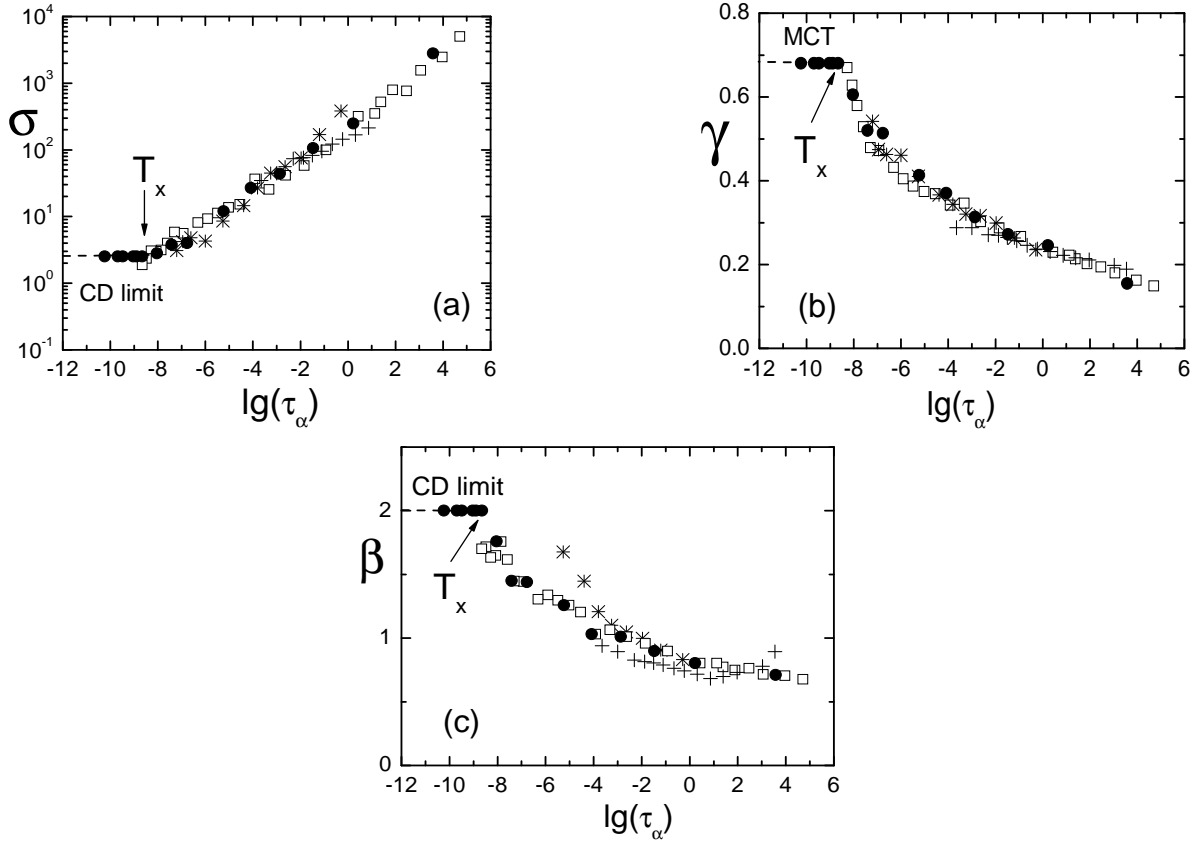


**Figure 5.5:** Fit parameters: (a)  $\sigma$ ; (b)  $\gamma$ ; and (c)  $\beta$  of the susceptibility of the  $\alpha$ -process as a function of  $\lg\tau_\alpha$ ; included are the corresponding data for glycerol, propylene carbonate and 2-picoline from [53, 54]

Since at high temperatures the exponent  $\gamma$  strongly increases,  $\sigma$  becomes close to 1 and  $\beta$  becomes larger than 1 (cf. Fig. 5.4(c)), this is an indication that the *CD limit* is reached (cf. Section 5.2). In other words, at  $T > 289K$  or  $\tau_\alpha < 2 \cdot 10^{-9}$  the excess wing has disappeared, and one finds  $\beta_{CD} = \gamma$  when a CD function is chosen to interpolate the high temperature susceptibility. Therefore, we apply for higher temperatures ( $T > 289K$ ) the GGE distribution together with the constraint Eq. 5.5 which, as discussed, provides an interpolation of a simple peak susceptibility which is very close to a CD function. The result of this fitting procedure is shown in Fig. 5.6 where we display the normalized high temperature data of glycerol.

Here, we included a power-law contribution with a temperature independent exponent  $a = 0.337$  (cf. MCT analysis below) in order to account

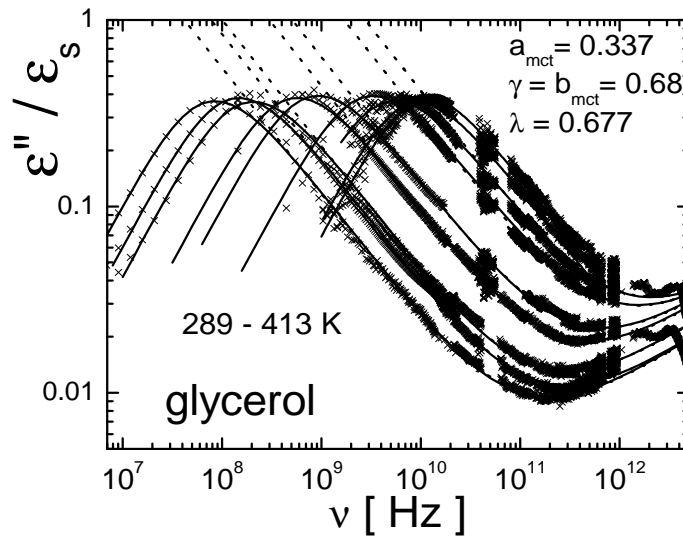


**Figure 5.6:** Normalized imaginary part of the complex permittivity at high temperatures in K (289, 295, 303, 323, 333, 363, 382, 403, 413); interpolation of both  $\alpha$ -process and fast dynamics contribution by the GGE distribution with applying the constraint, Eq. 5.5, and  $\gamma = b_{mct} = 0.68$  (solid lines) together with a power law contribution with  $a = a_{mct} = 0.337$  accounting for the fast dynamics contribution, Eq. 5.6 ; for comparison MCT interpolation of the minimum with  $b_{mct} = 0.68$  and  $a_{mct} = 0.337$  (dashed lines) is shown; at 403 K and 413 K a fit by CD susceptibility is shown.

properly for the fast dynamics contribution up to say 200 GHz. It turns out that the data are compatible with keeping  $\gamma = 0.68$  ( $= \beta_{CD}$ ) independent of temperature. Clearly, also this phenomenological fit yields a satisfying interpolation of the data. Here, we want to note that the data are characterized by very different point densities in the frequency intervals covered by the different dielectric techniques. Also, the scatter is quite large at high frequencies. Therefore, the fits show small systematic deviations from the data in some cases. In Fig. 5.3 fits of the full data set are shown including the constrained fits above 289 K as well as those below by applying free fits with the GGE distribution together with a power law contribution for the fast dynamics. Clearly a very satisfying interpolation is obtained covering 17 decades in frequency. The temperature dependence of the GGE parameter, as well as the parameters of the fast dynamics contribution, *i.e.*, the exponent  $a$  and the corresponding weighting factors  $A$  and  $B$  of the  $\alpha$ -process and the fast dynamics contribution, respectively (cf. Eq. 5.6), are included in Fig. 5.4. At high

temperatures ( $T > 289K$ ) the exponents  $\gamma$  and  $a$  are essentially temperature independent, whereas at low temperatures they show a marked temperature dependence. Below 289 K the exponent  $a$  of the fast dynamics contribution shows a trend to increase. Again, we note that the present dielectric data of glycerol do not allow for an unambiguous determination of the exponent  $a$ . The weighting factor  $A$  is virtually constant whereas  $B$ , reflecting the fast dynamics contribution, decreases strongly below about 320 K. Regarding the evolution of the susceptibility the phenomenological approach provides clear evidence for a high temperature and a low temperature regime with a crossover temperature  $T_x \approx 290K$ . Whereas at high temperatures  $T > T_x$  a simple peak susceptibility with constant relaxation strength (reflected by  $A \approx const.$ ) describes the  $\alpha$ -process together with a temperature independent fast dynamics contribution (reflected by  $B \approx const.$ ) with a constant exponent  $a$ , a new spectral feature appears at low temperatures ( $T < 290K$ ), namely the excess wing. In addition, the weight of the fast dynamics contribution becomes strongly temperature dependent (cf. parameter  $B(T)$ ). In Fig. 5.4 the two regimes are marked and, as it will be demonstrated next, the high temperature scenario is also well described by the asymptotic laws of MCT.

### 5.3.2 Mode coupling theory analysis.

In a second approach we analyze the evolution of the susceptibility as described by the high temperature scenario of the MCT. The theory provides an interpolation of the susceptibility minimum according to Eq. 2.16. Regarding this minimum, a sum of the constrained GGE susceptibility (or a CD function) and a power law accounting for the fast dynamics is mathematically equivalent to Eq. 2.16 provided that  $\gamma = b_{mct}$  and  $a = a_{mct}$  are chosen. Actually, for the phenomenological fit shown in Fig. 5.6 (high temperature data, only) we have already incorporated the MCT relation among  $\gamma$  and  $\alpha$  derived from an exponent parameter  $\lambda = 0.677$  [9]. Consequently, the phenomenological fit (solid line) and the MCT interpolation by Eq. 2.16 (dashed line) of the susceptibility minimum are indistinguishable as is demonstrated in Fig. 5.6. The phenomenological approach covers the complete relaxational spectra whereas MCT provides a generic interpolation of the minimum, only. Thus, the high temperature regime is

described in the phenomenological approach by exponents which are compatible with MCT. Having obtained the minimum parameters (amplitude and position)  $\chi''_{min}$  and  $\nu_{min}$  by the MCT interpolation one is able to test the scaling laws of MCT, Eq. 2.17. Fig. 5.7 presents the results for the linearized relationships  $(\chi''_{min})^2(T)$ ,  $(\nu_{min})^{2a_{mct}}(T)$  and  $(\tau_\alpha)^{-1/\gamma_{mct}}$  as well as  $\eta^{-1/\gamma_{mct}}(T)$  as functions of temperature. Here,  $\tau_\alpha$  is obtained from the phenomenological fit and the viscosity  $\eta$  is taken from the literature [60]. Consistently, the critical temperature  $T_c = 288 \pm 3K$  can be extracted by

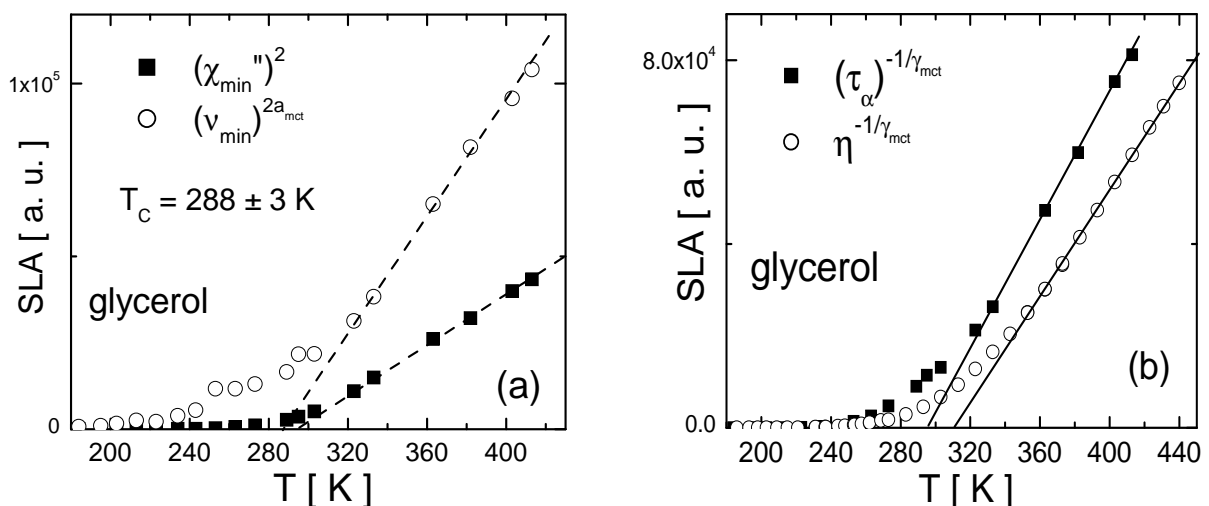


**Figure 5.7:** : Testing scaling laws of MCT; the linearized scaling law amplitudes (SLA) are plotted; the points at 403 K and 413 K in (a) have been obtained from the master curve (cf. Fig. 5.8).

extrapolating the high temperature data  $\chi''_{min}$ ,  $\nu_{min}$  and  $\tau_\alpha(T)$ . The viscosity data extrapolate to a somewhat higher value of  $T_c$ , a phenomenon indicating that  $\eta$  and  $\tau_\alpha$  may exhibit a slightly different temperature dependence at high temperatures. We emphasize that first deviations from the scaling laws appear at somewhat higher temperature than  $T_c$ . Once again we note that in the previous MCT analysis by Lunkenheimer *et al.* [41] the analysis was restricted to temperatures  $T \leq 333K$ . Also, their parameter  $b_{mct} = 0.63$  is somewhat different from that obtained within the present analysis ( $b_{mct} = 0.68$ ). Only including the high temperature data and a normalized susceptibility can a consistent critical temperature be extracted from all the observables, and consequently, the critical temperature is found to be significantly higher with respect to that of the



analysis of Lunkenheimer *et al.* [41].

Another way of demonstrating the validity of the MCT predictions is to re-scale the data  $\chi''(\nu)$  by  $\chi''_{min}$  and  $\nu_{min}$  in such a way as to obtain a master curve for the susceptibility minimum. This is demonstrated in Fig. 5.8. Here we present the data above the critical temperature  $T_c = 288K$  (solid points) as well as below (crosses). Clearly, all data above  $T_c = 288K$  can be collapsed on a master curve for the envelope which is well interpolated by the MCT formula with  $b_{mct} = 0.68$  and  $a_{mct} = 0.337$  as is also revealed by the minimum interpolation in Fig. 5.6, whereas below  $288K$  deviations show up, namely the minimum becomes broader and broader the lower the temperature. This feature reflects the appearance of the excess wing. In other words, the emergence of the excess wing terminates the high temperature scenario of MCT, and thus allows to identify unambiguously the critical temperature.

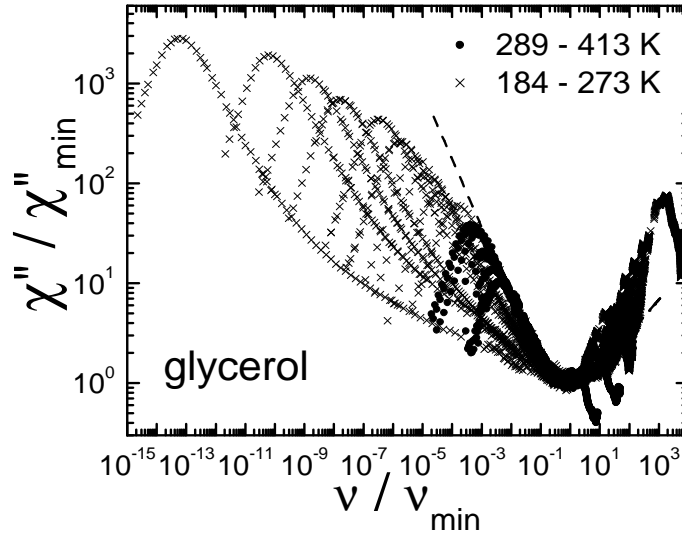


**Figure 5.8:** Rescaled minimum of the susceptibility obtained by scaling the original data (cf. Fig. 5.3) by  $\chi''_{min}$  and  $\nu_{min}$  respectively; solid circles: data at  $T \geq 289K$ , crosses: data at  $T < 289K$ ; dashed line: interpolation by MCT master curve, Eq. 2.16.

Finally, having achieved a complete interpolation of the susceptibility data we can proceed to checking another MCT prediction, namely the anomaly of the non-ergodicity parameter  $f$ , by applying Eq. 5.7. For the cut-off frequency we introduce  $\nu_c = 200$  GHz which ensures that essentially no spectral contribution of the boson peak is included in the integral. Of course, this limit is somewhat arbitrary, but a change from

$\nu_c = 200$  GHz to  $\nu_c = 400$  GHz leads to an increase of  $1 - f$  by a factor of roughly  $2^a$ , *i.e.* only 26% at high temperatures (as  $a \approx 0.3$ ). Fig. 5.9 displays  $1 - f$  as a function of temperature. Below about 300 K a

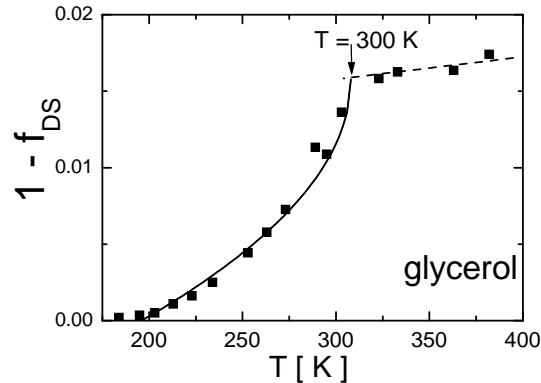


**Figure 5.9:** Non-ergodicity parameter  $1 - f_{DS}$ , cf. Eq. 5.7, as a function of temperature; solid line: square root law of MCT, dashed line: guide for the eye.

significant drop of  $1 - f$  is observed. This is nothing else than the expected *anomaly of the non-ergodicity parameter*, and the data in Fig.5.9 can be fitted with the square root behavior of MCT, Eq. 2.21, yielding a critical temperature  $T_c \approx 300K$ . We note that the absolute value of  $1 - f$  is quite small; the largest value found at high temperatures is  $1 - f \approx 0.017$ .

## 5.4 Discussion and conclusion.

The evolution of the relaxational contribution in the dielectric susceptibility of glycerol has successfully been interpolated covering 17 decades in frequency. Following the lines given by Adichtchev *et al.* [31] and Blochowicz *et al.* [53] we have analyzed the low frequency response at low temperatures (including  $\alpha$ -process and excess wing) within a phenomenological approach, on the one hand, and the high temperature data within MCT, on the other. In the phenomenological approach the crossover temperature  $T_x$  is defined by the disappearance of the excess wing and by reaching the *CD limit* which can be clearly identified in the temperature dependence of the parameters of the applied extended generalized gamma (GGE) distribution. Within asymptotic laws of MCT the crossover is given by the result of the scaling analysis.

Within the experimental error both crossover temperatures ( $T_x$  and  $T_c$ ) agree, and  $T_c \approx 288K$  is extracted from a MCT analysis. In contrast to the previous MCT analysis by Lunkenheimer *et al.* [41] the analysis in the present contribution uses all available high temperature data ( $T \leq 413K$ ) while Lunkenheimer *et al.* restricted their analysis to temperatures  $T \leq 333K$ . Also, dielectric spectra normalized by the static permittivity are analyzed. As a consequence of both, the critical temperature extracted shifted to higher temperatures by roughly 30 K as compared to 262 K in the previous analysis and consistent results are achieved from all scaling observables. As in the case of toluene [17] and 2-picoline (cf. Chapter 4), for reasons not completely understood, the asymptotic laws of MCT describe the dynamics even up to highest temperatures also in the case of glycerol. Only by including that high temperature data a safe foundation for extracting the critical temperature is guaranteed. This is particularly crucial for non-fragile organic glass formers for which the high temperature scenario of MCT may be observed only well above the room temperature. Thus, it may be possible that discrepancies in determining  $T_c$  found also for other systems disappear when the MCT analysis is extended to highest temperatures including even temperatures above the melting point.

We note that re-inspecting the data of a neutron scattering study of glycerol suggests  $T_c \approx 280K$  [43] and that Rössler *et al.* reported  $T_c \approx 310K$  from an analysis of the viscosity [19]. Applying the so-called Stickel plot Lunkenheimer *et al.* [41] found that the Vogel-Fulcher-Tammann equation holds well only below 285 K. Thus, better consistency is now reached among the results from different methods identifying the crossover temperature.

In addition to extracting  $T_c$  from the scaling analysis,  $T_c$  can equally well be identified by the anomaly of the non-ergodicity parameter  $f$  respectively  $1 - f$ . Evaluating the corresponding integrals over the susceptibility by using the fit curves obtained within the phenomenological approach  $1 - f(T)$  is easily determined. In fair agreement the square root behavior of MCT is rediscovered. The absolute value of  $1 - f$  is very small, *i.e.*  $1 - f \leq 0.02$  is observed. Thus, experimentally, it does not make much sense in most cases to determine the anomaly by extracting  $f(T)$  since the latter is always close to 1. This may have important consequences since small values of  $1 - f(T)$  may also show up in an analysis of

depolarized LS spectra. Assuming in first approximation that LS probes the reorientational correlation function of the second Legendre polynomial and dielectric spectroscopy the corresponding function of the first Legendre polynomial and that the fast motion can be described by a spatially highly restricted reorientation within, *e.g.*, a cone model, Blochowicz *et al.* showed that  $1 - f_{LS} = 3(1 - f_{DS})$  [53] (cf. also [61] for a similar discussion). Thus, even for LS experiments it might be difficult to identify the anomaly of the ergodicity parameter in  $f_{LS}(T)$ . In the case of NS  $1 - f$  may become larger [13, 43]. Within molecular mode coupling theory [61]  $1 - f_c(q = 0) \approx 0.02$  has been reported which is very close to the value observed experimentally. In the corresponding simulations it is again found that  $1 - f_{LS} = 3(1 - f_{DS})$  [62].

Concerning the evolution of the susceptibility, our analysis clearly discriminates between a high temperature and a low temperature regime. The first is well described by MCT with an  $\alpha$ -process and fast dynamics contribution being essentially unchanged in spectral shape and amplitude and only  $\tau_\alpha$  changing, whereas the second, the low temperature scenario, is characterized by the emergence of the excess wing. The appearance of the excess wing marks the sole change of the dynamic susceptibility while cooling a type *A* glass former and also marks the break down of the high temperature scenario of MCT. However, concerning the anomaly of the non-ergodicity parameter  $1 - f$  this feature is observed below  $T_c$  thus indicating that at least this MCT prediction remains valid also at  $T < T_c$ . This is the case although the evolution of the excess wing appears not to be included in MCT. Also, below  $T_c$  the exponent  $a$  of the fast dynamics contribution shows a trend to increase, which tentatively may be interpreted as a crossover to a white noise spectrum [31, 43], a feature also predicted by MCT though only at frequencies below the knee which actually is not found. Thus, one may be inclined to conclude that concerning the fast dynamics MCT works also below  $T_c$ . Comparing different glass formers such as glycerol, propylene carbonate and 2-picoline it appears that the crossover is found at a similar state of supercooling, *i.e.* always in the range  $10^{-9} < \tau_\alpha < 10^{-8}$  s. In the case of glycerol  $\tau_\alpha(T_c) \approx 10^{-9}$  s is observed. As discussed the excess wing is hardly to be taken as a part of a continuing ( $T < T_c$ )  $\alpha$ -process but rather as a special secondary relaxation process [56, 57]. This process manifests itself in a very simi-

lar way in all type  $A$  glass formers when the line shape parameters are plotted as function of the time constant  $\tau_\alpha$ . No significant difference is found between the fragile system propylene carbonate and glycerol exhibiting an intermediate degree of fragility and both systems follow the MCT predictions at high temperatures. The only important difference found for the spectral shape of the susceptibility refers to the shape of the  $\alpha$ -relaxation peak itself. The width parameter  $\alpha$  defining the time end of the distribution function  $G_G GE(\ln\tau)$  is temperature independent but different for the various systems. In other words only the slowest dynamics exhibit non universal features. Future experiments on other type  $A$  glass formers which essentially have to cover all experimentally accessible frequencies will tell whether this statement survives progress. First analysis of type  $B$  glass formers indicate that some universality is lost (depending on the relaxation strength of the  $\beta$ -process) but still both the excess wing as well as the  $\beta$ -process contribution itself happen to merge with the  $\alpha$ -process at the critical temperature [53]. Concluding, we say that although clarifying the physical nature of the slow response of a glass former with an emergence of the excess wing is still a future task to be solved, the proposed approach yields a complete interpolation of the susceptibility spectra of type  $A$  glass formers, provides a clear cut identification of the spectral changes occurring while supercooling and reproduces the MCT scenario at high temperatures, *i.e.* allows for determining unambiguously the critical temperature  $T_c$  also in the case of a non-fragile system.

# 6 Fast relaxation processes in glasses tested by quasi-elastic light scattering

## 6.1 Introduction

In the last decades, many experimental and theoretical works that addressed the problem of the glass transition were made [9, 18, 64, 66, 70, 117]. Understanding the dynamic susceptibility of simple glass formers as it evolves from high temperatures down to the glass transition temperature was the main goal. Here, significant progress was made. In contrast to that, the molecular dynamics persisting in the glass, *i.e.* below  $T_g$ , is less investigated. Since the main relaxation ( $\alpha$ -process) is frozen all persisting relaxational contributions are characterized by small amplitudes, and broad band spectra allowing for a systematic description down to cryogenic temperatures are rare. On the other hand, the anomalies of glasses at low temperatures attracted a lot of attention; however, most of the works focused on temperatures below say 4 K, and mainly inorganic network glasses were studied [25, 26, 27]. It is not clear whether such glasses exhibit the same relaxational patterns as molecular glasses. In some organic polymers the typical linear increase of the heat capacity was indeed identified [65]. However, at more elevated temperatures, the relaxational features of polymers are often obscured by side group or end group relaxation. Recently, a dielectric study covering the kHz range reported quite similar relaxation behavior in molecular glasses below say 30 K as found for silica [79]. Yet, further studies are needed, and the present contribution is intended to address this issue by presenting quasi-elastic light scattering (QELS) data to address the question of fast relaxation

processes in glasses.

In order to describe the low-temperature anomalies of glasses, in particular the anomalous specific heat, the tunneling model was introduced which postulates the existence of certain defects that are described by asymmetric double well potentials (ADWP), and at low temperatures the barrier is crossed via tunneling [25]. This standard tunneling (ST) model describes well the anomalous heat capacity, as well as, *e.g.*, the low-temperature internal friction; it turns out that the relaxational features of many glasses are remarkably similar up to temperatures of say 4K [25, 26, 27]. Though providing a satisfying phenomenological description of mostly inorganic systems, the model does not explain the origin of the defects, which is still an open question. It appears natural to extend the approach of ST model to higher temperatures, where thermally activated crossing of the barrier of the ADWP is expected to dominate. Jäckle [79] as well as Gilroy and Phillips (GP) [78] proposed such an approach, and the data of silica among others were interpreted within this frame [79, 81, 82, 83]. At  $T > 10\text{K}$  the relaxational behavior is determined only by the distribution of barrier heights  $g(V)$  of the ADWP's; GP discussed a simple exponential distribution without a cut-off at low energies [78]. Thus, the distribution  $g(V)$  can be estimated from high-temperature data, whilst it is not possible to directly extract it from the low-temperature tunneling data. However, it is not clear what fraction of the total ADWP's present in a glass is actually responsible for the tunneling states. Furthermore, it appears that the high-temperature relaxation processes exhibit a less degree of universality than the low temperature processes. Nevertheless, the typical barrier height  $V$  was found to be of the order of  $k_B T_g$ , as may be expected from freezing of density fluctuations at  $T_g$  [26, 65, 78, 82, 91]. Due to such relatively low barriers the relaxations are fast close to  $T_g$ , and they are expected to determine the response of glasses in the GHz regime and to show up in the QELS spectra.

Above  $T_g$ , in addition to the main  $\alpha$ -relaxation, fast relaxational features can likewise be identified. A relaxational process in the ps regime was identified by neutron and light scattering and attributed to in-cage motion within the mode coupling theory [9]. This process is found in the same frequency range where the fast dynamics in ADWP's is expected to

show up. Close to  $T_g$ , the so-called excess wing of the  $\alpha$ -process emerges, which can be described by a power-law contribution with an exponent significantly smaller than the corresponding one of the  $\alpha$ -peak itself [46, 47]. The exponent appears to decrease with temperature and below  $T_g$  becomes small and essentially temperature independent [47, 65]. In other words, the excess wing degenerates to a nearly constant loss (NCL) extending over decades in the Hz - MHz range. Finally, in some glasses, in addition, a more or less strong secondary relaxation peak was identified and attributed to the Johari-Goldstein (JG)  $\beta$ -process [48]. At  $T < T_g$  the temperature evolution of the  $\beta$ -process susceptibility can be described assuming a thermally activated process with a Gaussian distribution of barrier heights [48, 49]. Its mean activation energy  $E$  correlates with  $T_g$ ; a relation  $E = 24T_g$  was found in many systems, though there are exceptions to this rule [49, 50]. Recent experiments showed that the JG process involves small angle reorientation of essentially all molecules [51, 52]. Although both the fast ADWP dynamics and JG process can formally be described by a suitable distribution of activation energies, it turns out that the typical barrier heights are quite different.

The described processes may be called secondary relaxation processes in the sense that they involve spatially highly restricted motion of the entire molecule. Secondary relaxation processes are believed to be intrinsic to glass, since they are observed in all glass formers. Finally, we note that anharmonicity effects can also produce quasi-elastic contributions in scattering experiments and which may compete with the other relaxation sources [111]. Concluding, understanding the variety of relaxational features in glasses still provides a challenge.

In past years studying quasi-elastic light scattering (QELS) with tandem Fabry-Perot interferometer together with a double monochromator provided valuable information concerning the fast dynamics mainly above  $T_g$ . To obtain useful data in the GHz range below  $T_g$ , the LS technique has to be pushed to its limit [21, 81, 82]. Actually, given the small amplitudes of the secondary relaxation processes in glasses, the accessible frequency window narrows with decreasing the temperature. Nevertheless, first results for temperatures below  $T_g$  were recently presented [81, 82, 83, 84, 88]. The low-frequency part of the LS spectra was described by a power-law contributions with a positive exponent, and in the case of silica and potas-



sium calcium nitrate (CKN), the spectra can be described within the GP model with an exponential distribution  $g(V)$ .

Fig. 6.1(a) gives an example of the spectra for silica (cf. [82]).

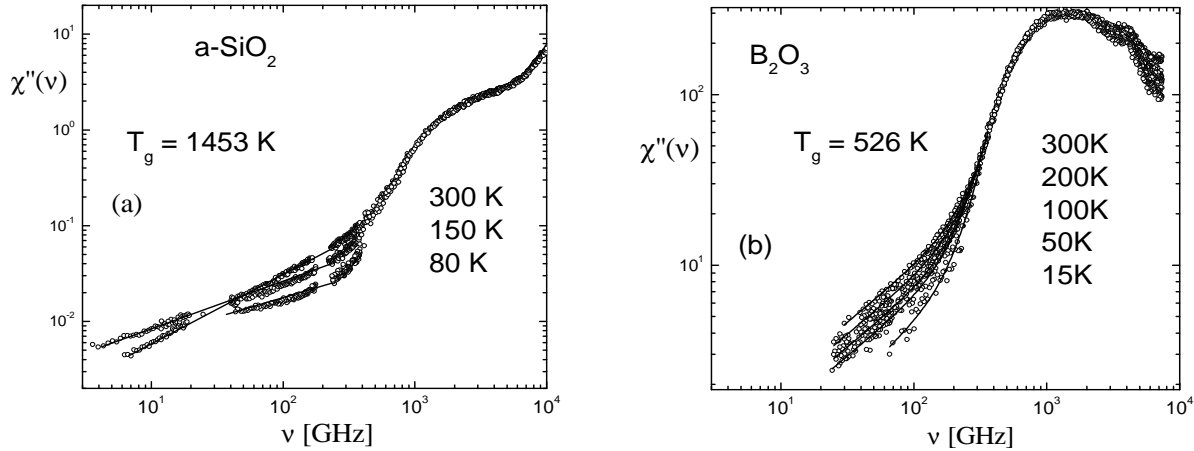


**Figure 6.1:** Depolarized light-scattering spectra in inorganic glasses (open circles): (a) silica glass (data from [82]) and (b)  $B_2O_3$  (data from [88]). Solid lines correspond to the fit by Eq. 6.1.

The exponent of the low-frequency power-law contribution is found to be proportional to temperature as expected from the GP model. However, for other systems such as boron oxide (cf. Fig. 6.1(b)) as well as several molecular glasses this model appeared not to work [84, 88]. The spectra increase in intensity with the temperature, while the shape is essentially temperature independent.

## 6.2 Light-scattering spectra

Figs. 6.2 show depolarized LS susceptibility spectra  $\chi''(\nu) = I(\nu)/[n(\nu) + 1]$  of the molecular glasses m-tricresyl phosphate (m-TCP), o-terphenyl (OTP), 2-picoline, ethanol. Here,  $I(\nu)$  is the LS spectral density and  $n(\nu) + 1$  the Bose factor. In all the spectra, the frequency range above 500 GHz is dominated by the vibrational contribution (including the boson peak) that at  $T < T_g$  is essentially temperature independent, and above about 1 THz by intramolecular vibrations. Thus, the spectra were normalized to the same integrated intensity at high frequencies in THz

6 Fast relaxation processes in glasses tested by quasi-elastic light scattering

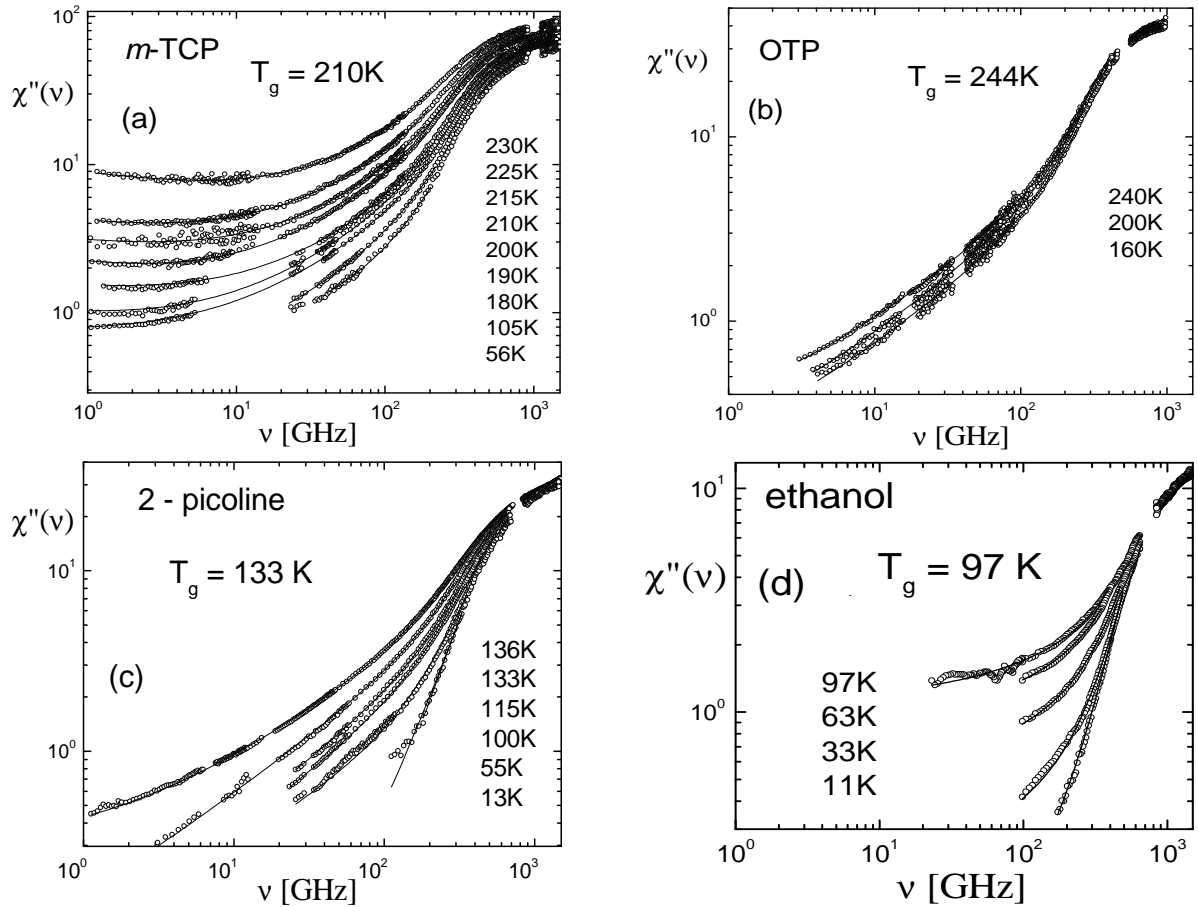


**Figure 6.2:** Depolarized light-scattering spectra of molecular glasses (open circles): (a) m-TCP, (b) OTP, (c) 2-picoline, (d) ethanol. Solid lines correspond to the fit by Eq. 6.1.

range. In the low-frequency part of the spectrum, say  $\nu < 300$  GHz, fast relaxation contributions dominate.

Qualitatively, the GHz relaxation spectra are similar in all the glasses under study. A common feature is an increase of the QELS intensity with temperature. In most cases, this relaxational part cannot be described by a simple power-law as is the case in silica or boron oxide (cf. Fig. 6.1). For m-TCP and ethanol, at least, there is a clear an apparent flattening of the spectra at the lowest attainable frequencies that we tentatively attribute to a NCL contribution. In ethanol this contribution is clearly seen at least at  $T = T_g = 97$  K where it dominates at  $\nu < 80$  GHz. For m-TCP, at the highest temperature  $T = 230$  K that is already above  $T_g$ , one actually recognizes a flat minimum. Thus, one can conclude that in

the spectra of all glasses presented in Fig.6.2 a more or less pronounced NCL contribution may be anticipated in order to explain the deviation from a simple power-law spectrum, the latter being attributed to the fast dynamics.

## 6.3 Spectra analysis

Thus, three contributions can be distinguished in the LS spectra of the various glasses originating from: i) vibrations ii) fast relaxation and iii) NCL. We are going to fit the LS spectra by assuming an additive superposition of these three spectral contributions. According to the Section 2.3, the vibrational contribution can be described by a power-law  $c\nu^h$ , where  $c$  is a constant. For the fast relaxation contribution again a power-law frequency dependence,  $b\nu^\alpha$ , is expected (cf. Eq. 2.26). Unfortunately, the accuracy and the frequency range of our data are insufficient to reliably distinguish a truly constant loss (CL),  $a$ , from NCL  $a\nu^{-\gamma}$  with a small exponent  $\gamma = 0 - 0.2$ . Thus, in order to decrease the number of fitting parameters we used the simplest case  $\gamma = 0$ , *i.e.*, we assume that adding a CL contribution is adequate for describing our LS spectra. Thus, we use the following fit function

$$F(\nu) = a + b\nu^\alpha + c\nu^h. \quad (6.1)$$

The exponent  $h$  of the vibrational term was found by fitting the spectra at the lowest temperatures, as shown in Figs. 6.1 and 6.2, *i.e.*, the spectrum at 80K in  $SiO_2$ , 15 K in  $B_2O_3$ , 56 K in m-TCP, 160K in OTP, 13 K in 2-picoline, 11 K in ethanol. It turned out that for a given glass the exponent exhibits only small variations with temperature. Thus, we assumed that the exponent  $h$  is temperature independent at  $T < T_g$  while the exponent  $\alpha$  as well as the amplitudes  $a$ ,  $b$  and  $c$  in Eq. 6.1 may depend on temperature. Thus, a four-parameter fit is used to interpolate the LS spectra covering 2 - 3 decades in frequency. The respective fits are shown in Figs. 6.2(a), (b), (c) and (d). Clearly, a very satisfying interpolation is found. Unfortunately, the LS spectra shown cannot be significantly improved with the state-of-the-art TFPI techniques, and that, since the

scattered light intensity decreases with temperature, the accessible low-frequency limit then moves up. Thus, at the most interesting lowest temperatures the available data are insufficient to satisfactorily justify the use of Eq. 6.1. Nevertheless, applying Eq. 6.1 may be taken as a first attempt to unravel some common spectral features of the LS spectra of glasses.

As said, in the fits of the data for m-TCP and ethanol there is an indication of the CL contribution at the lowest accessible frequencies. In OTP and 2-picoline the CL contribution is less clear; however free fits to Eq. 6.1 result in a non-negligible  $a$  also for these glasses. In  $B_2O_3$  the QELS spectra can be fitted equally well to either a combination of CL and a power law with the slope  $\alpha = 0.9 - 1$ , or to a power law with  $\alpha \cong 0.65$  alone. Measurements at lower frequencies are needed to discriminate the two cases.

The relaxation spectrum  $\chi''_{fast}(\nu)$  can be estimated by subtracting the CL and vibrational contributions from the total spectrum:

$$\chi''_{fast}(\nu) = \chi''(\nu) - a - c\nu^h. \quad (6.2)$$

The so-extracted  $\chi''_{fast}(\nu)$  of OTP is shown in Fig. 6.3 for a few temperatures. Clearly, the relaxation spectra have a power-law wing at the low-

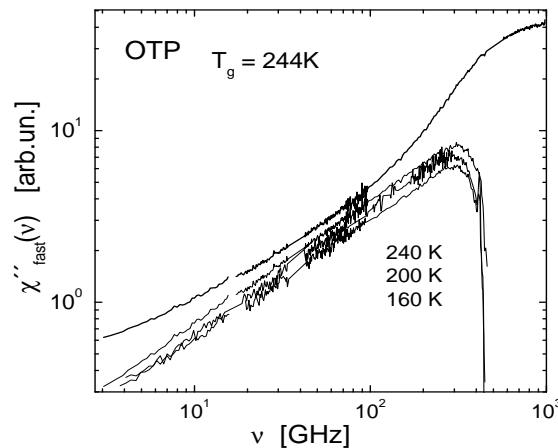


**Figure 6.3:** Light-scattering spectra of the fast relaxation in OTP obtained after subtracting the constant loss and vibrational contribution from the experimental spectra; for comparison the experimental spectrum at  $T = 240$  K is shown.

frequency side of the maximum and a cut-off at the high frequency side,

the latter being steeper than in the case of a Debye spectrum. Qualitatively, the shape of the spectrum reflects the distribution of the relaxation rates [78, 82]. The frequency of the maximum of  $\chi''_{fast}(\nu)$  is of the order of a typical molecular attempt frequency.

The exponent  $\alpha$  that characterizes the slope of the relaxation contribution is shown in Fig. 6.4 as a function of the reduced temperature  $T/T_g$ . For the rest of the glasses  $\alpha$  increases with the temperature below  $T_g$  in

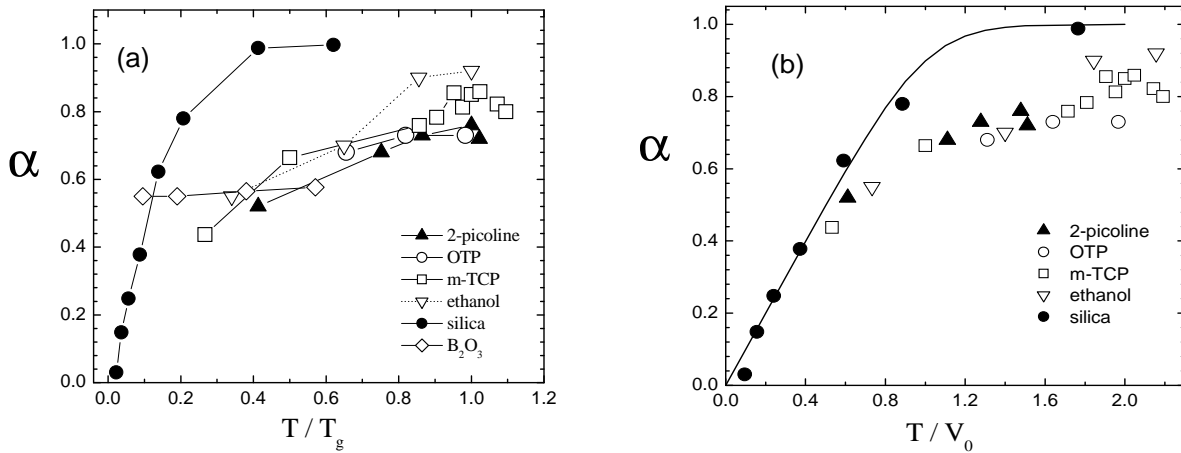


**Figure 6.4:** Temperature dependence of the exponent  $\alpha$  as a function of: (a)  $T/T_g$ , (b)  $T/V_0$ .  $\blacktriangle$  - 2-picoline,  $\circ$  - OTP,  $\square$  - m-TCP,  $\nabla$  - ethanol,  $\diamond$  -  $B_2O_3$ . For comparison,  $\alpha$  is shown also for silica ( $\bullet$ ). Solid line in Fig. (b) refers to prediction of the Gilroy-Phillips model with an exponential barrier distribution  $g(V)$ .

a somewhat different manner, so that three groups may be recognized in Fig. 6.4(a): i) silica, ii) molecular glasses, and iii)  $B_2O_3$ . In silica  $\alpha(T/T_g)$  increases quite fast and reaches 1 already at low value of  $T/T_g$ . In all the molecular glasses  $\alpha(T/T_g)$  data approximately fall on a common master curve and  $\alpha$  is steadily increasing with  $T/T_g$ . In  $B_2O_3$   $\alpha(T/T_g)$  is virtually temperature independent ( $\alpha \approx 0.55$ ). All the data may be collapsed on a single master curve when  $\alpha$  is plotted as a function of  $T/V_0$ , where  $V_0$  defines the starting slope of  $\alpha(T)$  at the lowest temperatures (cf. Fig. 6.4(b)). In 2-picoline, OTP and ethanol there is not enough low-temperature data to reliably identify the slope  $\alpha$ , so the parameter  $V_0$  was chosen in such a way that the experimental points lie on the master curve. Except for silica, for which the data at highest  $T/V_0$  lie somewhat above, all the data follow a common curve.

In the fit function, Eq. 6.1, the vibrational contribution is represented by the term  $\chi''_{vib} \propto \nu^h$ . A Debye-like density of states,  $g_{Deb}(\nu) \propto \nu^2$  corresponds to  $h = 2$ . The boson peak by definition shows a higher exponent  $h$ . Indeed, the results of the fit demonstrate that the exponent  $h$  is higher than 2, but it is less than 4, the exponent predicted by the soft potential model [84].

We now consider the CL amplitude relative to the amplitude  $\chi''_{max}$  of the vibrational band at 1 – 2 GHz

$$a_n = \frac{a}{\chi''_{max}} \quad (6.3)$$

and show its temperature variation for different glasses in Fig. 6.5. Inspecting Fig. 6.5, the parameter  $a_n$  in molecular glasses is  $\sim 10^{-2} - 10^{-1}$

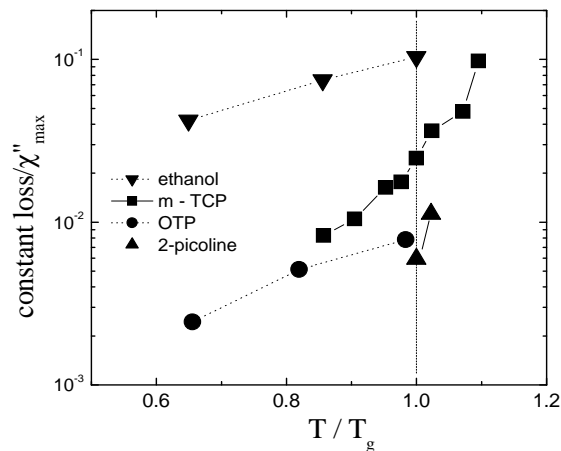


**Figure 6.5:** Temperature dependence of the constant loss intensity  $a_n$  normalized to the maximum of the microscopic vibrational band (cf. Eqs. 6.1 and 6.3). ▼ - ethanol, ■ - m-TCP, ● - OTP, ▲ - 2-picoline.

at  $T_g$ . In OTP and 2-picoline  $a_n$  is less by an order of magnitude than in ethanol and m-TCP. Below  $T_g$ , the temperature dependence of the CL amplitude can be described in fair approximation by an exponential,

$$a \propto \exp\left(\frac{T}{T_0}\right) \quad (6.4)$$

with  $T_0 = 30 - 40$  K for ethanol, m-TCP, 80 K for OTP.

In the glasses with pronounced temperature dependence of the exponent  $\alpha$  of the fast relaxation spectrum, the behavior is qualitatively similar to that in silica, studied earlier [82]. At low temperatures,  $\alpha$  increases linearly with the temperature, in agreement with the GP model [78] and shows a trend to saturate at higher temperatures. The curve  $\alpha(T/T_g)$  for molecular glasses is quite similar and lies below the curve of silica. Thus, one can assume that thermally activated ADWP dynamics is the main source of the fast relaxation also in molecular glasses. In the GP model (cf. Section 2.3), it is assumed that the distribution of barriers  $g(V)$  decays exponentially as a function of  $V$  with no cut-off at low energies. This yields  $\alpha = T/V_0$  at  $T \ll V_0$  and  $\alpha = 1$  at  $T \gg V_0$ . More generally, as a function of  $T/V_0$ , the exponent  $\alpha$  is expected to follow a master curve. This is shown in Fig. 6.4(b). In these coordinates, the temperature dependence of  $\alpha$  is quite similar in molecular glasses and silica, *i.e.*, a master curve is observed at least up to  $T/V_0 \cong 2$ . As noted, in the GP model  $\alpha$  should approach 1 at high temperatures and this is indeed observed in the case of silica at  $T > 500$  K [80]. Thus, the available data for silica are in full agreement with the quantitative prediction of the GP model (cf. Eq. 2.25) assuming an exponential distribution  $g(V)$  (solid line in Fig. 6.4(b)). The somewhat weaker increase of  $\alpha$  with  $T/V_0$  in the molecular glasses as compared to that of silica may indicate deviations from a simple exponential distribution  $g(V)$ . In the molecular glasses the analysis yields  $V_0 \sim T_g/2$ . We stress that in the cases of glassy 2-picoline, ethanol, OTP, and m-TCP we can only conclude that the data do not contradict the GP model, the absence of low-temperature data precluding further analysis. If ADWP dynamics is the main source of the fast relaxation, the relaxation strength of the fast relaxations is expected to be temperature independent [81]; more exactly, it is proportional to the number of ADWPs, which is supposed to be constant in the glassy state ( $T < T_g$ ).

# 7 Study of the structural glass and glassy crystal of ethanol and cyano cyclohexane

This chapter follows the publication [85].

## 7.1 Introduction

In structural glasses, coupling between the translational and orientational degrees of freedom makes it difficult to understand the essential mechanism underlying the glass transition phenomenon. Fortunately, there are substances which exhibit only orientational disorder: plastic crystals and orientational glasses. In plastic crystals, the molecular centers of mass preserve the crystalline order but the molecules rotate more or less freely. Upon cooling, such plastic crystals can form a glassy crystal at  $T = T_g$ , where the molecular orientation freezes, exhibiting features characteristic of a glass transition as found in structural glasses. If cooled sufficiently slow, the plastic crystal may transform into an orientationally ordered crystal via a solid-solid phase transition. In contrast, so-called orientational glasses cannot be brought into an ordered phase due to strong frustration effects. In glassy crystals, the dynamics associated with the glass transition presumably may be simpler to understand in comparison with that of structural glass formers where both rotations and structural disorder coexist. Thus, glassy crystal may be taken as simplified model of the glassy state in which translational degrees of freedom essentially are excluded from the dynamics because of structural periodicity but exhibiting all the characteristic features of structural glasses including a boson peak and low temperature anomalies [95, 102].



The investigation of the fast relaxation processes in the glassy crystal phase of ethanol and in the glassy/plastically crystalline phase of cyano cyclohexane (CCH) by LS is presented in this chapter. For comparison, the same measurements are performed for the structural glass of ethanol. Ethanol is convenient for comparative investigations of the dynamics in the structural glass and glassy crystal since it can be easily prepared in both phases, and the same  $T_g = 97$  K is found [96, 97]. In the case of ethanol only a rather short temperature range above  $T_g$  is accessible where it can be studied in the supercooled plastic crystal before transformation to the ordered phase occurs. Below  $T_g$  both phases are stable, allowing QELS measurements. There is no such limitation in the case of CCH, which is stable in the glassy/plastically crystalline state over a large temperature range up to the melting point  $T_m = 285$  K ( $\sim 2T_g$ ). For both ethanol and CCH dielectric spectroscopy (DS) data were reported [96, 98, 99, 102] and also measurements of the heat capacity [95]. In addition to an  $\alpha$ -process a comparatively fast Johari-Goldstein process was identified by DS for both materials.

Two kinds of experiments were performed: Measurement of the polarized LS spectra including the Brillouin line, that provide information on the damping of 5 – 20 GHz phonons, *i.e.* on the corresponding internal friction, and measurement of the depolarized LS spectra in the range 1 GHz – 1500 GHz.

## 7.2 Experimental conditions

a) **Samples.** Ethanol and cyano cyclohexane (CCH) were purchased from Aldrich, Germany. The ethanol sample had water content  $< 0.001$  % and was used without further purification. The CCH sample was of 98% purity and was distilled prior to measurement. The samples were sealed in Duran cuvettes after several freeze-and-pump degassing cycles.

b) **Light scattering experiments.** Low frequency (1–1500 GHz) light scattering (LS) spectra were measured applying a six-pass Sandercock Tandem Fabry-Perot interferometer (TFPI) [23] and an Ar<sup>+</sup> laser at a wavelength 514.5 nm with a power 250 mW. Details of the experiment are described in the experimental chapter. In order to study position

$\nu_{\text{Br}}$  and width  $\Gamma_{\text{Br}}$  of the Brillouin line measurements of the polarized LS with a FSR = 30 GHz and single scan were performed in backscattering geometry. The frequency and the width are obtained as discussed in detail in the Appendix.

c) **Preparation of the different phases**

1. *Ethanol.* The structural glass of ethanol was obtained by cooling the liquid through the glass transition temperature ( $T_g = 97$  K [98]) with a cooling rate of about 10 K/min which is sufficient to avoid crystallization. In order to obtain the plastically crystalline phase of ethanol, the supercooled liquid was annealed at  $T = 105.0$  K or 106.5 K. The transformation process was controlled by monitoring the Brillouin line position. Since the supercooled liquid and plastic crystal have different Brillouin line positions (14.7 and 15.1 GHz, respectively, at  $T = T_g$ ), the kinetics of the transformation can easily be followed. The transformation time  $\tau_p$  (the time when 50 % of the substance had transformed into the plastic crystal) was found to be 3 hours and 1.5 hours at  $T = 105.0$  K and 106.5 K, respectively. This is in a good agreement with a study of the transition by dielectric spectroscopy [96]. For waiting times  $> 2\tau_p$ , the Brillouin lines did not undergo detectable changes any longer. The total annealing time was  $\approx 5\tau_p$ . At low temperatures ( $T < T_g$ ) the Brillouin spectrum of ethanol in the glassy crystal revealed a low-frequency shoulder. Its position corresponded to the Brillouin line position in the structural glass. Quantitative decomposition of the experimental spectrum by two contours indicated the presence of about 5% of the structural glass in the sample of the plastic crystal of ethanol. As it will be seen in what follows, the LS spectra of the two phases are very similar; that is why we neglect the small fraction of the structural glass in our analysis.

2. *Cyano cyclohexane.* At room temperature cyano cyclohexane (CCH) is a liquid. At the melting temperature  $T_m = 285$  K the liquid transforms into the plastic crystal, and at  $T_g = 134$  K into the glassy crystal [98]. It was found that in the temperature range 250 – 285 K the cooling rate influences the optical quality of the sample. The best quality was obtained for a cooling rate 0.1 K/min. Moreover, the QELS measurements in the temperature range 270 – 285 K were not reproducible due to phase instability. That is, not only the optical quality but also the dynamics was strongly influenced by the speed of cooling from the liquid to the plasti-

cal crystal. For example, the manifestation of the primary  $\alpha$ -relaxation contribution to the LS spectra changed by different cooling rates. In Fig. 7.1 the QELS spectra of CCH recorded at  $T = 250$  K are compared for two different cooling rates. It is seen that while the spectra are the same in the range where the fast relaxation and the boson peak dominate ( $\nu > 30$  GHz), the  $\alpha$ -relaxation contribution shows up only in the case of the sample with a high cooling rate. This sample exhibits a broad Brillouin peak around 10 GHz probably due to the development of high stresses during rapid cooling. We observed also that slow cooling through the phase transition in the presence of the focused laser beam can lead to a spectrum like in the case of the rapid cooling. These facts can be explained if there are two plastically crystalline phases. Indeed, the DSC curve of CCH reveals a small peak at  $T = 270$  K. This situation is not an exception, the existence of two phases of plastic crystals distinguished by different  $\alpha$ -relaxation time was reported also for adamantanone [102]. For obtaining the depolarized LS experiment we used only the temperature regions  $T \leq 250$  K and  $T \geq 285$  K. In Fig. 7.1 the dielectric data from [98] are added for comparison. There is a good agreement between the

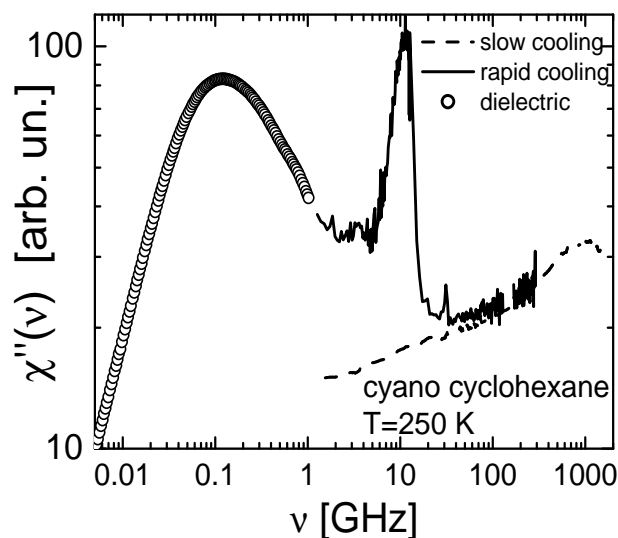


**Figure 7.1:** Light scattering spectra of cyano cyclohexane recorded at  $T = 250$  K for two different cooling rates. Solid line: rapid cooling, dashed line: slow cooling. For comparison, the dielectric spectrum of cyano cyclohexane (amplitude adjusted) at the same temperature obtained by rapid cooling is shown by open circles (data from [98])

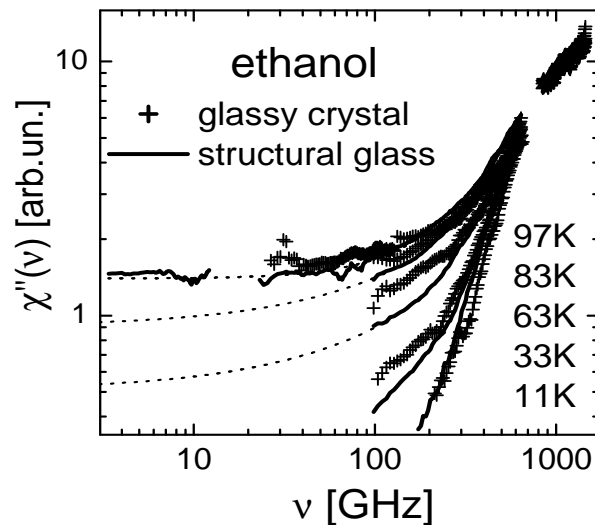
LS spectrum of the rapidly cooled sample and the dielectric spectrum.

There is no agreement in the case of slow cooling. Actually, rapid cooling rates were also applied in dielectric spectroscopy measurements [98]. On the other hand, the cooling with a low rate (0.1 K/min) always leads to a well defined phase with reproducible LS spectra. In the rest of this chapter will be discussed the results only for this plastically crystalline phase of CCH, and when comparing the LS results with those from dielectric spectroscopy one has to keep this difference in mind.

## 7.3 Results and analysis

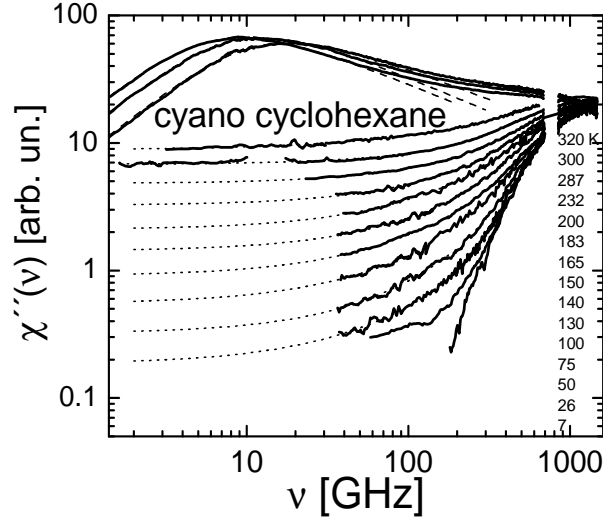
### 7.3.1 Depolarized light scattering

Fig. 7.2 exhibits the depolarized LS susceptibility spectra,  $\chi''(\nu) = I/[n(\nu) + 1]$ , of the structural glass of ethanol as well as of the glassy crystal at various temperatures  $T \leq T_g$ ,  $I$  being the LS intensity and  $n(\nu)$  the Bose factor. In Fig. 7.3 the corresponding spectra of cyano cy-



**Figure 7.2:** Depolarized light scattering susceptibility for the structural glass (solid line) and the glassy crystal (crosses) of ethanol ( $T_g = 98$  K). Dotted line: fit by Eq. 7.1.

clohexane (CCH) are shown. In the case of CCH the data from the liquid phase are also included. One can clearly see a main relaxation peak ( $\alpha$ -process) in the spectra of liquids.



**Figure 7.3:** Depolarized light scattering susceptibility of the glassy crystal of cyano cyclohexane ( $T_g = 134$  K); dotted line: fit by the function (7.1); data at  $T \geq 287$  K from the liquid phase, dashed line: fit with a Cole-Davidson susceptibility

The corresponding time constants  $\tau_\alpha$ , as obtained by fitting these spectra with a Cole-Davidson susceptibility, are plotted in Fig. 7.10(b). In the frequency range above 300 GHz all spectra are dominated by vibrational contribution (boson peak). Relaxational processes are responsible for the strong increase of the susceptibility's amplitude with temperature in the low frequency part of the spectrum ( $\lesssim 300$  GHz). Qualitatively, the fast relaxation spectra of the structural glass and the glassy crystal of ethanol look very similar. Comparing the differences quantitatively two features are observed. First, the vibrational spectrum exhibits differences which are best recognized when the data measured at the lowest temperature, *i.e.*, 11 K, is displayed in the spectral density representation, *i.e.*, as  $\chi''(\nu)/\nu$  (cf. Fig. 7.4). At this temperature, the vibrational spectrum dominates down to  $\sim 0.25$  THz, *i.e.*, the relaxational contribution has become very small. In the frequency range 0.3 – 1 THz the boson peak amplitude is smaller by about 10 – 20% in the case of the glassy crystal. The second difference is that the relaxational contribution in ethanol is higher for the glassy crystal by about 10 – 20% (cf. Fig. 7.2). In other words, in the structural glass a stronger boson peak is connected with weaker relaxation contribution, the opposite relation is found in the glassy crystal. These findings well correspond to the difference in the respective

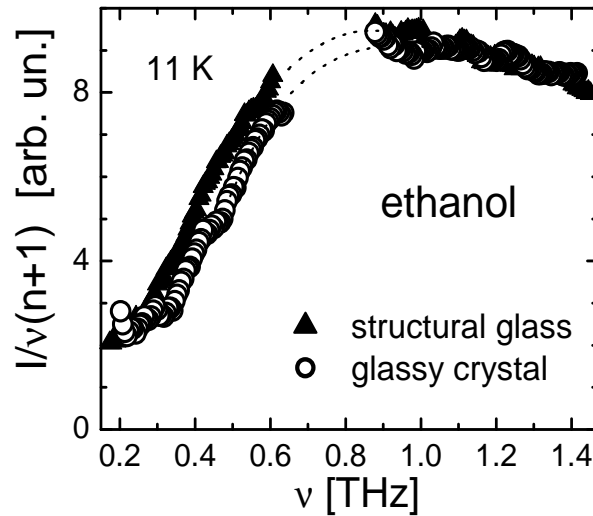


**Figure 7.4:** Boson peak in the depolarized light scattering spectra of ethanol at  $T = 11$  K in the spectral density representation; dotted line: guide for the eye.

vibrational density of states as found by Ramos *et al.* [95] investigating the low temperature specific heat.

Regarding the shape of the relaxation spectrum and its evolution with temperature again high similarity is found for both ethanol phases as well as for the glassy crystal of CCH. For CCH, at  $T = 232$  K and 200 K the spectra are measured down to 2 – 3 GHz. At these temperatures, the spectra exhibit a frequency independent behavior, explicitly  $\chi''(\nu) = const$ , from lowest frequencies up to a few tens GHz. Tentatively, this behavior can be attributed to a nearly constant loss (NCL) contribution. At lower temperatures it was possible to measure spectra only down to 20 – 30 GHz. Here, the crossover to somewhat flatter spectra at low frequencies may be indicative for a significant NCL contribution also at these temperatures. In the case of ethanol, data at  $T = 97$  K were compiled down to 4 GHz for the structural glass and down to 20 GHz for the glassy crystal. The spectrum also exhibits a NCL behavior from lowest frequencies up to  $\sim 60$  GHz. At lower temperatures, data are only available at  $\nu \geq 100$  GHz because ethanol (as CCH) scatters light very weakly, *i.e.*, here a NCL contribution, if any, is again not explicitly measured, although the decreasing of the apparent slope of the spectra below  $\nu \sim 100$  GHz may be a signature of a NCL contribution increasing with temperature. At these low temperatures, the spectra (displayed on a double logarithmic scale)

of both phases exhibit an increase of the slope (power-law exponent) from 0.5 – 0.8 at  $\nu \sim 100$  GHz, where relaxation still dominates, to  $\sim 3$  in the vibrational part of the spectra at  $\nu \sim 250 - 300$  GHz.

Fig. 7.5 presents a comparison of the polarized (VV) and depolarized (VH) LS spectra of ethanol at  $T = 97$ K. At frequencies above the Brillouin frequency  $\nu_{\text{Br}}$  both spectra coincide well; however, at  $\nu < \nu_{\text{Br}}$  the VV spectrum exhibits a step-like increase of the intensity in comparison with the VH spectrum.

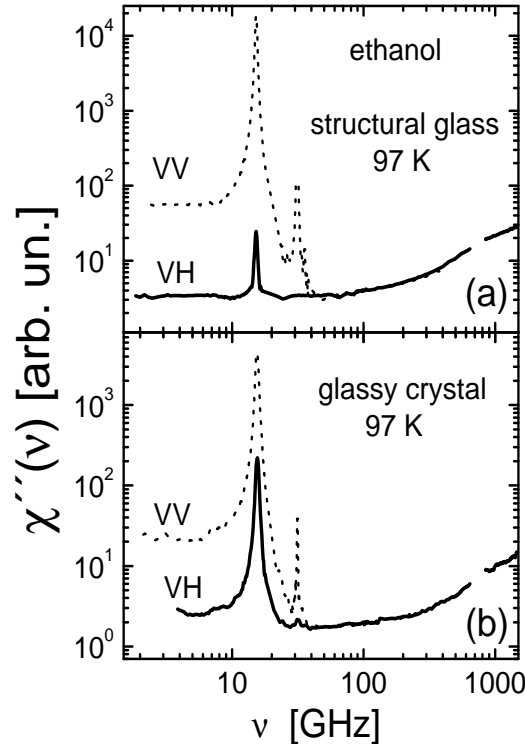


**Figure 7.5:** Comparison of polarized (VV, dotted line) and depolarized light scattering spectra (VH, solid line) of the structural glass (a) and the glassy crystal (b) of ethanol

As demonstrated by Novikov *et al.* [104] this feature can be explained by the contribution of the relaxational response of the longitudinal phonon at the Brillouin frequency. This is an analog of the Mountain mode observed in liquids [105]. Such contribution does not exist in the case of the VH spectra. The ratio of the VV and VH intensities at  $\nu < \nu_{\text{Br}}$ , explicitly  $k = I_{\text{VV}}(\nu < \nu_{\text{Br}})/I_{\text{VH}}(\nu < \nu_{\text{Br}})$ , is  $k_{\text{glass}} = 16.7$  for the structural glass and  $k_{\text{gc}} = 13.6$  for the glassy crystal, so that  $k_{\text{glass}}/k_{\text{gc}} = 1.25 \pm 0.15$ . Compar-

ing the shape of the relaxational contribution in the VV and VH spectra high similarity is observed indicating that similar relaxation processes are probed in either case.

In this part a quantitative analysis of the depolarized QELS spectra of ethanol and CCH will be discussed. From analyzing the QELS spectra of 2-picoline and the dielectric spectra of glycerol [17, 31, 89] (cf. Chapter 4) it was found that the susceptibility minimum close to  $T_g$  can be interpolated by assuming a superposition of the high-frequency contribution of the  $\alpha$ -process as given by its excess wing with a power-law exponent  $\gamma$  and a contribution from the fast relaxation characterized by an exponent  $a$ . Below  $T_g$ , the exponent  $a$  was found to be essentially temperature independent and equal to  $a = 0.7 - 1$ , and the exponent  $\gamma$  to become very small, say  $\gamma \simeq 0.1$ . Thus, below  $T_g$  the excess wing of the  $\alpha$ -process degenerates to a NCL contribution which may extend up to the 50 MHz regime as was proven by  $^2\text{H}$  NMR in the case of glycerol [109]. In other words, the excess wing in the supercooled liquid can be interpreted as the precursor of the NCL in the glass, and one can assume that it extends to the GHz range where it is probed by QELS. In order to reduce the number of fit variables, it was assumed for the narrow frequency interval of the QELS data that the NCL contribution can be approximated by a true constant loss, *i.e.*  $\gamma \simeq 0$ . Therefore, let's try to apply as a fit function a sum of a constant loss contribution,  $C(T)$ , and a power-law contribution,  $B(T)\nu^a$ . To take into account also the vibrational contribution, we add another power-law term  $D\nu^s$  found from the lowest temperature spectrum (11 K in ethanol and 7 K in CCH) where the vibrational contribution dominates. Thus, the fit function reads

$$\chi''(\nu) = C(T) + B(T)\nu^a + D\nu^s. \quad (7.1)$$

The exponents  $a$  and  $s$ , characterizing the fast relaxation and the vibrational spectrum, respectively, were kept constant at all temperatures ( $T < T_g$ ) reducing the number of free parameters. In ethanol  $a = 0.75$ ,  $s = 3$ , and in CCH,  $a = 0.8$ ,  $s = 2.5$  are found. The resulting fits are shown by the dotted lines in the Figs. 7.2 and 7.3. As can be seen, to describe the change of the slope in the QELS spectra a significant NCL contribution results in both phases of ethanol as well as in CCH at temperatures even as low as some 10 K. In Fig. 7.6(b) for ethanol and in



Fig. 7.7(b) for CCH, the temperature dependence of the NCL contribution  $C(T)$  is displayed, where it is compared with the respective internal friction data  $Q^{-1}(T)$  (cf. below).

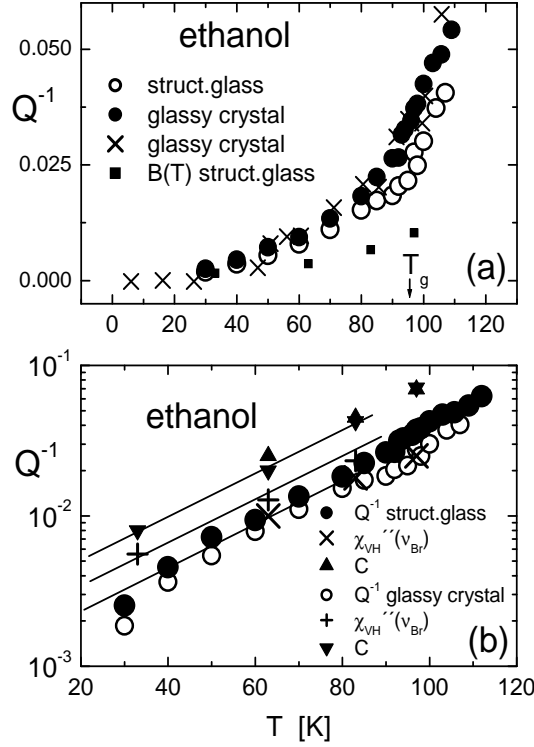


**Figure 7.6:** Comparison of internal friction  $Q^{-1}$  and depolarized light scattering (LS) data in ethanol, linear plot (a) and semi-logarithmic plot (b); open and solid circle:  $Q^{-1}$  for the structural glass and the glassy crystal, respectively; cross in (a): the corresponding data from [107]; solid squares: amplitude of the ps dynamics B; cross in (b): intensity of the depolarized LS spectra at the Brillouin frequency in the glassy crystal found from the fit of the spectra in Fig. 7.2 and scaled by an arbitrary factor, plus sign: respective data for the structural glass; upward triangle: intensity of the constant loss contribution C in the structural glass, downward triangle: in the glassy crystal, also scaled; solid lines: exponential temperature dependence with  $T_{\text{NCL}} = 30$  K.

For comparison, the temperature dependence of the LS susceptibility at the Brillouin frequency,  $\chi''(\nu_{\text{Br}}, T)$ , as obtained from the fit, is also shown in these figures. Essentially, the same temperature dependence is observed for both  $\chi''(\nu_{\text{Br}}, T)$  and  $C(T)$ , and the data can be well fitted by an exponential temperature dependence (solid lines), explicitly

$$C(T) \propto \chi''(T; \nu_{\text{Br}}) \propto \exp(T/T_{\text{NCL}}) \quad (7.2)$$

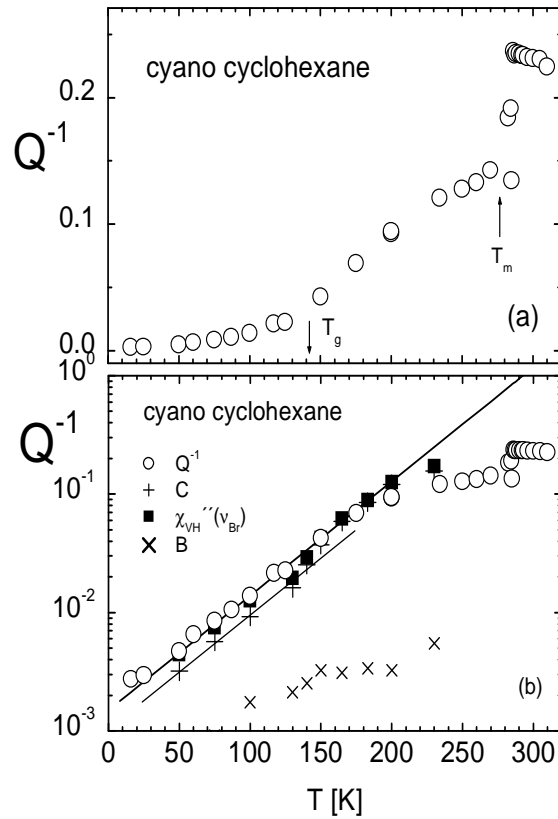


**Figure 7.7:** (a) Internal friction  $Q^{-1}$  for cyano cyclohexane, linear scale; (b) semi-logarithmic scale; solid circles: internal friction, open squares: intensity of the depolarized light scattering spectra at the Brillouin frequency (from Fig. 7.3 scaled by an arbitrary factor), plus sign: constant loss intensity C; cross: intensity of the ps relaxation; straight lines: exponential fit with  $T_{\text{NCL}} = 45$  K

In ethanol,  $T_{\text{NCL}} = 30 \pm 4$  K is found for both glassy crystal and structural glass. In the glassy crystal CCH  $T_{\text{NCL}} = 45 \pm 3$  K is observed. The intensity of the fast relaxation, *i.e.*, parameter  $B(T)$  in Eq. 7.1 is shown in fig. 7.7(b) for CCH. In comparison with the NCL behavior, it shows a weaker temperature dependence.

### 7.3.2 Brillouin scattering

In Fig. 7.8 the frequency  $\nu_{\text{Br}}$  and the width (FWHM)  $\Gamma_{\text{Br}}$  of the Brillouin line of ethanol in the glassy crystal and structural glass are shown. Fig. 7.9 exhibits the corresponding data for the glassy crystal cyano cyclohexane

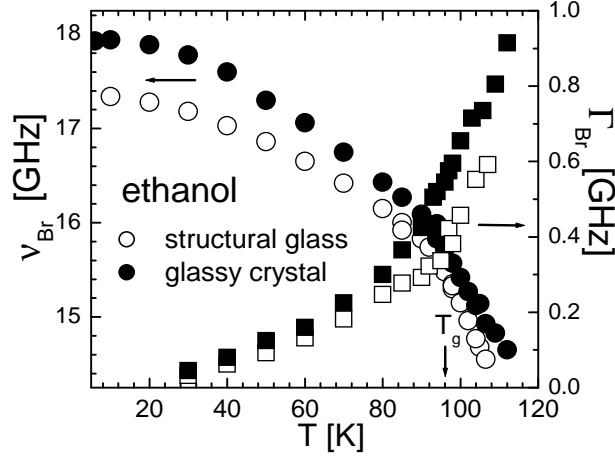


**Figure 7.8:** Position  $\nu_{\text{Br}}$  and width  $\Gamma_{\text{Br}}$  of the Brillouin line in ethanol; solid symbols: glassy crystal, open symbols: structural glass; glass transition temperature  $T_g$  and melting point  $T_m$  indicated.

(CCH). In the case of CCH also data in the liquid phase ( $T > T_m \simeq 285\text{K}$ )

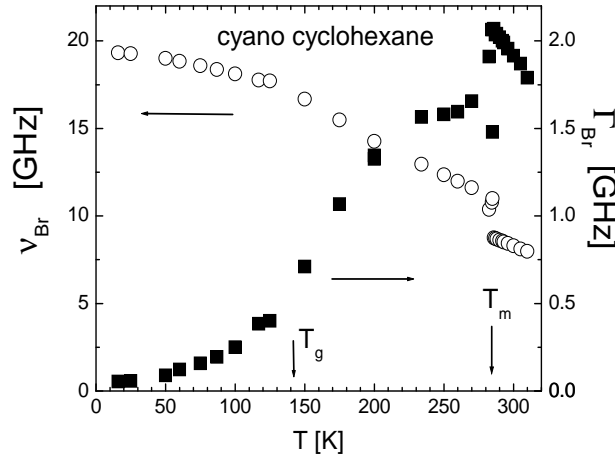


**Figure 7.9:** Position  $\nu_{\text{Br}}$  and width  $\Gamma_{\text{Br}}$  of the Brillouin line in ethanol; solid symbols: glassy crystal, open symbols: structural glass; glass transition temperature  $T_g$  is indicated.

are displayed. The parameters  $\nu_{\text{Br}}$  and  $\Gamma_{\text{Br}}$  are extracted from the fits of the Brillouin spectra as described in the Appendix. The Brillouin frequency and the width were used for calculating the internal friction  $Q^{-1}$  at  $\nu = \nu_{\text{Br}}$ ,

$$Q^{-1}(T) = \Gamma_{\text{rel}}/\nu_{\text{Br}}. \quad (7.3)$$

Figs. 7.6(a,b) show the data of  $Q^{-1}(T)$  for both phases of ethanol, and Fig. 7.7 for the internal friction of CCH. Both linear (a) and semi-

logarithmic plots of the data (b) are displayed. The internal friction data of ethanol shown in Fig. 7.6(a) is in a good agreement with the data of Criado *et al.* [106] included in Fig. 7.6(a). In the glassy crystal

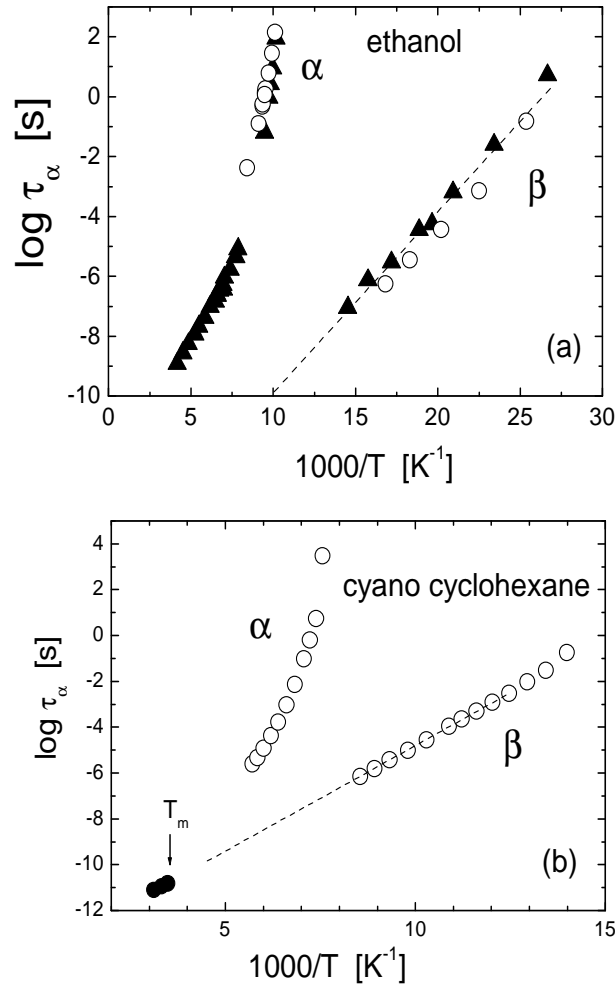


**Figure 7.10:** Relaxation time constants of  $\alpha$ - process and  $\beta$ -process in ethanol and cyano cyclohexane as found by dielectric spectroscopy (data from [96, 98]). (a) Ethanol, open circles: glassy crystal, solid triangles: structural glass; (b) cyano cyclohexane, solid circle: time constant taken from the QELS spectra in the liquid phase.

both in ethanol and CCH as well as in the structural glass of ethanol (cf. Figs. 7.6(a), 7.7(a))  $Q^{-1}$  increases with temperature monotonically showing a somewhat stronger increase above the glass transition temperature  $T_g$  when plotted linearly as a function of temperature. In a semi-logarithmic representation of  $Q^{-1}(T)$  (cf. Figs. 7.6(b), 7.7(b)), this change at  $T_g$  is almost undiscernible, and the data can be reproduced by

an exponential temperature dependence which is actually very similar to that obtained from analyzing the depolarized QELS spectra. Explicitly,

$$Q^{-1}(T; \nu_{\text{Br}}) \propto \chi''(\nu_{\text{Br};T}) \propto C(T) \quad (7.4)$$

holds. One can conclude that the NCL contribution with its exponential temperature dependence dominates both polarized and depolarized LS spectra in the low frequency limit.

## 7.4 Discussion

As demonstrated the relaxation processes revealed by investigating both the depolarized and polarized QELS spectra and the internal friction in the glassy crystal and structural glass of ethanol as well as in the glassy crystal of CCH are very similar. It is interesting to note, that fast relaxations show up stronger in the plastic crystal than in the structural glass, as observed both in LS and in acoustic attenuation  $Q^{-1}$ . In the fit function, Eq. 7.1, two relaxational contributions in the LS spectra are distinguished: the NCL (approximated actually by a constant loss) and the fast relaxation process, the latter is described by a power-law contribution,  $\nu^a$  with  $a > 0$ . The assumption of such a NCL contribution was motivated by analyzes of dielectric spectra and spin-lattice relaxation, the latter indicating that the NCL may extend up to say 50 MHz, at least [47, 109]. The NCL contribution at  $T < T_g$  can be interpreted as a reminiscence of the high-frequency excess wing of the  $\alpha$ -relaxation [47] showing up at  $T > T_g$ . A similar interpolation of the GHz spectra was discussed also by other authors [13, 72]. The exponential temperature dependence of the NCL corresponds to that observed in the dielectric spectra, *e.g.* of glycerol and propylene carbonate [47] where  $T_{\text{NCL}} \sim 33 \text{ K}$  was reported. Thus, a consistent interpretation of the QELS spectra is found although, due to the limited frequency window covered by the QELS spectra (in particular in the case of such weak scatterers like ethanol and cyano cyclohexane), the spectral analysis remains model dependent.

Both ethanol and CCH are actually type B glass formers, *i.e.*, they exhibit a Johari-Goldstein (JG)  $\beta$ -process as revealed by dielectric spectroscopy measurements [96, 98, 99, 102]. That means that in the dielectric

experiments the excess wing is more or less obscured by the presence of the  $\beta$ -peak. In both systems the characteristic relaxation time of the JG relaxation,  $\tau_{\text{JG}}$ , is anomalously short, corresponding to a mean activation energy of  $14 T_g$  (ethanol) and  $19 T_g$  (CCH), being significantly lower than the typical value  $\sim 24 T_g$  [47]. For comparison, in Fig. 7.10 the data for  $\tau_{\text{JG}}$  and  $\tau_\alpha$  as reported by dielectric spectroscopy [96, 98] are shown for the case of ethanol and CCH. We included the time constant  $\tau_\alpha$  as obtained from our QELS study on the liquid phase of CCH Fig. 7.3. Typically, a merging of  $\tau_{\text{JG}}$  and  $\tau_\alpha$  occurs at high temperature, where the relaxation times are on the order of  $10^{-7} - 10^{-8}$  sec [110]. According to Fig. 7.10, the merging, if any, should occur at significantly shorter correlation time. If one supposes that  $\tau_{\text{JG}}$  can be extrapolated to higher temperatures as it is shown in Fig. 7.10 by a dashed line, then the JG relaxation reaches the GHz frequency range at 90 K for ethanol and for 185 K for CCH. Thus, one could expect it to be observable in the LS experiment, and in this case the constant loss contribution may also be interpreted as a reminiscence of the JG relaxation with spectral contributions extending into the LS frequency window. However, there are indications that LS experiments, for reasons not yet understood, do not probe the JG process but only the excess wing [17, 31, 107].

As was discussed in Chapters 2 and 4, a relaxation process in the ps time regime is predicted by MCT. It corresponds to relaxation in the cage formed by the neighbouring molecules in the supercooled liquid. Above the critical temperature of MCT,  $T_c$ , the fast relaxation is temperature independent and has a power-law spectrum with an exponent  $a$  found to be in the range of  $0.3 - 0.4$  (cf. Chapter 4). With decreasing temperature below  $T_c$  but above  $T_g$ , the exponent  $a$  increases, but below  $T_g$  it is fixed. This may be interpreted as a crossover to a white noise spectrum as expected by the theory. A temperature independent exponent is also assumed for our analysis of the QELS spectra revealing  $a = 0.7 - 0.8$  for ethanol and CCH. Thus, the ps dynamics may be interpreted as a reminiscence of the “cage rattling”.

Two further mechanisms of the fast relaxation in glasses are discussed in the literature: dynamics in asymmetric double well potentials (ADWP) [78, 83] and the anharmonic effect [111]. The ADWP mechanism is dominant in silica and CKN glasses [81, 83]. In the spectra it leads to a power-

law wing  $\nu^a$  with an exponent  $a \propto T$ , and the susceptibility, as a function of temperature, is expected to exhibit a maximum. In the case of the ADWP mechanism the integral over the spectral density should be a constant; this reflects the constant density of ADWPs in the glass. Clearly, the experimental data of the present chapter can not be described by the ADWP mechanism. This follows, first, from the temperature independent exponent  $a$ . Second, the internal friction  $Q^{-1}(T)$  has no maximum. And third, the amplitude of the fast relaxation,  $B(T)$ , increases with temperature which together with the temperature independent exponent  $a$  signals an increase of the integral over the fast relaxation spectrum. The absence of any trace from thermally activated ADWP dynamics is quite remarkable since its presence is usually taken as a direct consequence of the standard tunneling model which is applied to describe the low temperature anomalies of glasses, i.e., whereas at low temperatures the ADWPs provide the energy landscape for tunneling, at high temperatures thermally activated crossing of the ADWP barrier is expected [116].

Anharmonicity as the source of the fast relaxation [111, 112] may, in principle, be relevant in ethanol and in CCH. This mechanism predicts a temperature independent exponent  $a$  of the relaxation spectrum and a linear dependence of its amplitude on temperature.

The comparison of polarized (VV) and depolarized (VH) LS spectra of ethanol glass (cf. Fig. 7.5) shows that there is a Mountain mode [105] like relaxation contribution to the VV spectrum at the low-frequency wing of the Brillouin line. This contribution has a 16.7 times stronger intensity than that of the VH spectrum at the same frequency. It was shown that the QELS spectrum in GHz range may originate from the relaxation damping of the boson peak vibrations within the model of vibration mediated LS [104, 113, 114]. Then, the ratio of VV to VH intensities at  $\nu < \nu_{\text{Br}}$  is determined by the ratio of the integrated Brillouin line intensity to that of the boson peak. For the case of the ethanol glass the value  $k \approx 17$  was predicted in [104] what corresponds well to the experimental value of the present work. In the case of the glassy crystal of ethanol the ratio of the integral over the Brillouin line to the integral over the boson peak is by a factor  $\sim 1.25$  less than in the structural glass (cf. Fig. 7.4). Therefore, according to that model the parameter  $k$  should be less by this factor in the glassy crystal than in the structural glass. Indeed, presented in this chap-

ter experimental results well correspond to this situation:  $k_{\text{glass}}/k_{\text{gc}}=1.25 \pm 0.15$ . Thus, the present result supports the assumption that in the QELS spectra relaxations show up via the vibrational response.

## 7.5 Conclusion

The fast relaxation processes in the structural glass and glassy crystal of ethanol as well as in the glassy crystal of cyano cyclohexane were studied by quasi-elastic light scattering (QELS). Both depolarized and polarized LS spectra as well as the width and the position of the Brillouin line were measured. It was found that all the systems exhibit very similar behavior of the QELS spectra, boson peak and internal friction at the Brillouin frequency. The LS spectra are similar to those observed in other molecular glasses [17, 31, 81]. Thus, these results show that positional order in glassy crystal does not significantly alter the fast relaxation processes. The depolarized LS spectra both in ethanol and CCH may be consistently described by a constant loss contribution which dominates in the frequency range from 1 GHz to a few tens GHz and a fast dynamics contribution at higher frequencies up to the onset of the boson peak. The NCL amplitude increases exponentially with temperature, *i.e.*  $\exp(T/T_{\text{NCL}})$ . The parameter  $T_{\text{NCL}} \sim 30 - 45$  K is similar as was found by dielectric spectroscopy in type A glass formers where the NCL emerges below  $T_g$  as a degenerated excess wing of the  $\alpha$ -process at  $T > T_g$  [47, 89, 91, 109]. The intensity of the depolarized LS at the Brillouin frequency depends on temperature in a good agreement with that of the internal friction data indicating that polarized and depolarized spectra probe essentially the same relaxation process. The fast relaxation spectrum in the 100 GHz range is described by a power-law with a temperature independent exponent  $a$ , and an amplitude which only weakly increases with temperature ( $T < T_g$ ). Such behavior is quite different from that observed in the archetypical silica and CKN glass [83, 82] where the QELS spectra are well explained by assuming solely thermally activated transitions in AD-WPs. Thus, in molecular glasses and glassy crystals investigated so far, another mechanism of the relaxation has to be assumed to be dominating, *e.g.*, the anharmonicity of vibrations, and an inconsistency with the ex-



tension of the standard tunneling model for high temperatures forecasting thermally activated ADWP dynamics above say 10 K has to be stated.

## 8 Summary

The present work is devoted to studying the dynamics in molecular glass formers applying the light-scattering (LS) technique, in particular tandem Fabry-Perot interferometry which allows to cover the frequency range from 0.3 GHz to 1000 GHz. Chapters 4 to 7 each present, in a self-contained way, different aspects of the dynamics, as summarized below.

In Chapter 4, the results of the study of the molecular glass formers 2-picoline and m-tricresyl phosphate are presented. The LS spectra are analyzed in the frame of the Mode Coupling Theory (MCT). At high temperatures the evolution of the susceptibility minimum is well described by MCT. Below the critical temperature  $T_c$ , the asymptotic scaling laws of MCT fail due to the appearance of the excess wing of the  $\alpha$ -process, which shows a universal evolution as a function of relaxation time  $\tau_\alpha$ , as was demonstrated by dielectric spectroscopy. A phenomenological approach, which allows to separate slow ( $\alpha$ -process) and fast relaxation processes in the LS spectra is developed. Applying this approach, the temperature dependence of the non-ergodicity parameter  $f$  is obtained. The anomaly of  $f$  as well as a crossover to "white noise" of the fast dynamics spectra is found.

In Chapter 5, the most extensive dielectric data of glycerol compiled by Lunkenheimer *et al.* [Contemp. Phys. **41**, 15 (2000)] are reanalyzed. In contrast to the analysis of Lunkenheimer *et al.*, the normalized susceptibility spectra, *i.e.*, the dielectric loss data normalized by the static susceptibility, including the high temperature data, are analyzed. For this purpose a phenomenological approach, which describes the whole dielectric spectrum including the  $\alpha$ -peak, its high frequency wing, and fast dynamics, is applied. The crossover temperature extracted from the phenomenological analysis and defined by the emergence of the high frequency wing upon cooling agrees well with the critical temperature extracted from the MCT analysis. The crossover temperature  $T_c = 288 \pm 3K$  is significantly

---

higher than reported before. Extracting the non-ergodicity parameter  $f$ , the characteristic anomaly similar to the one of 2-picoline and m-TCP discussed in Chapter 4, is found.

In Chapter 6, the study of the fast relaxation below  $T_g$  in the molecular glasses 2-picoline, m-TCP, o-terphenyl (OTP), as well as in ethanol is presented. In addition to the boson peak, the depolarized LS spectra reveal quasi-elastic contributions that we attribute to i) the nearly constant loss (NCL) in the frequency range below  $\cong 10$  GHz and ii) a power law contribution with positive exponent  $\alpha$  at higher frequencies. In the majority of glasses the latter may be attributed to thermally activated dynamics in asymmetric double well potentials (ADWP), as was previously found for the DLS spectra in silica. Following the Gilroy-Phillips model, the exponent  $\alpha$  shows a master curve as a function of  $T/V_0$  for the various glasses where  $V_0$  specifies the width of the exponential distribution of barriers  $g(V)$ , *i.e.*,  $g(V) \propto \exp(-V/V_0)$ .

In Chapter 7, the investigation of the fast relaxation processes in the structural glass ( $T < T_g$ ) and in the glassy crystal phase of ethanol, as well as in cyano cyclohexane, is presented. Depolarized and polarized LS spectra including the Brillouin lines were measured. It was found that depolarized, polarized LS and internal friction data exhibit fairly similar behavior, and thus reflect the same relaxations. The DLS spectra were described by assuming that the NCL contribution dominates below a few tens GHz, while the fast relaxational dynamics dominates at higher frequencies.

## 9 Zusammenfassung

Im Rahmen der vorliegenden Arbeit wurde die Dynamik in molekularen Glasbildnern mittels Lichtstreuung (LS), insbesondere durch die Tandem-Fabry-Perot-Interferometrie, welche den Frequenzbereich von 0.3 GHz bis 1000 GHz zugänglich macht, untersucht. Die im folgenden zusammengefassten Kapitel 4 bis 7 beinhalten, in sich geschlossen, jeweils Ausführungen zu verschiedenen Aspekten der Dynamik.

In Kapitel 4 wurden die LS Spektren der molekularen Glasbildner 2-Picolin und meta-Tricresylphosphat (m-TCP) im Rahmen der Modenkopplungstheorie (MCT) analysiert. Bei hohen Temperaturen wird die experimentell gefundene Entwicklung des Suszeptibilitätsminimums durch die MCT gut beschrieben. Unterhalb der kritischen Temperatur  $T_c$  versagen jedoch die asymptotischen Skalierungsgesetze der MCT aufgrund der Ausbildung des Excess-Wings des  $\alpha$ -Prozesses, welcher, wie mittels Dielektrischer Spektroskopie gezeigt, eine universelle Entwicklung als Funktion der Relaxationszeit  $\tau_\alpha$  aufweist. Es wurde ein phänomenologischer Ansatz entwickelt, welcher es erlaubt langsame ( $\alpha$ -) und schnelle Relaxationsprozesse in den LS Spektren zu trennen. Somit wurde die Temperaturabhängigkeit des Nichtergodizitäts-Parameters  $f$  erhalten; dessen Anomalie ebenso gefunden wurde wie ein Übergang zu weissem Rauschen in den Spektren der schnellen Dynamik.

In Kapitel 5 wurden die umfangreichsten dielektrischen Daten von Glycerol, zusammengestellt von Lunkenheimer *et al.* [Contemp. Phys. **41**, 15 (2000)] erneut analysiert. Im Gegensatz zur Analyse von Lunkenheimer *et al.* wurden die normalisierten Suszeptibilitätsspektren, im besonderen der dielektrische Verlust, normalisiert über die statische Suszeptibilität, betrachtet. Zu diesem Zweck wurde ein phänomenologischer Ansatz verwendet, welcher das gesamte dielektrische Spektrum inkl.  $\alpha$ -Peak, dessen Hochfrequenzflügel und der schnellen Dynamik beschreibt. Die auf diesem Wege erhaltene bergangstemperatur und jene definiert

---

durch das Aufkommen des Hochfrequenzflügels während der Abkühlung stimmen gut mit der kritischen Temperatur aus der MCT überein. Diese Übergangstemperatur  $T_c = 288 \pm 3K$  ist deutlich höher als bisher publizierte Werte. Extraktion des Nichtergodizitäts-Parameters  $f$  lieferte eine charakteristische Anomalie ähnlich zu jener von 2-Picolin und m-TCP aus Kapitel 4.

Untersuchungen der schnellen Relaxation in den molekularen Gläsern 2-Picolin, m-TCP, o-Terphenyl (OTP) und in Ethanol unterhalb von  $T_g$  bilden das Kapitel 6. Zusätzlich zum Bosonenpeak wiesen die depolarisierten LS (DLS) Spektren quasielastische Beiträge auf, 1.) den nearly constant loss (NCL) im Frequenzbereich unterhalb  $\cong 10$  GHz und 2.) den Beitrag eines Potenzgesetzes mit positivem Exponenten  $\alpha$  bei hohen Frequenzen. In einem Großteil der Gläser kann letzterer Beitrag thermisch aktivierter Dynamik in Doppelmuldenpotentialen (ADWP) zugeordnet werden, wie schon zuvor gefunden für Silica anhand der DLS Spektren. Im Gilroy-Phillips Model weist der Exponent  $\alpha$  eine Masterkurve als Funktion von  $T/V_0$  für jene Gläser auf, bei denen  $V_0$  die Breite der exponentiellen Verteilung von Barrieren  $g(V)$ , *d.h.*,  $g(V) \propto \exp(-V/V_0)$  spezifiziert.

Kapitel 7 behandelt Studien zum schnellen Relaxationsprozess im strukturellen Glas- ( $T < T_g$ ) sowie in der plastisch-kristallinen Phase von Ethanol und Cyanocyclohexan. Depolarisierte und polarisierte LS Spektren inklusive der Brillouin-Linien wurden gemessen. Es stellte sich heraus, dass depolarisierte, polarisierte LS und die Daten aus der Inneren Reibung ziemlich ähnliches Verhalten aufweisen und somit die selben Relaxationsprozesse widerspiegeln. Beschrieben wurden die DLS Spektren anhand der Annahme, dass der NCL Beitrag unterhalb einiger zehn GHz dominiert, während die schnellen Relaxationsprozesse bei höheren Frequenzen dominant werden.

# A Appendix

In this Appendix described the Brillouin lineshape analysis providing the homogeneous width  $\Gamma_{\text{rel}}$  is described. The broadening of the Brillouin line is typically governed by three sources: finite phonon lifetime due to relaxations (homogeneous, or relaxational broadening which one is interested in), distribution of phonon velocities due to some inhomogeneous broadening, and the finite resolution of the spectrometer. A detailed analysis allows to distinguish all the three different type of broadening.

The relaxational broadening of the Brillouin spectra in the damped-harmonic oscillator approximation leads to the following spectral shape of the Brillouin line [115]:

$$I(\nu) \propto \frac{\nu_{\text{Br}}^2 \Gamma_{\text{rel}}}{(\nu^2 - \nu_{\text{Br}}^2)^2 + \nu^2 \Gamma_{\text{rel}}^2} \quad (\text{A.1})$$

where  $\nu_{\text{Br}}$  and  $\Gamma_{\text{rel}}$  are the Brillouin frequency and the full width at half maximum (FWHM) of the Brillouin peak, respectively. If one transforms to the susceptibility spectrum,

$$\chi''(\nu) = I(\nu) / [n(\nu) + 1] \quad (\text{A.2})$$

one finds that it is well approximated by a Lorentzian  $L$ ,

$$\chi''_{LS}(\nu) \simeq \frac{\Gamma_{\text{rel}}/[4(n(\nu_{\text{Br}}) + 1)]}{(\nu - \nu_{\text{Br}})^2 + \Gamma_{\text{rel}}^2/4} = L(\Gamma_{\text{rel}}, \nu) \quad (\text{A.3})$$

as is shown for ethanol in the left inset of Fig. A.1 For the inhomogeneous distribution of  $\nu_{\text{Br}}$  a Gaussian distribution may be expected. Since usually this broadening is narrow in comparison with  $\nu_{\text{Br}}$ , a Gaussian approximation is also a good approximation for the corresponding susceptibility.

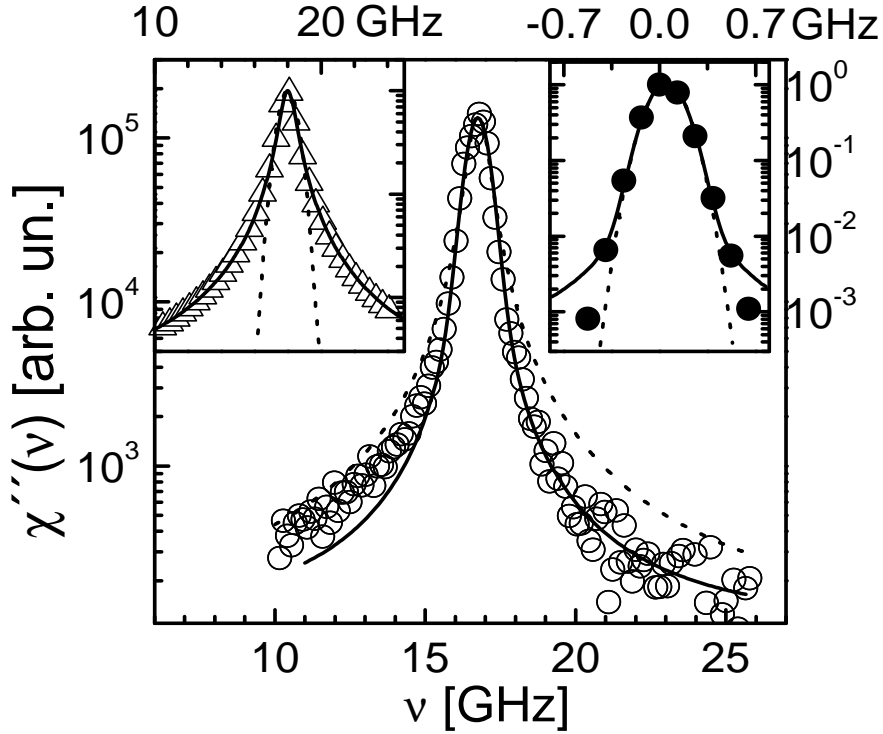


**Figure A.1:** Brillouin line shape in the susceptibility representation in the glassy crystal of ethanol at  $T = 70$  K (open circles), dotted and solid line are fits by the Voigt function as described in the text; left inset: open triangles: damped oscillator approximation, solid line: Lorentzian fit, dotted line: Gaussian, we used  $\nu_{\text{Br}} = 18$  GHz and  $\Gamma_{\text{rel}} = 1$  GHz, that are typical values for our experiment; right inset: experimental resolution function (solid circles), dotted line: fit by a Gaussian, solid line: fit by a Voigt function.

Thus, the LS susceptibility can be described by a convolution of Gaussian  $G$  and Lorentzian  $L$ , known as the Voigt function,

$$\chi''_{\text{Voigt}}(\nu) = \int_0^{\infty} G(\Gamma_{\text{inh}}, \nu - \nu_1) L(\Gamma_{\text{rel}}, \nu_1) d\nu_1 \quad (\text{A.4})$$

where  $G(\Gamma_{\text{inh}}, \nu)$  is the Gaussian contour with the width  $\Gamma_{\text{inh}}$ .

The instrumental transmission function of the Sandercock TFPI is the 3-times-3-pass Airy function. Again a Gaussian function is a good approximation of that Airy function down to about 1 – 10% of its maximum. Therefore, the experimental resolution function was fitted by a Gaussian revealing a good agreement down to  $\sim 3$  % of the maximum (see dashed

line in the right inset of Fig. A.1). The solid line in this inset shows the fit by a Voigt function that allows one to describe the resolution function down to  $\sim 0.5\%$  of the maximum. Hence, an additional Lorentzian broadening with a width  $\Gamma_L^{res} = 0.028$  GHz appears. It follows that the resolution function  $R(\nu)$  can be described as

$$R(\nu) = \int_0^{\infty} G(\Gamma_G^{res}, \nu - \nu_1) L(\Gamma_L^{res}, \nu_1) d\nu_1 \quad (\text{A.5})$$

where  $\Gamma_G^{res}$  and  $\Gamma_L^{res}$  are the Gaussian and the Lorentzian widths parameters.

The measured spectrum  $\chi''(\nu)$  is given by a convolution of the spectrum  $\chi''_{LS}(\nu)$  and the resolution function  $R(\nu)$ . When the instrumental width is negligible in comparison with  $\nu_{Br}$ , the susceptibility spectrum  $\chi''(\nu)$  is well described by the convolution of  $\chi''_{Voigt}(\nu)$  and  $R(\nu)$ . This convolution is again a Voigt function

$$\chi''(\nu) = \int_0^{\infty} G(\Gamma_G, \nu - \nu_1) L(\Gamma_L, \nu_1) d\nu_1 \quad (\text{A.6})$$

with

$$\begin{aligned} \Gamma_L &= \Gamma_L^{res} + \Gamma_{rel} \\ \Gamma_G^2 &= \Gamma_G^{res\ 2} + \Gamma_{inh}^2 \end{aligned}$$

Thus, by fitting the experimental spectrum by the Voigt function one can obtain the parameters  $\Gamma_G$  and  $\Gamma_L$ . Fitting the resolution function allows one to get independently the parameters  $\Gamma_G^{res}$  and  $\Gamma_L^{res}$  (like in the right inset of Fig. A.1). Both the Lorentzian and the Gaussian of the Voigt contour (Eq. A.6) determine the width of the experimental spectrum and it is difficult to separate the two contributions. Usually, in this case it is assumed that  $\Gamma_{inh}$  is temperature independent; then  $\Gamma_{inh}$  can be found independently by measuring the Brillouin line at very low temperature (since relaxational broadening can be ignored here). One can see, however, that this assumption does not give satisfactory results, especially for the glassy crystal. For example, in Fig. A.1 the Brillouin spectrum of glassy



---

crystal ethanol at  $T = 70$  K is fitted by a Voigt contour (dotted line) whose Gaussian width  $\Gamma_G$  was determined from the low temperature ( $T = 10$  K) spectrum. While the fit works well in the main part of the spectrum, it fails to describe the wings. The reason for this may be that at  $T = 70$  K the sample has a larger inhomogeneous broadening than at  $T = 10$  K due to, *e.g.*, appearance of mechanical stresses upon cooling. An underestimated Gaussian width leads to an overestimated Lorentzian width; as a result one has a poor description of the wings of the experimental spectrum.

However, if the experimental spectra cover a few orders in intensity then Gaussian and Lorentzian contributions can be separated already from a single spectrum. The reason for this is that the wing of a Gaussian contour decreases much faster with frequency than that of the Lorentzian. The left inset in Fig. A.1 exhibits the fit of the damped oscillator curve, eq. (A.4), by the Gaussian function. A different behavior is seen in the wings of the contours. The requirement of a good agreement for the whole spectrum allows one to determine both  $\Gamma_G$  and  $\Gamma_L$ . The solid line in Fig. A.1 presents the fit by the Voigt function. The fit works well in the whole intensity range (small deviations in the low-frequency part are due to the memory term in the phonon response function [104]). The fits of the Brillouin spectra in the present work were performed as described above.

# Bibliography

- [1] C.A. Angell *Relaxation in liquids, polymers and plastic crystals-strong/frigile patterns and problems*, J. Non-Cryst. Solids , 131-133 (1991).
- [2] M.D. Ediger, C.A. Angell, S.R. Nagel, *Supercooled Liquids and Glasses*, J. Phys. Chem. , **100**, 13200 (1996).
- [3] J. Jäckle *Models of the glass transition*, Rep. Prog. Phys. , **49**, 2 (1986).
- [4] G. Adam, J.H. Gibbs, *On the Temperature Dependence of Cooperative Relaxation Properties in Glass-Forming Liquids*, **43**, 139 (1965).
- [5] Morrel H. Cohen and G.S. Grest, *Liquid-glass transition, a free-volume approach*, Phys. Rev. B **20**, 1077 (1979).
- [6] H.Z. Cummins *The liquid-glass transition: mode-coupling perspective*, J. Phys.: Condens. Matter **11**, A95-A117 (1999).
- [7] U. Bengtzelius W. Götze and A. Sjölander, *Dynamics of supercooled liquids and the glass transition*, J. Phys. C: Solid State Phys., **17**, 5915 (1984).
- [8] E. Leutheusser, *Dynamical model of the liquid – glass transition*, Phys. Rev. A , **29**, 2765 (1984).
- [9] W. Götze and L. Sjögren *Relaxation processes in supercooled liquids*, Rep. Prog. Phys. , **55** (1992), pp. 241-376.
- [10] W. Götze, *in Liquids, Freezing and the Glass Transition*, edited by J. P. Hansen, D. Levesque, and J. Zinn-Justin (North-Holland, Amsterdam, 1991), p.287

- 
- [11] B.J. Berne and R. Pecora, *Dynamic Light Scattering*, J. Wiley, New York (1976).
- [12] J. Wiedersich, N.V. Surovtsev, V.N. Novikov, E. Rössler, and A.P. Sokolov, *Light scattering spectra of fast relaxation in silica and  $Ca_{0.4}K_{0.6}(NO_3)_{1.4}$  glasses*, Phys. Rev. B , **64**, 064207 (2001).
- [13] P. Lunkenheimer, U. Schneider, R. Brand nad A. Loidl, *Glassy dynamics*, Contemporary Physics, volume 41, number 1 (2000), pp. 15-36.
- [14] N.J. Tao, G. Li, and H.Z. Cummins, *Self-Similar Light-scattering spectra of  $\beta$  Relaxation near the Liquid-Glass Transition*, Phys. Rev. Lett. , **66**, 10 (1991), pp.1334-1337.
- [15] G.Li, W.M. Du, X.K. Chen, H.Z. Cummins, and N.J. Tao, *Testing mode – coupling predictions for  $\alpha$  and  $\beta$  relaxation in  $Ca_{0.4}K_{0.6}(NO_3)_{1.4}$  near the liquid – glass transition by light – scattering*, Phys. Rev. A , **45**, 6 (1991), pp.3867-3879.
- [16] W. Kob, H.C. Andersen, *Testing mode-coupling theory for a supercooled binary Lennard-Jones mixture: The Van Hove correlation function*, Phys. Rev. E , **51**, 4626 (1995).
- [17] J. Wiedersich, N.V. Surovtsev, and E. Rössler, *A comprehensive light scattering study of the glass former toluene*, J. Chem.Phys. , **113**, 3 (2000).
- [18] C.A. Angell, K.L. Ngai, G.B. McKenna, P.F. McMillan, S.W. Martin, J. Appl. Phys., **88**, 3113 (2000).
- [19] E. Rössler, A.P. Sokolov, A. Kisliuk, and D. Quitmann, *Low-frequency Raman scattering on different types of glass formers used to test predictions of mode-coupling theory*, Phys. Rev. B , **49**, 21 (1994).
- [20] J. Gapinski, W. Steffen, A. Patkowski, A.P. Sokolov, A. Kisliuk, U. Buchenau, M. Russina, F. Mezei, H. Schober, *Spectrum of fast dynamics in glass forming liquids: Does the "knee" exist?* J. Chem. Phys. **110**, 5 (1999).

- [21] H.C. Barshilia, G. Li, G.Q. Shen, and H.Z. Cummins, *Depolarized light scattering spectroscopy of  $Ca_{0.4}K_{0.6}(NO_3)_{1.4}$ : A reexamination of the "knee"*, Phys. Rev. E **59**, 5625 (1998).
- [22] G. Hernandez, *Fabry-Perot Interferometers*, Cambridge University Press, (1986).
- [23] S.M. Lindsay, M.W. Anderson, and J.R. Sandercock, *Construction and alignment of a high performing multipass vernier tandem Fabry-Perot interferometer*, Rev. Sci. Instrum. , **52**, 1478 (1981).
- [24] J.R. Sandercock, *Operator Manual for Tandem Interferometer*, (1993).
- [25] W.A. Philips, *Two-level states in glasses*, Rep. Prog. Phys. **50**, 1657 (1987).
- [26] S. Rau, C. Enss, S. Hunklinger, P. Neu, A. Würger, *Acoustic properties of oxided glasses at low temperatures*, Phys. Rev. B **52**, 7179 (1995).
- [27] R.O. Pohl, X. Liu, E. Thompson, *Low-temperature thermal conductivity and acoustic attenuation in amorphous solids*, Rev. Mod. Phys, **74**, 991 (2002).
- [28] W. Götze, *Recent tests of the mode-coupling theory for glassy dynamics*, J. Phys.: Condens. Matter , **11** (1999) A1-A45.
- [29] J. Wuttke, J. Hernandez, G. Li, G. Coddens, H.Z. Cummins, F. Fujara, W. Petry, and H. Sillescu, *Neutron and Light Scattering Study of supercooled Glycerol*, Phys. Rev. Lett. **72**, 19 (1994).
- [30] L. Andrussov, in Landoff-Börnstein Vol. 2, Pt. 5a (Springler, Berlin, 1969), 6th ed.
- [31] S.V. Adichtchev, St. Senkhof, V.N. Novikov, E. Rössler, Ch. Tschirwitz, and J. Wiedersich, *Anomaly of the non-ergodicity parameter and crossover to white noise in the fast relaxation spectrum of a simple glass former*, Phys. Rev. Lett. , **88**, 055703-1 (2002)

- 
- [32] A. Kisliuk, V.N. Novikov, A.P Sokolov, J. Polym. Sci., **b** **40**, 313-327 (2001).
- [33] E. Rössler, A.P. Sokolov, P. Eiermann, and U. Warschewske, Physica A, **201**, 237 (1993).
- [34] C.I.F. Böttcher and P. Borderwijk, *Theory of Electric Polarization* (Elsevier, Amsterdam, 1978), Vol 2.
- [35] Ch. Tschirwitz, C. Alba-Simonesco, unpublished data.
- [36] A. Kudlik, Ch. Tschirwitz, unpublished data.
- [37] G.P. Johari and M. Goldstein *Viscous liquids and the Glass Transition 2. Secondary Relaxation in Glasses of Rigid Molecules*. J. Chem. Phys. , **53**, 2372 (1970).
- [38] L.M. Torrel, L. Borjesson, and A.P. Sokolov, Trans. Theory. Stat. Phys., **24**, 1097 (1995).
- [39] E. Rössler, A.P. Sokolov, Chem. Geol. **128**, 143 (1996).
- [40] T. Franosch, W. Götze, M.R. Mayr, and A.P. Singh, *Evolution of structural relaxation spectra of glycerol within the gigahertz band*, Phys. Rev. E , **55**, 3183 (1997).
- [41] P. Lunkenheimer, A. Pimenov, M. Dressel, Yu.G. Goncharov, R. Böhmer, and A. Loidl, *Fast Dynamics of Glass-Forming Glycerol Studied by Dielectric Spectroscopy*, Phys. Rev. Lett. , **77**, 318 (1996).
- [42] A.P. Sokolov, *The glass transition: general scenario and crossover temperature*, J. Non-Cryst. Solids , **235-237**, 190-195 (1998).
- [43] W. Petry and J. Wuttke, Trans. Theory. Stat. Phys., **24**, 1075 (1995)
- [44] A. Tölle, *Neutron scattering studies of the model glass former ortho-terphenyl*, Rep. Prog. Phys. , **64**, 1473 (2001).
- [45] D. Prevosto, P. Bartolini, R. Torre, M. Ricci, A. Taschin, S. Cappacioli, M. Lucchesi, and P. Rolla, Phys. Rev. E , **66**, 011502 (2002).
- [46] W. Götze, J. Phys.: Condens. Matter **11**, A1 (1999).

- [47] A. Kudlik, S. Benkhof, T. Blochowicz, C. Tschirwitz, E. Rössler, *The dielectric response of simple organic glass formers*, J. Mol. Struct., **479**, 201 (1999).
- [48] L. Wu, S.R. Nagel, Phys. Rev. B **46**, 11198 (1992).
- [49] A. Kudlik, C. Tschirwitz, T. Blochowicz, S. Benkhof, E. Rössler, J. Non-Cryst. Solids **235-237**, 406 (1998).
- [50] K.L. Ngai, and S. Capaccioli, Phys. Rev. E **69**, 031501 (2004).
- [51] H. Wagner, and R. Richert, J. Non-Cryst. Solids **242**, 19 (1998).
- [52] M. Vogel, P. Medic, and E.A. Rössler, Annual. Rep. NMR Spectrosc. **56**, 231 (2005).
- [53] Th. Blochowicz, Ch. Tschirwitz, St. Benkhof, and E. Rössler, *Susceptibility functions for slow relaxation processes in supercooled liquids and the search for universal relaxation patterns*, J. Chem. Phys. , **118**, 16 (2003).
- [54] Th. Blochowicz, *Broadband Dielectric Spectroscopy in Neat and Binary Molecular Glass Formers* (Logos Verlag Berlin 2003).
- [55] S. Adichtchev, T. Blochowicz, C. Tschirwitz, V.N. Novikov, and E. Rössler, *Reexamination of the evolution of the dynamic susceptibility of the glass former glycerol*, Phys. Rev. E , **68**(1) (2003).
- [56] U. Schneider, R. Brand, P. Lunkenheimer, and A. Liodl, *Excess Wing in the Dielectric Loss of Glass Formers: A Johary-Goldstein  $\beta$ -relaxation?* Phys. Rev. Lett. , **84**, 24 (2000).
- [57] M. Vogel, C. Tschirwitz, G. Schneider, C. Koplin, P. Medick, and E. Rössler, J. Non-Cryst. Solids , **307-310**, 326 (2002).
- [58] P. Lunkenheimer, *Habilitationsarbeit*, Augsburg, 2000.
- [59] A. Schönhal, Europhys. Lett., **56**, 815 (2001).

- 
- [60] Landolt-Börnstein, II. Band, Teil 5, Bandteil a (Transportphänomene I), Berlin, 1969.
- [61] R. Schilling and T. Scheidstiger, Phys. Rev. E , **58**, 2932 (1997).
- [62] S. Kämmerer, W. Kob, and R. Schilling, Phys. Rev. E , **58**, 2141 (1998).
- [63] K.L.Ngai, *Dynamic and thermodynamic properties of glass-forming substances*, J. Non-Cryst. Solids , **275**, 7 (2000).
- [64] E. Rössler, V.N. Novikov, A.P. Sokolov, Phase Transit. **63**, 201 (1997).
- [65] C. Gainaru, A. Rivera, S. Pitselyk, G. Eska, and E.A. Rössler *Does frequency-temperature superposition hold in deeply super-cooled liquids?*, Phys. Rev. B **72**, 174203 (2005).
- [66] R. Böhmer, G. Diezemann, G. Hinze, E. Rössler, Prog. Nucl. Mag. Res. Spect. **39**, 191 (2001).
- [67] G. Johari, M. Goldstein, J. Chem. Phys. **53**, 2372 (1970)
- [68] H.Z. Cummins, G. Li, W. M. Du, J. Hernandez, , N.J. Tao, Transp. Theory and Statist. Physics, **24**, 981 (1995).
- [69] H.Z. Cummins, G. Li, W. Du, R.M. Pick, C. Dreyfus, Phys. Rev. E **53**, 896 (1996).
- [70] B. Frick and D. Richter, Science, **267**, 1939 (1995).
- [71] A.P. Sokolov, V.N. Novikov, B. Strube, Phys. Rev. B **56**, 5042 (1997).
- [72] U. Schneider, P. Lunkenheimer, R. Brand, A. Loidl, Phys. Rev. E **59**, 6924 (1999).
- [73] R. Torre, P. Bartolini M. Ricci, and R. M. Pick, Europhys. Lett. **52**, 324 (2000).
- [74] G. Hinze, D. D. Brace, S. D. Gottke, and M. D. Fayer, Phys. Rev. Lett. **84**, 2437 (2000).
- [75] W. Götze, L. Sjögren, Rep. Progr. Phys. **55**, 241 (1992).

- [76] N. Theodorakopoulos, J. Jäckle, Phys.Rev. B **14**, 2637 (1976).
- [77] V.G. Karpov, M.I. Klinger, and F.N. Ignatiev, Zh. Exp. Teor. Fiz. **84**, 760 (1983)(Sov. Phys. JETP **57**, 439 (1983)).
- [78] K.S. Gilroy and W.A. Phillips, Phil. Mag. B **43**, 735 (1981).
- [79] J. Jäckle, in: *Amorphous solids: Low-Temperature Properties*, W.A. Philips, (Springer, Berlin, 1981).
- [80] R. Shuker and R.W. Gammon, Phys. Rev. Lett. **25**, 222 (1970).
- [81] N.V. Surovtsev, J. Wiedersich, V.N. Novikov, A.P. Sokolov, E. Rössler, Phys. Rev. B **58**, 14888 (1998).
- [82] J. Wiedersich, S. V. Adichtchev, and E. Rössler. Phys. Rev. Lett. **84**, 2718 (2000).
- [83] J. Wiedersich, N.V. Surovtsev, N.V. Novikov, E. Rössler, and A.P. Sokolov, Phys. Rev. B **64**, 064207 (2001).
- [84] V.K. Malynovsky, V.N. Novikov, P.P. Parshin, A.P. Sokolov, M.G. Zemlyanov, Europhys. Lett. **11**, 43 (1992).
- [85] N.V. Surovtsev, S.V. Adichtchev, J. Wiedersich, V.N. Novikov, E.A. Rössler, J. Chem. Phys. **119**, 23 (2003).
- [86] J. Gapinski, W. Steffen, A. Patkowski, A.P. Sokolov, A. Kisliuk, U. Buchenau, M. Russina, F. Mezei, and H. Schober, J. Chem. Phys. **110**, 2312 (1999).
- [87] G. Li, M. Du, A. Sakai, H.Z. Cummins, Phys. Rev. A **346**, 3343 (1992)
- [88] N.V. Surovtsev, J.A.H. Wiedersich, E. Duval, V.N. Novikov, E. Rössler, A.P. Sokolov, J. Chem. Phys.**112**, 2319 (2000).
- [89] A.P. Sokolov, A. Kisliuk, V.N. Novikov, K. Ngai, Phys. Rev. B **63**, 172204 (2001).
- [90] A. Kisliuk, V. N. Novikov, A. P. Sokolov, J. Polym. Sci. B: Polym. Phys. **40**, 201 (2002).
- [91] G. Caliskan, A. Kisliuk, V. N. Novikov, and A. P. Sokolov, J. Chem. Phys. **114**, 10189 (2001).



- [92] V. N. Novikov, N. V. Surovtsev, J. Wiedersich, S. Adichtchev, S. Kojima and E. Rössler, *Europhys. Lett.* **57**, 838 (2002).
- [93] S.V. Adichtchev, N. Bagdassarov, St. Benkhof, Th. Blochowicz, V.N. Novikov, E. Rössler, N.V. Surovtsev, Ch. Tschirwitz, J. Wiedersich, *J. Non. Cryst. Sol.* **307-310**, 24 (2002).
- [94] S. Adichtchev, T. Blochowicz, C. Gainaru, E. A. Rössler, V.N. Novikov, C. Tschirwitz, *J. Phys. Cond. Matt.* **15**, S835 (2003)
- [95] M. A. Ramos, S. Vieira, F. J. Bermejo, J. Dawidowski, H. E. Fischer, H. Schober, M. A. González, C.K. Loong, and D. L. Price, *Phys. Rev. Lett.* **78**, 82 (1997).
- [96] S. Benkhof, A. Kudlik, T. Blochowicz, and E. Rössler, *J. Phys.: Condens. Matter* **10**, 8155 (1998).
- [97] A. Srinivasan, F. J. Bermejo, A. de Andrés, J. Dawidowski, J. Zúniga, and A. Criado, *Phys. Rev. B* **53**, 8172 (1996).
- [98] C. Tschirwitz, S. Benkhof, T. Blochowicz, E. Rössler, *J. Chem. Phys.* **117**, 6281 (2002).
- [99] M. A. Miller, M. Jimenez-Ruiz, F. J. Bermejo, and N. O. Birge, *Phys. Rev. B* **57**, R13977 (1998).
- [100] J. Wiedersich, PhD thesis, Universität Bayreuth, 2000.
- [101] H. C. Barshilia, G. Li, G. Q. Shen, and H. Z. Cummins, *Phys. Rev. E* **59**, 5625 (1999).
- [102] R. Brand, P. Lunkenheimer, A. Loidl, *J. Chem. Phys.* **116**, 10386 (2002).
- [103] The sharp peak at around 20 GHz in the polarized spectra results from Brillouin scattering of the cuvette.
- [104] V. N. Novikov, N. V. Surovtsev, J. Wiedersich, S. V. Adichtchev, S. Kojima, and E. Rössler, *Europhys. Lett.* **57**, 838 (2002).
- [105] R.D. Mountain, *J. Res. Natl. Bur. Stand. A* **70**, 207 (1966).

- [106] A. Criado, M. Jiménez-Ruiz, C. Cabrillo, F. J. Bermejo, M. Grimsditch, H. E. Fischer, S. M. Bennington, and R. S. Eccleston, *Phys. Rev. B* **61**, 8778 (2000).
- [107] L. Comez, D. Fioretto, L. Palmieri, L. Verdini, P.A. Rolla, J. Gapinski, T. Pakula, A. Patkowski, W. Steffen, E.W. Fischer, *Phys. Rev. E* **60**, 3086 (1999)
- [108] K.L. Ngai, *J. Non-Cryst. Solids* **274**, 155 (2000)
- [109] T. Blochowicz, A. Kudlik, S. Benkhof, J. Senker, E. Rössler, and G. Hinze, *J. Chem. Phys.* **110**, 12011 (1999).
- [110] V.N. Novikov, A.P. Sokolov, *Phys. Rev. E*, submitted.
- [111] V. N. Novikov, *Phys. Rev. B* **58**, 3867 (1998).
- [112] V. N. Novikov, *Phys. Rev. B* **55**, R14685 (1997).
- [113] V.Z. Gochiyaev, V.K. Malinovsky, V.N. Novikov, A.P. Sokolov, *Phil. Mag. B* **63**, 777 (1991).
- [114] A.P. Sokolov, V.N. Novikov, B. Strube, *Europhys. Lett.* **38**, 49 (1997).
- [115] G. Ruocco and F. Sette, *J. Phys.: Condens. Matter* **13**, 9141 (2001).
- [116] P. Esquinazi (Ed.), *Tunneling Systems in Amorphous and Crystalline Solids*, Springer, Berlin 1998
- [117] C.A. Angell, *Science* **267**, 1924 (1995).

## List of publications

- 1. N V Surovtsev, S V Adichtchev, V K Malinovsky, A A Kalinin, and Yu N Pal'yanov**, *Fast relaxation intensity versus silica glass density: Existence of sharp peculiarity*, J. Phys.:Condens. Matter 18 (2006) pp. 4763-4771
- 2. Surovtsev N.V., Adichtchev S.V., Rossler E., Ramos M.A.**, *Density of vibrational states and light-scattering coupling coefficient in the structural glass and glassy crystal of ethanol*, J. Phys.:Condens. Matter 16 (3): 223-230 JAN 28 2004
- 3. Surovtsev N.V., Adichtchev S.V., Wiedersich J., Novikov V.N., Rossler E.A.**, *Fast relaxation in the structural glass and glassy crystal of ethanol and cyano cyclohexane: a quasielastic light scattering study*, J. Chem. Phys., 119 (23): 12399-12408 DEC 15 2003
- 4. Adichtchev S., Blochowicz T., Tschirwitz C., Novikov V.N., Rossler E.A.**, *Reexamination of the evolution of the dynamic susceptibility of the glass former glycerol*, Phys. Rev. E, 68 (1): Art. No. 011504 Part 1, JUL 2003
- 5. Adichtchev S., Blochowicz T., Gainaru C., Novikov V.N., Rossler E.A., Tschirwitz C.**, *Evolution of the dynamic susceptibility of simple glass formers in the strongly supercooled regime*, J. Phys.:Condens. Matter 15 (11): S835-S847 Sp. Iss. SI, MAR 26 2003
- 6. Adichtchev S.V., Bagdassarov N., Benkhof S., Blochowicz T., Novikov V.N., Rossler E., Surovtsev N.V., Tschirwitz C., Wiedersich J.**, *Evolution of the dynamic susceptibility of paradigmatic glass formers below the critical temperature  $T_c$  as revealed by light scattering*, J. Non-Cryst. Solids, 307: 24-31 SEP 2002
- 7. Novikov V.N., Surovtsev N.V., Wiedersich J., Adichtchev S., Kojima S., Rossler E.**, *On the origin of quasi-elastic light scattering in glasses*, Europhys. Lett. 57 (6): 838-844 MAR 2002
- 8. Adichtchev S.V., Benkhof S., Blochowicz T., Novikov V.N., Rossler E., Tschirwitz C., Wiedersich J.**, *Anomaly of the nonergodicity parameter and crossover to white noise in the fast relaxation spectrum of a simple glass former*, Pys. Rev. Lett 88 (5): Art. No. 055703 FEB 4 2002
- 9. Wiedersich J., Adichtchev S., Rossler E.**, *Spectral shape of relaxations in silica glass*, Pys. Rev. Lett 84 (12): 2718-2721 MAR 20 2000

# Acknowledgments

First of all I would like to express my special thanks to my supervisor Professor E.A. Rössler for giving me the opportunity to work in Bayreuth and for very helpful discussions of my experimental results.

I would like to express my gratitude to Dr. Johannes Wiedersich who taught me how to work with the light-scattering setup and helped me a lot in my first days in Bayreuth.

I would like to thank to Jürgen Gmeiner and Irene Bauer for their assistance in the preparations of my samples.

Many thanks to my Russian colleagues Professor V.K. Malinovsky, Professor V.N. Novikov and Dr. N.V. Surovtsev. I learned a lot working with them.

I also would like to say thanks to Christian Tschirwicz, Thomas Blochowicz, Andreas Feldner, Catalin Gainaru, Sorin Lusceac, Carmen, Alberto Rivera, and Viktor Porokhonsky for many nice and unforgettable moments in Bayreuth.

I thank to my parents for supporting me in difficult times.